Development of a Flotation Rate Equation from First Principles under Turbulent Flow Conditions

Ian Michael Sherrell

Dissertation submitted to the faculty of the Virginia Polytechnic Institute and State University in partial fulfillment of the requirements for the degree of

Doctor of Philosophy

In

Mining and Minerals Engineering

R.H. Yoon, Chair
G.H. Luttrell
G.T. Adel
D. Telionis
P. Vlachos

July 30, 2004
Blacksburg, Virginia

Keywords: rate constant, flotation model, turbulence, extended DLVO, collision frequency, attachment energy, detachment energy

Development of a Flotation Rate Equation from First Principles under Turbulent Flow Conditions

Ian Michael Sherrell

(ABSTRACT)

A flotation model has been proposed that is applicable in a turbulent environment. It is the first turbulent model that takes into account hydrodynamics of the flotation cell as well as all relevant surface forces (van der Waals, electrostatic, and hydrophobic) by use of the Extended DLVO theory. The model includes probabilities for attachment, detachment, and froth recovery as well as a collision frequency. A review of the effects fluids have on the flotation process has also been given. This includes collision frequencies, attachment and detachment energies, and how the energies of the turbulent system relate to them. Flotation experiments have been conducted to verify this model. Model predictions were comparable to experimental results with similar trends. Simulations were also run that show trends and values seen in industrial flotation systems. These simulations show the many uses of the model and how it can benefit the industries that use flotation.

ACKNOWLEDGEMENTS

The author would like to express his deepest appreciation to Dr. Roe-Hoan Yoon. His guidance and support throughout this work were of the utmost importance. Also, the support of Dr. Demetri Telionis and Dr. Pavlos Vlachos were immeasurable. With their significant and incisive advice, this project was able to succeed. Great appreciation and thanks is extended towards them. The author would also like to thank Dr. Gerald Luttrell for his words of wisdom, inspiration, and support. The author also thanks Dr. Greg T. Adel for his timely and insightful advice.

The author would like to thank the Center for Advanced Separation Technology as well as the Department of Energy for their financial support.

Sincere appreciations are extended to Hubert Schimann, Emilio Lobato, Selahattin Baris Yazgan, and Mariano Velázquez. With their friendship, support, and guidance, research went smoothly, but more importantly was enjoyable. Their friendships will be treasured.

The author is also grateful to all of his other friends for their love and support. A special thank you to David Gray. He provided great understanding, sympathy, and encouragement, as well as a lasting friendship.

Lastly, the author would like to express his deepest gratitude and appreciation to his family. Particular thanks are expressed to his wife, Cam, for her love, support, understanding, and tremendous patience.

TABLE OF CONTENTS

ABSTRACT II

ACKNOWLEDGEMENTS III

TABLE OF CONTENTS IV

LIST OF FIGURES VII

LIST OF TABLES IX

INTRODUCTION 1

BACKGROUND 1

MODELING 1

SURFACE FORCES (ENERGIES) 5

OBJECTIVES 8

ORGANIZATION 8

NOMENCLATURE 9

REFERENCES 11

PAPER 1 FLUID DYNAMICS OF BUBBLES AND PARTICLES UNDER TURBULENT FLOTATION CONDITIONS: A REVIEW 13

ABSTRACT 13

INTRODUCTION 13

COLLISION FREQUENCIES 14

ATTACHMENT AND DETACHMENT ENERGIES 19

SUMMARY 22

NOMENCLATURE 23

REFERENCES 24

PAPER 2 DEVELOPING A TURBULENT FLOTATION MODEL FROM FIRST PRINCIPLES 26

ABSTRACT 26

INTRODUCTION 26

MODEL 27

RATE CONSTANT 28

PARTICLE COLLECTION 28

ENERGIES 30

FROTH RECOVERY 31

RESULTS 34

Conclusions 39
Nomenclature 40
References 41
Paper 3 A Comprehensive Model for Flotation under Turbulent Flow Conditions: Verification 44
Abstract 44
Introduction 44
Model 45
Collision Frequency 45
Particle Collection 46
Froth Recovery 48
Experimental 49
Sample 49
Surfactants 49
Continuous Testing 50
Experimental Setup 50
Experimental Procedure 52
Sample Analysis 53
Variables 53
Rate Constant 53
Air Fraction 55
Surface Tension 55
Contact Angle 55
Zeta Potential 55
Particle Size 56
Bubble Size 56
Results 58
Conclusions 61
Nomenclature 61
References 62
Summary 65
Recommendations for Future Work 67
Appendix A – Experimental Data and Model Predictions 69

VITA 95

List of Figures

INTRODUCTION

FIGURE 1. SURFACE ENERGY VS. DISTANCE OF SEPARATION BETWEEN TWO PARTICLES 5

PAPER 1

FIGURE 1. EFFECTS OF STREAMLINES FOR PARTICLE COLLISIONS WITH A RISING BUBBLE 14
FIGURE 2. COLLISION DUE TO SHEAR MECHANISM 15
FIGURE 3. COLLISION DUE TO ACCELERATION MECHANISM 16
FIGURE 4. COMPARISON OF COLLISION FREQUENCY MODELS 18
FIGURE 5. SURFACE ENERGY VS. DISTANCE OF SEPARATION BETWEEN TWO PARTICLES 20
FIGURE 6. TURBULENT KINETIC ENERGY SPECTRUM SHOWING ATTACHMENT AND DETACHMENT ENRGIES 21

PAPER 2

FIGURE 1. SURFACE ENERGY VS. DISTANCE OF SEPARATION BETWEEN TWO PARTICLES 29
FIGURE 2. TURBULENT KIENTIC ENERGY SPECTRUM 31
FIGURE 3. PARTICLE SIZE EFFECT ON FROTH PARTICLE EFFECT AND FROTH RECOVERY 33
FIGURE 4. EFFECT OF THE COLLISION KERNEL ON THE RATE CONSTANT 34
FIGURE 5. EFFECT OF FROTH RECOVERY ON THE RATE CONSTANT 35
FIGURE 6. EFFECT OF ATTACHMENT AND DETACHMENT PROBABILITIES ON THE RATE CONSTANT 35
FIGURE 7. EFFECT OF BUBBLE SIZE ON THE FLOTATION RATE CONSTANT 36
FIGURE 8. EFFECT OF ENERGY INPUT ON THE FLOTATION RATE CONSTANT 37
FIGURE 9. EFFECT OF CONTACT ANGLE ON THE FLOTATION RATE CONSTANT 38
FIGURE 10. EFFECT OF LIQUID-VAPOR SURFACE TENSION ON THE FLOTATION RATE CONSTANT 39

PAPER 3

FIGURE 1. SURFACE ENERGY VS. DISTANCE OF SEPARATION BETWEEN TWO PARTICLES 46
FIGURE 2. FLOTATION CIRCUIT SCHEMATIC 50
FIGURE 3. FLOTATION CELL DIMENSIONS 51
FIGURE 4. SAMPLING POINTS AROUND FLOTATION CELL 52
FIGURE 5. BUBBLE SAMPLING DEVICE 56
FIGURE 6. ORIGINAL AND MODIFIED BUBBLE PICTURES 57
FIGURE 7. BUBBLE SIZE POPULATION DISTRIBUTION 57
FIGURE 8. RELATIONSHIP BETWEEN EXPERIMENTAL AND THEORETICAL RATE CONSTANTS WITH VARIATIONS IN CONTACT ANGLE 58
FIGURE 9. RELATIONSHIP BETWEEN EXPERIMENTAL AND THEORETICAL RATE CONSTANTS WITH VARIATIONS IN PERCENT SOLIDS. ENTIRE DATA SET 59

FIGURE 10. RELATIONSHIP BETWEEN EXPERIMENTAL AND THEORETICAL RATE CONSTANTS WITH VARIATIONS IN PERCENT SOLIDS. EXCLUDING LARGE PARTICLE-HIGH PERCENT SOLIDS DATA SET 59
FIGURE 11. RELATIONSHIP BETWEEN EXPERIMENTAL AND THEORETICAL RATE CONSTANTS WITH VARIATIONS IN ENERGY DISSIPATION 60

List of Tables

PAPER 3

TABLE 1. FLOTATION TEST VARIABLES 53
TABLE 2. EXPERIMENTAL DATA 54

Introduction

Background

Flotation is widely used throughout the mining industry as well as the chemical, and petroleum industries. It can be a highly efficient process for solid-solid separation of minerals. It is now more diverse in its application, with uses such as separation of ink from paper, plastics from each other, radioactive contaminants from soil, and carbon from fly ash. The entire industry is growing along with knowledge of the process and sub-processes. With this increased knowledge, a more reliable flotation model can be derived from first principles. This results in a general flotation model, and allows its use in the mining industry, regardless of machine type and material being recovered.

Generally, flotation is a three-phase process, which uses a medium of water (liquid) to separate various particles (solid) by the addition of air bubbles (gas). Hydrophobic particles attach to the bubbles and rise to the top of the flotation cell where they are extracted while hydrophilic (or less hydrophobic) particles remain in the slurry. The attachment of particles to bubbles is the most important sub process in flotation. Without a selective attachment, no separation would be possible. To enhance this selective attachment, surfactants may be added to alter surface properties. The surfactants control the surface tension and contact angles of the particles in the flotation process.

Flotation occurs within a turbulent environment. Turbulence within a conventional flotation cell is produced by the action of the impeller, which is used for mixing purposes, while turbulence within a column flotation cell is induced by rising air bubbles and settling particles. The combination of the hydrodynamic forces in a turbulent environment and the surface forces controlled by the addition of surfactants makes modeling of the entire flotation process very complex.

Modeling

Modeling of flotation has two major benefits. The main benefit being the control and improvement of the flotation process within an industrial situation. The model will be able to predict a recovery from certain known inputs. If possible, the controller, either

human or computer, may be able to improve the recovery by modifying those inputs. The model has the benefit of instantly knowing what that modification will do. The model can also find the maximum recovery within certain input ranges. The second benefit is that process design can be more easily accomplished. For a typical flotation circuit design within a processing plant, many lab tests are run and scale up of those tests are then performed. A flotation model can bypass the inaccuracy of the scale up process and do away with many of the flotation lab tests. As long as certain input variables are known the flotation recovery can be calculated.

A flotation model is similar to a chemical kinetics model, with one form of that being shown in Equation 1.

$$\frac{dN_1}{dt} = f\left(k, N_i\right) = -k_1 N_1^{f} - k_2 N_2^{g} \qquad 1$$

The model directly predicts the change in particle concentration, N_1, with respect to time, t, as a function of a certain concentration(s), N_i, and rate constant(s), k_i. The negative sign indicates that the concentration is diminishing due to the loss of particles being floated. The exponents f and g signify the order of the process. Most researchers believe that flotation is a first order process and a function of only the particle concentration and a rate constant (Kelsall 1961; Arbiter and Harris 1962; Mao and Yoon 1997).

$$\frac{dN_1}{dt} = -kN_1 \qquad 2$$

The rate constant, k, within this equation conveys how rapidly one species floats. A high rate constant indicates that certain species floats quickly while a low rate constant indicates slow flotation. Knowing the rate constants of two (or more) species within a separation process reveals the efficiency of the process. The greater the difference between the two rate constants, the better the separation is. The recoveries of each individual species, R, can also be calculated knowing the rate constant as well as the residence time within the cell, τ.

$$R = \frac{k\tau}{1 + k\tau} \qquad 3$$

Since recoveries are the desired output from modeling flotation, the rate constant is the useful component of Equation 2. Throughout flotation modeling history, the attempt has been made to produce a general flotation rate constant equation.

The most recent general turbulent flotation rate model was given by Pyke, Fornasiero, and Ralston (2003).

$$k = -2.39 \frac{G_{fr}}{d_2 V_{cell} u_2} \left(\frac{0.33 \varepsilon_d^{4/9} d_2^{7/9}}{\nu^{1/3}} \right) \left(\frac{\Delta \rho_2}{\rho_3} \right)^{2/3} E_C E_A E_S \qquad 4$$

Rate constants are usually modeled as a function of a collision frequency, and probabilities of attachment and detachment (Schulze 1993; Yoon and Mao 1996; Mao and Yoon 1997; Lu 2000; Bloom and Heindel 2002; Pyke, Fornasiero et al. 2003). In Equation 4, the attachment efficiency, E_A, is taken to be the probability of attachment while the stability efficiency, E_S, is an inverse probability of detachment. There is also a collision efficiency, E_C, which takes hydrodynamic effects into account during the collisions of particles and bubbles. The remainder of the equation is the collision frequency. The true number of collisions, that may or may not become attached, results from the combination of the collision efficiency and collision frequency. The collision frequency shown in Equation 4 is a modified equation given by Abrahamson (1975) that is divided by the number density of particles. The turbulent velocity used within Abrahamson's model is given by Liepe and Mockel (1976).

The collision efficiency within Equation 4 takes into account the fact that particles may deviate from the fluid flow and may not collide due to this deviation. Pyke, Fornasiero, and Ralston (2003) use a solution of the BBO equation referred to as the Generalized Sutherland Equation. This takes into account interception and inertial forces.

The attachment efficiency makes use of the angle of collision, which results in a certain maximum sliding time, and relates that to the amount of time needed for the bubble and particle to become attached once collision occurs. When collisions occur, a certain amount of time, referred to as the induction time, is required for the liquid film to be drained between the bubble and particle as well as the three-phase-contact line to spread and become stable. Enough time must be available during the collision process for the attachment to take place.

The stability efficiency is a relationship between the attachment and detachment forces. The attachment forces include capillary and hydrostatic forces. The detachment

forces include buoyancy, gravitational, machine acceleration, and capillary force. Knowing these, the stability of the aggregate can be determined.

Equation 4 provides a model of the flotation process based upon turbulent characteristics of the flow as well as hydrodynamic forces. What the model does not account for is the effects of surface forces. Surface forces are known to have an effect on the outcome of flotation as shown by Mao and Yoon (1997). Without the inclusion of surface forces a model can predict only a certain percentage of cases and is not general in nature. A flotation model has been proposed that accounts for surface forces in a quiescent environment (Yoon and Mao 1996).

$$k = \frac{1}{4} S_b \left[\frac{3}{2} + \frac{4\,\mathrm{Re}^{0.72}}{15} \right] \left(\frac{R_1}{R_2} \right)^2 \exp\left(-\frac{E_1}{E_k} \right) \left[1 - \exp\left(-\frac{W_a + E_1}{E_k^{'}} \right) \right] \qquad 5$$

This model is derived from first principles and is the most rigorous flotation model, to date, dealing with all dominant surface forces found in flotation. These surface forces are the electrostatic, van der Waals, and hydrophobic forces and are modeled based upon the extended DLVO theory. The surface forces are used in calculating the probability of attachment (first exponential term) and the probability of detachment (second exponential term). The energies that must be overcome, by the kinetic energies of the particles and bubbles, for the attachment and detachment processes to occur are related to the surface forces.

The first half of Equation 5 is a combination of the collision frequency ($¼S_b$) and collision efficiency. The collision frequency is derived from the number of particles one bubble would collide with assuming it traveled vertically the entire length of the cell and particles were completely stationary and evenly distributed throughout the cell. This becomes a function of the surface area rate, S_b, of the air. Since particles are not stationary, a collision efficiency is used to take into account hydrodynamic effects. This assumes that particles follow the fluid completely (no inertial effects) and that there is a governing stream function that takes into account the Reynolds number of the bubble.

The problem with this model is that it was derived for a quiescent environment. Due to this, no turbulent effects are present. Since turbulence is found in all flotation situations, this model can not be applied for flotation purposes. It does, on the other

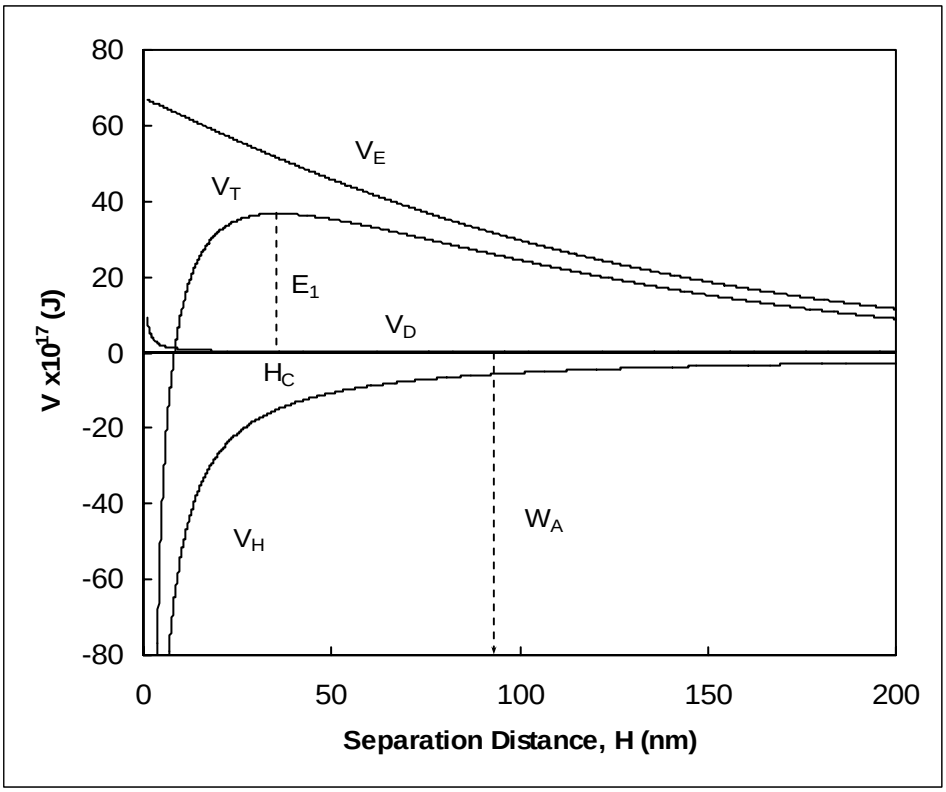

Figure 1. Surface energy vs. distance of separation between two particles (i.e. particle-bubble)

hand, provide a valuable relationship between the hydrodynamics of the system and the surface forces.

Surface Forces (Energies)

Surface forces are interactions between surfaces usually on a scale of less then 100 nanometers. The forces can be converted into energies of interaction based upon the radii of the two interacting surfaces. Surface force modeling in flotation employs the extended DLVO theory. This theory combines the van der Waals (dispersion) energy (force), V_D, electrostatic energy (force), V_E, as well as the hydrophobic energy (force), V_H, into one total surface energy (force), V_T (see Figure 1). These surface energies are additive as shown in Equation 6.

$$V_T = V_E + V_D + V_H \qquad 6$$

All three forces (energies) are either known or shown to have an effect on interactions between particles and bubbles in a water medium (Yoon and Mao 1996; Yoon 2000).

The electrostatic energy is given by Equation 7 (Shaw 1992).

$$V_E = \frac{\pi\varepsilon_0\varepsilon R_1 R_2\left(\Psi_1^2+\Psi_2^2\right)}{\left(R_1+R_2\right)}\left[\frac{2\Psi_1\Psi_2}{\Psi_1^2+\Psi_2^2}\ln\left(\frac{1+e^{-\kappa H}}{1-e^{-\kappa H}}\right)+\ln\left(1-e^{-2\kappa H}\right)\right] \quad 7$$

The Stern potential for the particle and bubble, Ψ_i, is substituted with the zeta-potential, ζ_i, which can be measured.

The dispersion energy is given by Equation 8 (Rabinovich and Churaev 1979)

$$V_D = -\frac{A_{132}R_1R_2}{6H\left(R_1+R_2\right)}\left[1-\frac{1+2bl}{1+bc/H}\right] \quad 8$$

where A_{132} is the Hamaker constant for particle 1 and particle 2 (a bubble in flotation) interacting in a medium (3). The last half of the equation is a correction factor for the retardation effect, where b is a parameter characterizing materials of interacting particles ($3\text{x}10^{-17}$ s for most materials), l is a parameter characterizing the medium ($3.3\text{x}10^{15}$ s^{-1} for water) and c is the speed of light (Yoon and Mao 1996). The retardation effect can usually be omitted due to the small effect that it has on the overall energy of interaction.

The equation for hydrophobic energy is an empirical formula as opposed to Equations 7 and 8 which are theoretical in nature. The most recent proposed form is similar to the dispersion energy equation (Yoon and Mao 1996).

$$V_H = -\frac{R_1R_2K_{132}}{6\left(R_1+R_2\right)H} \quad 9$$

The Hamaker constant, A_{132}, is replaced by the hydrophobic force constant, K_{132}, and there is no retardation effect. The hydrophobic force constant can be found by using Equation 10, which includes the interactions between similar particles in a medium (Yoon, Flinn et al. 1997).

$$K_{132} = \sqrt{K_{131}K_{232}} \quad 10$$

K_{131} and K_{232} are given by Equations 11 & 12, where [F] is the dodecylammonium hydrochloride concentration.

$$K_{131} = a\exp\left(b_k\theta\right) \quad 11$$

for θ<86.89°	a = 2.732E-21,	b_k = 0.04136
for 86.89°<θ<92.28°	a = 4.888E-44,	b_k = 0.6441
for θ>92.28°	a = 6.327E-27,	b_k = 0.2172

$$K_{232} = \exp\left(d + e\sqrt{[F]}\right) \qquad 12$$

for all $[F]$ $\qquad$ d = -39.67, $\qquad$ e = -117.7

Equation 11 was derived from data obtained from Yoon and Ravishankar (1994; 1996), Rabinovich and Yoon (1994), Vivek (1998), and Pazhianur (1999). Equation 12 was derived from data obtained by Yoon and Aksoy (1999).

There is an ongoing debate as to the validity and origin of the hydrophobic force. There has been a tremendous amount of research on this subject, with only a few examples included here. Most, but not all, researchers believe that the force can be measured at long ranges (up to 200 nanometers). Of those, there are varying explanations as to the origin of the force. Attard (1989) proposed that the hydrophobic force is actually a part of the van der Waals force. This can be discredited in flotation due to the fact that the van der Waals force is repulsive between a particle and air bubble in a water medium. This would result in no attractive forces seen in flotation. Another explanation must be given in view of the fact that an attractive force is still seen under these circumstances (Ducker, Xu et al. 1994; Lu 2000; Yoon 2000). The force also might originate from the ordering of water molecules away from the hydrophobic surface (Eriksson, Ljunggren et al. 1989) or from a hydrodynamic fluctuation at the hydrophobic surface and liquid interface that might produce an attractive force (Ruckenstein and Churaev 1991). The most recent explanation is the formation of a microscopic bridging bubble between the two surfaces. The surface tension along the liquid-vapor interface creates the long range hydrophobic force. The bridging bubble can be formed by cavitation of the liquid when the two surfaces approach each other (Berard, Attard et al. 1993; Parker and Claesson 1994) or by stable nano-bubbles that have previously adhered to the hydrophobic surface (Carambassis, Jonker et al. 1998; Ishida, Sakamoto et al. 2000; Ederth, Tamada et al. 2001; Sakamoto, Kanda et al. 2002). Arguments against microscopic bridging bubbles state that they are thermodynamically unstable (Eriksson and Ljunggren 1995; Eriksson and Ljunggren 1999) and too short lived to have a noticeable effect on experimental measurements (Ljunggren and Eriksson 1997). The debate as to the cause of the hydrophobic force will continue until a theoretical model for the interaction can be proposed and verified. Regardless of the origin of the hydrophobic

force, a long range attraction exists between hydrophobic surfaces. Therefore, it is appropriate to use Equation 9 to quantify that attractive force.

Knowing the total surface force energy (Figure 1), there exists a maximum repulsive (positive) energy that must be overcome, E_1. This maximum energy occurs at the critical rupture distance, H_c. At distances smaller than this the free energy continuously drops. This means there is nothing preventing the particle and bubble from coming together. Once this maximum is reached, and overcome, the particle and bubble will spontaneously adhere to each other, and a three-phase contact will occur. Due to vibrations along the liquid-vapor interface, the average critical rupture thickness is greater than the instantaneous critical rupture thickness (Yoon 2000). The vibrations cause the instantaneous distance between the bubble and particle, which is smaller than the average distance, to be equal to the critical rupture thickness. This smaller distance overcomes the energy barrier. These vibrations will result in a higher average critical rupture thickness and a lower energy barrier.

Objectives

The objective of the present research is to derive a general flotation model that takes into account turbulence within a flotation cell as well as all applicable surface forces. The main focus of the model is within the slurry portion of the flotation cell. This model is to be derived, as much as possible, from first principles that relate turbulent parameters of the fluid to physical and chemical properties of the particles, bubbles and fluid. With the addition of a froth recovery model, an entire flotation model will be available.

To accomplish this, a review of flotation fluid dynamics will be performed. Experiments will also be undertaken to verify the model. Simulations using the model will show the applicability to industrial systems. It is hoped that the proposed model will be able to improve upon these systems and be a benefit to the mineral processing industry.

Organization

The body of this thesis has been presented as three independent papers. Paper 1 is titled "Fluid Dynamics of Bubbles and Particles under Turbulent Flotation Conditions: A Review". This paper presents turbulence effects upon flotation. Included within this paper is a review of collision frequencies as well as the proposed attachment and detachment energies imparted by the turbulence. Paper 2 is titled "Developing a Turbulent Flotation Model from First Principles". This paper presents the flotation model that has been derived as well as simulations using this model. Paper 3 is titled "A Comprehensive Model for Flotation under Turbulent Flow Conditions: Verification". This paper demonstrates the validity of the proposed flotation model by experimental verification. The summary of the entire research is presented following these three papers. Recommendations for future work follow the summary.

Nomenclature

1	subscript – refers to particle
2	subscript – refers to bubble
3	subscript – refers to liquid
a	K_{131} parameter [-]
b	material parameter (V_D) [s]
b_k	K_{131} parameter [-]
c	speed of light [$m \cdot s^{-1}$]
d	K_{232} parameter [-]
d_i	diameter of i [m]
e	K_{232} parameter [-]
k	rate constant [s^{-1}]
l	medium parameter (V_D) [s^{-1}]
u_b	bubble velocity [m]
A_{132}	Hamaker constant for 1 interacting with 2 in 3 [-]
E_1	surface energy barrier [J]
E_A	attachment efficiency [-]
E_C	collision efficiency [-]
E_S	stability efficiency [-]

E'_k	kinetic energy of detachment [J]
E_k	kinetic energy of attachment [J]
F	concentration of dodecylammonium hydrochloride [$mol \cdot L^{-1}$]
G_{fr}	gas flow rate through flotation cell [$m^3 \cdot s^{-1}$]
H	distance of separation [m]
H_c	critical rupture thickness [m]
K_{132}	hydrophobic constant for particle 1 interacting with particle 2 in a medium 3 [-]
N_i	number density of i – number per unit volume [m^{-3}]
R	recovery [-]
R_i	radius of i [m]
Re	Reynolds number of a rising bubble [-]
S_b	surface area rate [s^{-1}]
V_{cell}	volume of cell [m^3]
V_D	dispersion free energy of interaction [J]
V_E	electrostatic free energy of interaction [J]
V_H	hydrophobic free energy of interaction [J]
V_T	total free energy of interaction [J]
W_a	work of adhesion [J]
ε	dielectric constant of medium (liquid) [-]
ε_0	permittivity of vacuum [$C^2 \cdot N^{-1} \cdot m^{-2}$]
ε_d	energy dissipation [$m^2 \cdot s^{-3}$]
ζ_i	zeta potential of i [mV]
θ	contact angle [rad] – measured through liquid
κ	inverse Debye length [m^{-1}]
ν	kinematic viscosity [$m^2 \cdot s^{-1}$]
ρ_i	density of i [$kg \cdot m^{-3}$]
τ	retention time within flotation cell [s]
Ψ_i	Stern potential of i [V]

References

Abrahamson, J. (1975). "Collision rates of small particles in a vigorously turbulent fluid." Chemical Engineering Science **30**(11): 1371-9.

Arbiter, N. and C. C. Harris (1962). Flotation Kinetics. Froth flotation - 50th anniversary volume. D. W. Fuerstenau, American Institute of Mining, Metallurgical, and Petroleum Engineers.

Attard, P. (1989). "Long-range attractions between hydrophobic surfaces." Journal of Physical Chemistry **93**: 6441-6444.

Berard, D. R., P. Attard, et al. (1993). "Cavitation of a Lennard-Jones fluid between hard walls, and the possible relevance to the attraction measured between hydrophobic surfaces." J. Chem. Phys. **93**(9): 7236-7244.

Bloom, F. and T. J. Heindel (2002). "On the structure of collision and detachment frequencies in flotation models." Chemical Engineering Science **57**(13): 2467-2473.

Carambassis, A., L. C. Jonker, et al. (1998). "Forces measured between hydrophobic surfaces due to a submicroscopic bridging bubble." Physical Review Letters **80**(24): 5357-5360.

Ducker, W. A., Z. Xu, et al. (1994). "Measurements of hydrophobic and DLVO forces in bubble-surface interactions in aqueous solutions." Langmuir **10**(9): 3279-3289.

Ederth, T., K. Tamada, et al. (2001). "Force measurements between semifluorinated thiolate self-assembled monolayers: long-range hydrophobic interactions and surface charge." Journal of Colloid and Interface Science **235**: 391-397.

Eriksson, J. C. and S. Ljunggren (1995). "Comments on the alleged formation of bridging cavities/bubbles between planar hydrophobic surfaces." Langmuir **11**: 2325-2328.

Eriksson, J. C. and S. Ljunggren (1999). "On the mechanically unstable free energy minimum of a gas bubble which is submerged in water and adheres to a hydrophobic wall." Colloids and Surfaces A: Physicochemical and Engineering Aspects **159**: 159-163.

Eriksson, J. C., S. Ljunggren, et al. (1989). "A phenomenological theory of long-range hydrophobic attraction forces based on a square-gradient variational approach." Journal of the Chemical Society, Faraday Transactions 2 **85**(part 3): 163-176.

Ishida, N., M. Sakamoto, et al. (2000). "Attraction between hydrophobic surfaces with and without gas phase." Langmuir **16**: 5681-5687.

Kelsall, D. F. (1961). "Application of probability in the assessment of flotation systems." Bull. Instn. Min. Metall. **650**: 191-204.

Liepe, F. and H. O. Moeckel (1976). "Studies of the combination of substances in liquid phase. Part 6: The influence of the turbulence on the mass transfer of suspended particles." Chemische Technik (Leipzig, Germany) **28**(4): 205-209.

Ljunggren, S. and J. C. Eriksson (1997). "The lifetime of a colloid-sized gas bubble in water and the cause of the hydrophobic attraction." Colloids and Surfaces A: Physicochemical and Engineering Aspects **129-130**: 151-155.

Lu, S.-c. (2000). "Bubble-particle interaction in flotation cell." Trans. Nonferrous Met. Soc. China **10**(Special Issue): 40-44.

Mao, L. and R.-H. Yoon (1997). "Predicting flotation rates using a rate equation derived from first principles." International Journal of Mineral Processing **51**(1-4): 171-181.

Parker, J. L. and P. M. Claesson (1994). "Bubbles, cavities, and the long-ranged attraction between hydrophobic surfaces." Journal of Physical Chemistry **98**: 8468-8480.

Pazhianur, R. (1999). Hydrophobic force in flotation, Virginia Polytechnic Institute and State University.

Pyke, B., D. Fornasiero, et al. (2003). "Bubble particle heterocoagulation under turbulent conditions." Journal of Colloid and Interface Science **265**(1): 141-151.

Rabinovich, Y. I. and N. V. Churaev (1979). "Effect of electromagnetic delay on the forces of molecular attraction." Kolloidnyi Zhurnal **41**(3): 468-74.

Rabinovich, Y. I. and R. H. Yoon (1994). "Use of atomic force microscope for the measurements of hydrophobic forces." Colloids and Surfaces, A: Physicochemical and Engineering Aspects **93**: 263-73.

Ruckenstein, E. and N. Churaev (1991). "A possible hydrodynamic origin of the forces of hydrophobic attraction." Journal of Colloid and Interface Science **147**(2): 535-538.

Sakamoto, M., Y. Kanda, et al. (2002). "Origin of long-range attractive force between surfaces hydrophobized by surfactant adsorption." Langmuir **18**(5713-5719).

Schulze, H. J. (1993). Flotation as a heterocoagulation process: Possibilities of calculating the probability of flotation. Coagulation and Flocculation. B. Dobias, Marcel Dekker.

Shaw, D. J. (1992). Introduction to colloid and surface chemistry. Boston, Butterworth-Heinemann.

Vivek, S. (1998). Effects of long-chain surfactants, short-chain alcohols and hydrolysable cations on the hydrophobic and hydration forces, Virginia Polytechnic Institute and State University.

Yoon, R. H. (2000). "The role of hydrodynamic and surface forces in bubble-particle interaction." International Journal of Mineral Processing **58**(1-4): 129-143.

Yoon, R. H. and S. B. Aksoy (1999). "Hydrophobic forces in thin water films stabilized by dodecylammonium chloride." Journal of Colloid and Interface Science **211**(1): 1-10.

Yoon, R.-H., D. H. Flinn, et al. (1997). "Hydrophobic interactions between dissimilar surfaces." Journal of Colloid and Interface Science **185**(2): 363-370.

Yoon, R.-H. and L. Mao (1996). "Application of extended DLVO theory, IV. Derivation of flotation rate equation from first principles." Journal of Colloid and Interface Science **181**(2): 613-626.

Yoon, R.-H. and S. A. Ravishankar (1994). "Application of extended DLVO theory III. Effect of octanol on the long-range hydrophobic forces between dodecylamine-coated mica surfaces." Journal of Colloid and Interface Science **166**(1): 215-24.

Yoon, R.-H. and S. A. Ravishankar (1996). "Long-range hydrophobic forces between mica surfaces in alkaline dodecylammonium chloride solutions." Journal of Colloid and Interface Science **179**(2): 403-411.

Fluid Dynamics of Bubbles and Particles under Turbulent Flotation Conditions: a Review

I. M. Sherrell

Abstract

A review and assessment of the current knowledge of the effects of turbulent flow on the flotation process has been undertaken. This includes a review of probabilistic models of collision frequencies with all underlying assumptions. Although there is no model that takes into account all turbulent effects and conditions for the collisions of particles and bubbles, a model proposed by Abrahamson (1975) is the most applicable for flotation purposes. Our review revealed that there are more appropriate models in the literature but modifications are needed to take into account bubble and particle density effects in a liquid. Attachment and detachment energies are also described. Attachment energies are related to the Kolmogorov length scale and the length scales of the particles and bubbles. Detachment energies are related to the system's largest length scale (i.e. the impeller).

Introduction

Fluid effects are seen in all flotation processes. Modeling of the process, therefore, must take this fact into account. Flotation modeling aims at obtaining a rate constant for different components (e.g. minerals, surface chemistry types, particle sizes) of a feed to a flotation circuit. These rate constants are usually modeled as a function of collision frequencies, and probabilities of attachment and detachment (Schulze 1993; Yoon and Mao 1996; Mao and Yoon 1997; Lu 2000; Bloom and Heindel 2002; Pyke, Fornasiero et al. 2003). Since fluid effects are seen in all aspects of flotation, they must be reflected in the collision frequency, attachment and detachment model sections.

To model these processes, assumptions must be made. There are many simplifications in flotation modeling including particle and bubble effects. Shape is assumed to be spherical due to the great difficulty in accounting for non-spherical particles. Particle surface chemistry is assumed to be uniform across the entire surface of the particle. Particle composition (e.g. hydrophobicity) is also assumed to be uniform either throughout the entire flotation cell or component being modeled or divisions of that cell or component. These are only a few of the simplifications encountered in flotation modeling, but the greatest simplification comes from modeling the fluid itself.

Turbulence has always been an extremely complicated subject, and the only way to model it, except under very special circumstances, is to assume that the turbulence is locally homogeneous and isotropic. Although, for certain flow fields, this is not as far-fetched as it may seem, the large scales encountered in flotation modeling do not satisfy this condition and the assumption is needed. This allows statistical modeling of turbulence to be adopted, based mostly

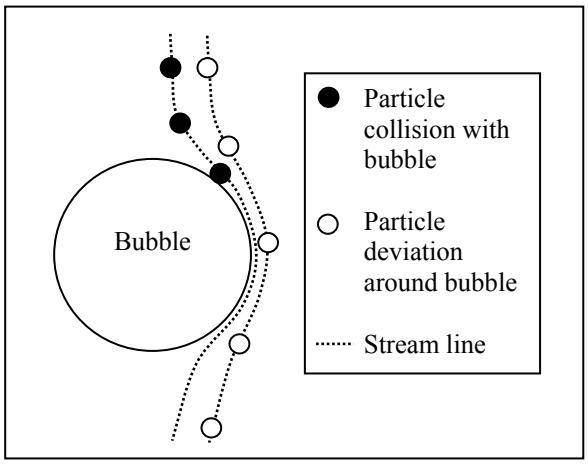

Figure 1. Effects of streamlines for particle collisions with a rising bubble. The assumption is made that particles follow the fluid completely.

on the Kolmogorov theory, which in turn allows the establishment of a relationship between turbulent data such as energy dissipation and root-mean-squared (rms) slip velocity.

Kolmogorov theory is a way of relating scales of turbulence (and in flotation modeling, what those scales are affecting) to their respective energies. Energy is added at the integral scale and from there cascades down through the inertial scales to the dissipative scales where it is lost as heat due to viscous effects. The assumption is that energy is not lost at any scale but the dissipative scale and is only transferred through the intermediate scales. In the flotation process, energy is added by the impeller (integral scale), acts upon the particles and bubbles (inertial scale) and is dissipated from the system at the Kolmogorov microscale (dissipative). Statistical simplification, such as the Kolmogorov theory, allows modeling of turbulent processes, such as flotation, to take place.

Collision Frequencies

Although the Kolmogorov theory is not explicitly used in collision frequency modeling, the assumption that the turbulence is homogeneous and isotropic is still required. Mao and Yoon bypassed this assumption by modeling flotation in a quiescent environment (1996; 1997). This required the use of streamlines and the assumption that particles followed the fluid flow completely.

The total number of collisions was found by multiplying the total possible collisions, Z_C, by a collision efficiency, P_C.

$$Z_{12} = Z_C P_C \qquad [1]$$

The total possible number of collisions was found by multiplying the volume swept by one bubble, assuming that the bubble rises straight up through the entire cell, and the number density of particles to get the number of particle collisions with one bubble. Knowing this and the number of bubbles per unit time through the cell results in the total possible collisions (Equation [2]).

$$Z_C = \frac{3V_g}{4R_2} N_1 = \frac{1}{4} S_b N_1 \qquad [2]$$

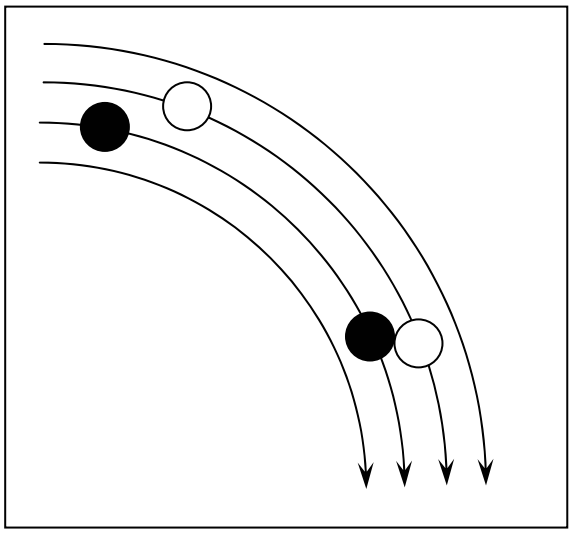

Figure 2. Collision due to shear mechanism.

The collision efficiency, P_C, was obtained by knowing the stream function for the flow around the bubble (Figure 1). Assuming that the particles completely followed the fluid flow (no Brownian or inertial effects) the collision efficiency would then be a function of that stream function and the particle and bubble radii (Luttrell and Yoon 1992; Yoon and Mao 1996; Dai, Fornasiero et al. 2000). There are forms of collision efficiencies that can also take into account, among other things, the inertial effects of particles (Dai, Fornasiero et al. 2000).

When turbulence is encountered, an analysis such as this can not be used. For one, bubbles take meandering paths through the liquid and a total volume that they travel through can not be accounted for. Also, streamlines are not stationary in turbulence. They are constantly changing throughout time and space. A more statistical approach must be taken.

Collision frequencies are all based around one simple model

$$Z_{12} = \beta N_1 N_2 \qquad [3]$$

where β, the collision kernel, is

$$\beta = f\left(C, d_{12}, w\right) \qquad [4]$$

a function of some constant, C, the average diameter of collision, $d_{12} = (R_1+R_2)$, and the relative velocities between the colliding particles, w. A form similar to this was first used by von Smoluchowski (1917) to model coagulation kinetics.

$$Z_{12} = \frac{4}{3} N_1 N_2 d_{12}^3 G \qquad [5]$$

G in Equation [5] is the velocity gradient perpendicular to the direction of particle motion. Only laminar flows with collisions occurring due to shear were considered. In shear flows, particles are able to interact and collide with each other the same way fluid particles can collide with other fluid particles (Figure 2). There is no deviation from the fluid path with this assumption. Camp and Stein (1943) were the first to apply this concept to turbulent collisions.

$$Z_{12} = \frac{4}{3} N_1 N_2 d_{12}^3 \sqrt{\frac{\varepsilon}{\nu}} \qquad [6]$$

They related G to turbulent fluid parameters, ε and ν. In their assumptions, they considered only collisions due to shear fields produced by large eddies. Again, there was the

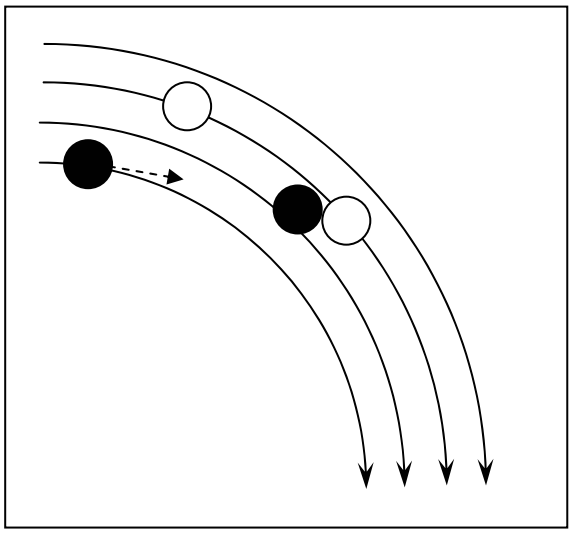

Figure 3. Collision due to acceleration mechanism. Heavy particle deviates from streamline to collide with inertia-less particle.

assumption that particles did not deviate from the fluid path. Saffman and Turner (1956) were later able to refine Camp and Stein's model by a slight modification of the constant *C*.

$$Z_{12} = \sqrt{\frac{8\pi}{15}} N_1 N_2 d_{12}^3 \sqrt{\frac{\varepsilon}{\nu}} \qquad [7]$$

For Equation [7] to be valid the collision diameter (d_{12}) must be small compared to the smallest eddies and the particles and bubbles must follow the fluid completely. In Saffman and Turner's case, Equation [7] was used to model droplet collisions in cloud formations, which followed these assumptions. In flotation these assumptions can not be followed, but Saffman and Turner also produced another model with the addition of an accelerative mechanism of collision.

$$Z_{12} = \sqrt{8\pi} N_1 N_2 d_{12}^2 \left[\left(1 - \frac{\rho_p}{\rho_f} \right)^2 (\tau_1 - \tau_2)^2 \left(\overline{\left(\frac{Du}{Dt} \right)^2} + \frac{1}{3} g^2 \right) + \frac{1}{9} d_{12}^2 \frac{\varepsilon}{\nu} \right]^{1/2} \qquad [8]$$

The accelerative mechanism accounts for inertial effects in turbulent collisions (Figure 3). This indicates that particles do not have to follow the fluid flow and can, therefore, be larger than the smallest eddies. For Equation [8] to be valid particles and bubbles must already be close together (within the same eddy) and must have very similar particle radii ($1 \leq R_1/R_2 \leq 2$).

Abrahamson (1975) then proposed a model for high turbulent energy dissipation, ε. This is shown in equation [9]

$$Z_{12} = \sqrt{8\pi} N_1 N_2 d_{12}^2 \sqrt{\overline{U_1^2} + \overline{U_2^2}} \qquad [9]$$

where the mean squared particle velocity

$$\overline{U_i^2} = \frac{\overline{U_f^2}}{1 + \frac{1.5\tau_i \varepsilon}{\overline{U_f^2}}} \qquad [10]$$

comes from a simplification of a model for particle relative velocity in an oscillating (sinusoidal) fluid given by Levins and Glastonbury (1972). Only the assumptions that very energetic isotropic turbulence was being considered, and that particle velocities were independent and followed some distribution, needed to be made.

Particle size is not an issue in this model. As long as the particle stokes number is high, the model is valid. The Stokes number is a ratio of the particle relaxation (response) time to the smallest fluid relaxation time (for fully developed turbulent flow, this timescale will correspond to the Kolmogorov timescale).

$$St = \frac{\tau_i}{\tau_\eta} = \tau_i \Big/ \left(\frac{\nu}{\varepsilon}\right)^{1/2} \qquad [11]$$

It represents how well a particle follows the fluid flow and is a way to measure this deviation. If a particle's relaxation time is less than the Kolmogorov timescale then the lag time between the fluid movement and the particle movement will be small and the particle will follow the fluid. For particles to accurately follow the flow their Stokes number should be much less than one. Any particles with relaxation times above the Kolmogorov timescale will have some lag in their response to flow fluctuations. Particle and bubble relaxation times are given by various authors throughout the literature (Govan 1989; Ceylan, Altunbas et al. 2001; Bourloutski and Sommerfeld 2002). With a high Stokes number assumption, the retarding effect due to lubrication theory, for particles nearly in contact, can be ignored (Reade and Collins 1998). Therefore, no collision efficiency is needed while using Abrahamson's collision frequency model.

Sundaram and Collins (1997) compared Abrahamson's model with Saffman and Turners' on the basis of particle Stokes numbers. As the Stokes number approached zero, the numerical simulation approached Saffman and Turner's prediction. As the Stokes number increased, Abrahamson's model more closely predicted the true collision frequency. At a Stokes number of, roughly, 1, both models had equal error, with Saffman and Turner under predicting and Abrahamson over predicting. With many flotation particles having Stokes numbers above 1 and with less assumptions being violated, Abrahamson's model is more representative of the flotation process, and, as a result, most flotation models use Equation [9] to determine collision frequency (Schubert 1999; Bloom and Heindel 2002; Pyke, Fornasiero et al. 2003).

Despite its widespread acceptance and use, Abrahamson's model is not the most appropriate for flotation purposes. This stems from the fact that a number of significant assumptions are violated. The greatest assumption being violated is that all colliding particles have an infinite Stokes number. This is not the case in flotation. When the particle Stokes number is above 10, the collision prediction by Equation [9] is fairly accurate, but for Stokes numbers below 10 it will over predict the true number of collisions taking place within the flotation cell.

A more comprehensive model would be one that would account for the full range of Stokes numbers and include both the shear and accelerative mechanisms of collision. Several authors have proposed models for just this scenario (Yuu 1984; Kruis and Kusters 1997). These models also include an added mass term for particle flows in liquid environments. This is very important for flotation modeling since all processes occur within a liquid environment.

One problem with the model proposed by Yuu is its applicability to very small particles (Kruis and Kusters 1997). This is not the case with Kruis and Kusters' model (Equations [12]-[14]).

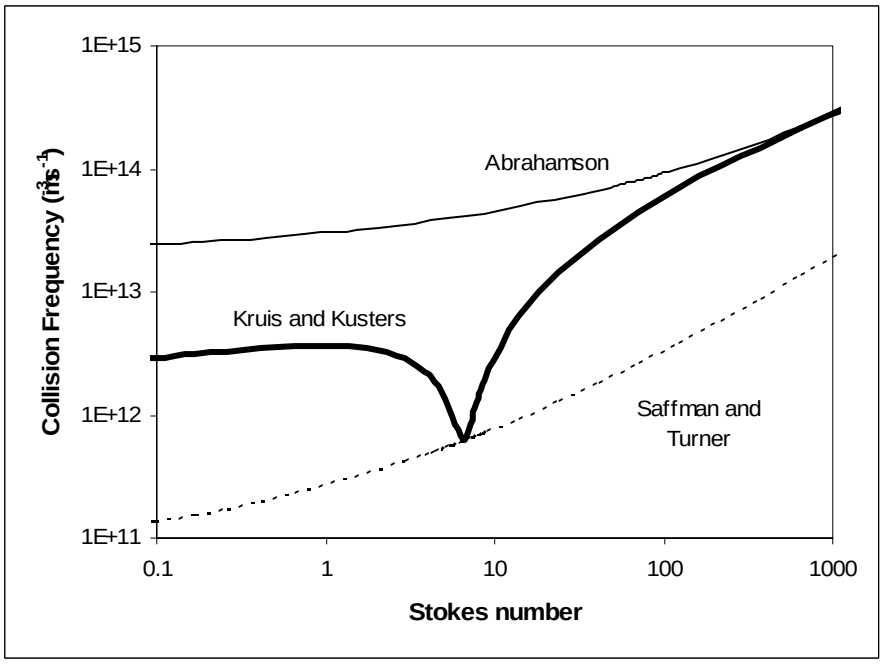

Figure 4. Comparison of collision frequency models. Model predictions are calculated with one colliding particle type's diameter steady at 100 microns, with the other particle type's diameter varying. Both colliding species have the same density.

$$Z_{12} = \sqrt{\frac{8\pi}{3}} N_1 N_2 d_{12}^2 \sqrt{w_{accel}^2 + w_{shear}^2} \qquad [12]$$

$$\frac{w_{shear}^2}{U_f^2} = 0.238b\left(\frac{U_1^2}{U_f^2}\frac{\theta_1}{C_{c,1}} + \frac{U_2^2}{U_f^2}\frac{\theta_2}{C_{c,2}} + \sqrt{\frac{\theta_1\theta_2}{C_{c,1}C_{c,2}}\frac{U_1^2 U_2^2}{U_f^2}} \right) \qquad [13]$$

$$\frac{w_{accel}^2}{U_f^2} = 3(1-b)^2 \frac{\gamma}{\gamma - 1}\left[(\theta_1 + \theta_2) - \frac{4\theta_1\theta_2\sqrt{\frac{1+\theta_1+\theta_2}{(1+\theta_1)(1+\theta_2)}}}{(\theta_1+\theta_2)} \right] \left(\frac{1}{(1+\theta_1)(1+\theta_2)} - \frac{1}{(1+\gamma\theta_1)(1+\gamma\theta_2)} \right) \qquad [14]$$

In Equations [12] - [14] w is the relative velocity between two particles due to either shear or acceleration, U_f is the root-mean-squared fluid velocity, U_i is the root-mean-squared particle velocity, b is the added mass coefficient, γ is the turbulence constant, and θ_i is the dimensionless relaxation time (particle relaxation time with respect to the Lagrangian timescale).

By accounting for intermediate Stokes numbers, Equations [12] - [14] bridge the gap between Equation [7] and Equation [9]. This is shown in Figure 4. Collisions are calculated with one particle type's size being steady while the other varies. Abrahamson's equation over predicts the true collision rate while Saffman and Turner's equation under predicts, with a

difference of approximately 2 orders of magnitude between the two equations. By accounting for intermediate Stokes numbers, as suggested by Kruis and Kusters, an intermediate collision frequency can be calculated between the maximum and minimum predictions given by Abrahamson and Saffman and Turner. Some variations can be noted between Kruis and Kusters and the other two models due to the inclusion of the added mass term. The dip in Kruis and Kusters' prediction, at approximately a Stokes number of 10, is due to the difference in the relaxation time between one species and another. The dip corresponds to the Stokes number of the constant particle size species. When the two relaxation times of the colliding particles are equal, the collisions are minimized. Collisions at this point mostly occur due to the shear mechanism. When the difference between the relaxation times increases, collisions increase. This is shown on either side of the dip in Figure 4.

The current problem with this model is that only one particle density can be given. Flotation collisions, on the other hand, need to account for two different particle densities. This should be taken into account with the added mass coefficient, but Equations [12] - [14] can not properly do this. Since these models can not currently account for bubble-particle collisions, the best model, to date, that can account for different collision densities is Abrahamson's (Equation [9]).

To use Equation [9], the particle and bubble root-mean-squared velocity must be known. This can be determined using Equation [10], with prior knowledge of the fluid rms velocity. Since this velocity is not known in flotation practice, a more suitable equation must be used. Liepe and Moeckel (1976) derived an expression for the slip particle rms velocity from previous researchers experimental data.

$$\sqrt{\overline{U_1^2}} = 0.4 \frac{\varepsilon^{4/9} d_1^{7/9}}{\nu^{1/3}} \left(\frac{\rho_p - \rho_f}{\rho_f} \right)^{2/3} \qquad [15]$$

This equation ([15]) has recently been verified using a digital particle image velocimetry (DPIV) technique (Brady, Telionis et al. 2004). Although this equation is being used in current flotation modeling for bubble velocities (Pyke, Fornasiero et al. 2003) it was never derived for bubbles and should not be used without any experimental verification. For bubbles, a more appropriate velocity is given by Lee et al. (1987) in equation [16].

$$\overline{U_2^2} = C_0 \left(\varepsilon d_2 \right)^{2/3} \qquad [16]$$

C_0 is given by Batchelor (1951) as 2.

Attachment and Detachment Energies

For flotation modeling, the attachment and detachment processes are calculated as probabilities, similar in form to the Arrhenius equation.

$$P_{A/D} = \exp\left(\frac{E_B}{E_K} \right) \qquad [17]$$

A certain probability is given for attachment (P_A) and detachment (P_D) dependent on the energies needed to be overcome, E_B, and the energies available in the system, E_K, to overcome that energy barrier.

The attachment energy barrier, E_1, comes from surface forces, which are modeled using the Extended DLVO theory (see Figure 5) (Yoon and Mao 1996). There are three main surface forces found in flotation; the electrostatic, V_E, dispersion (van der Waals), V_D, and hydrophobic,

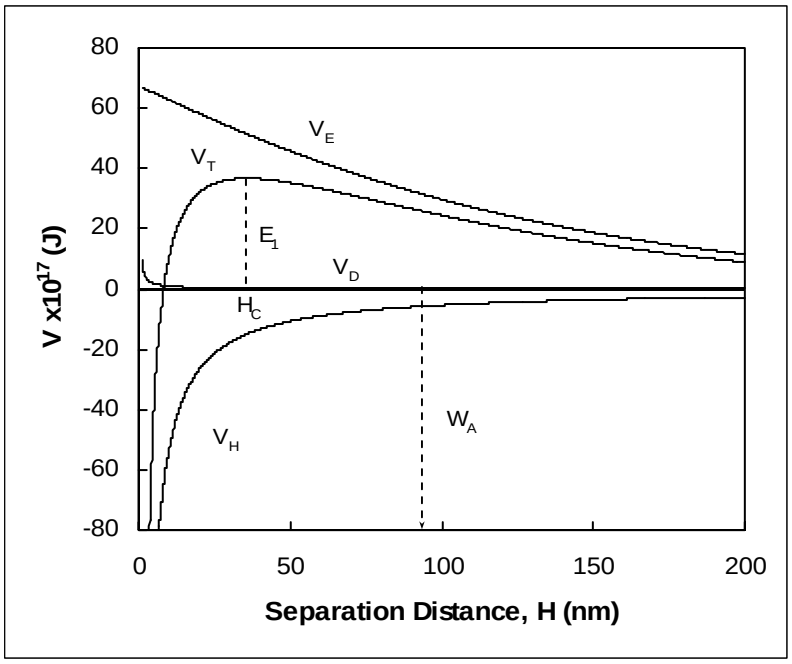

Figure 5. Surface energy vs. distance of separation between two particles (i.e. particle-bubble).

V_H, forces. These are additive and combine to produce the total surface force, V_T. These surface forces can easily be converted into energies. When two particles (e.g. particle/bubble) approach each other, they are initially repulsed (positive surface energy). They must overcome this repulsion to become attached. The repulsion increases until the energy barrier is overcome. Below that separation distance, also called the critical rupture distance, H_C, there is a continuous drop in surface energy. Once this occurs, there is nothing to stop the attachment of the particle and bubble.

The detachment barrier, W_A, comes from the change in surface energies when the detachment process occurs. The loss or gain in surface area of the solid, liquid, or vapor state during the detachment process is multiplied by the respective surface tension to obtain the required energy. The initial state in this process is the combined bubble and particle while the final stage is the separated bubble and particle. Both the attachment and detachment barriers are shown in Figure 5.

To overcome these barriers, a certain amount of energy is required. This energy is provided by the turbulent environment encountered within a flotation cell. The driving force within the cell is the motion of the impeller. The impeller produces the turbulent environment by the creation of eddies. The largest eddy is created by the impeller and is roughly equal to the impeller size. This eddy is where the energy is input into the turbulent environment. According to the Kolmogorov theory, this energy is then transferred through intermediate scales of turbulence to the smallest turbulent scale, the Kolmogorov microscale. This is shown in Figure 6.

The wave number ($\kappa=2\pi/d$) equivalent to the largest eddy size (impeller) corresponds to a kinetic energy equal to the tip-velocity of the impeller squared.

$$U_{T-large}^2 = \left(R_{Imp}\omega\right)^2 \qquad [18]$$

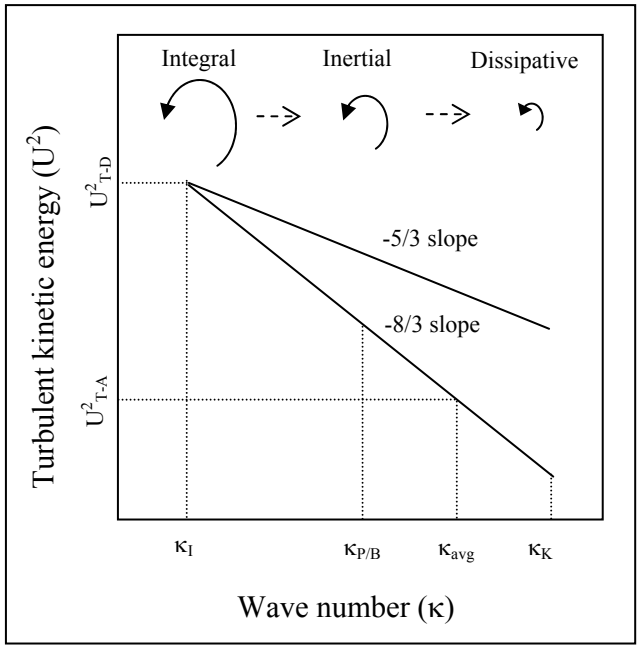

Figure 6. Turbulent kinetic energy spectrum showing attachment and detachment energies.

The cascade of energy on a log-log scale, as stated by the Kolmogorov theory, is represented by a straight line with a slope of -5/3. This is true for a pure liquid system, but with the introduction of bubbles the slope becomes -8/3 (Wang, Lee et al. 1990). With particles the slope is also decreased (Buurman 1990). It is assumed that with a combination of all three phases the slope will follow the -8/3 two-phase prediction. In these dispersed phase systems, the energy is dissipated much more quickly, due to the fact that a portion of the energy is transferred to the particles and bubbles (Gore and Crowe 1991). Because of this, at each wave number there is less energy with particles and bubbles than without. The energy spectrum is shown in Figure 6.

For the attachment and detachment processes, a certain range of these eddy sizes will have an effect on the particles and bubbles and give them their turbulent kinetic energies. For attachment to occur there must be a certain differential movement between the fluid and particle. This allows the particles and bubbles to collide. The attachment energy must, then, overcome the energy barrier, E_1, during this collision. Eddy sizes that allow this differential movement, correspond to the particle/bubble size through the Kolmogorov microscale. The fluid within this range has a different relaxation time than the particles and bubbles, as opposed to large eddies, where bubbles and particles follow their movement. This out of phase motion allows the particles and bubbles to move independent of the fluid and each other. It is assumed that the average amount of this energy over the associated wave numbers ($\kappa_{P/B}$ to κ_K) directly corresponds to the particle and bubble attachment energy, $U^2_{T\text{-}A}$.

$$E_{k-A} = \frac{1}{2}\left(m_1 + m_2\right)\mathrm{U}^2_{T-A} \qquad [19]$$

For the detachment process, bubbles and particles are already combined and do not need a differential relaxation time as they do in the attachment process. It is assumed that detachment comes about from the centrifugal motion of large eddies. When bubbles and particles are subjected to these eddies, they produce differing behavior. Bubbles tend to travel towards the

center of vortices, while particles travel outward (Chahine 1995; Crowe and Trout 1995). If a bubble-particle aggregate were subjected to this, it would tend to pull the aggregate in two which would lead to the detachment of the particle from the bubble. Given this scenario and the fact that all aggregates are subjected to the largest eddy produced by the impeller, which contains the largest available energy within the system, leads to the conclusion that the largest eddy provides the energy for detachment. The turbulent energy corresponding to the largest eddy, $U^2_{T-large}$, is, therefore, equal to the turbulent detachment energy, U^2_{T-D}.

$$E_{k-D} = \frac{1}{2}\left(m_1 + m_2\right)\mathrm{U}^2_{T-D} \qquad [20]$$

Summary

There are many different collision frequency models in the literature to date. All of these models have varying assumptions, with each model having some violation under flotation conditions. The best model for use in flotation modeling is one proposed by Abrahamson (1975). It is assumed that most particles in flotation follow the assumptions used in Abrahamson's derivation of the collision frequency model, which includes infinite (very high) Stokes numbers, independent particle velocities, a particle velocity distribution, and isotropic turbulence.

Newer models that account for the shear and accelerative mechanisms can also account for the entire range of Stokes numbers. These would be better suited for flotation purposes, except for the fact that they can not account for two different particle densities. Therefore, a particle-bubble collision can not be calculated using these models. When these models are updated to allow the use of greater and lesser than the surrounding medium densities, they will be able to account for all particles and bubbles, and their effects, in a turbulent liquid environment within a flotation cell.

Once particles collide, they have a probability of attaching, and once attached, of detaching. The forms of these probabilities are similar to the Arrhenius equation, with energy barriers being overcome by kinetic energies.

For the attachment process, the energy barrier is based upon the Extended DLVO theory and accounts for the electrostatic, dispersion, and hydrophobic surface forces. The energy needed to overcome this barrier is provided by the turbulent environment. For the attachment process to take place, some deviation from the fluid flow is required. The scales of turbulence that allow this are between the Kolmogorov microscale and the particle/bubble scale. It is assumed that the average wave number between these two scales accounts for the attachment energy that is needed to overcome the energy barrier. The Kolmogorov theory is used to calculate this energy. A modification of the theory is needed to account for particle and bubble effects on turbulence. This modification changes the slope of the energy spectrum from -5/3 to -8/3.

For the detachment process, the energy barrier is determined from the change in surface area of the different phases of the particle-bubble aggregate (i.e. solid, liquid, vapor), and the respective surface tensions of those phases. The largest scale of turbulence within the system, the impeller, is used to overcome this barrier. No deviation from the fluid is required for the detachment process. The detachment process follows from the differing effects vortices have on

particles and bubbles, with particles moving outwards, while bubbles move inward. The detachment energy follows from the turbulent energy of the largest scale.

Nomenclature

1,p	subscript – refers to particle
2	subscript – refers to bubble or second particle
b	added mass coefficienct [-]
C	constant within collision kernel [-]
C_0	constant equal to 2.0 [-]
$C_{c,i}$	Cunningham slip correction factor for i [-]
d_{12}	diameter of collision [m]
d_i	diameter of i [m]
E_1	surface energy barrier [J]
E_B	energy barrier [J]
E_K	generic kinetic energy [J]
$E_{k\text{-}D}$	kinetic energy of detachment [J]
$E_{k\text{-}A}$	kinetic energy of attachment [J]
g	gravity [$m \cdot s^{-2}$]
G	velocity gradient [s^{-1}]
H_c	critical rupture thickness [m]
m_i	mass of particle or bubble [kg]
N_i	number density of i – number per unit volume [m^{-3}]
P_A	probability of attachment [-]
P_C	collision efficiency [-]
P_D	probability of detachment [-]
R_i	radius of i [m]
R_{Imp}	radius of impeller [m]
S_b	surface area rate – within slurry [s^{-1}]
St	Stokes number [-]
U_f	fluid velocity [$m \cdot s^{-1}$]
$U^2_{T\text{-large}}$	large scale turbulent kinetic energy [$m^2 \cdot s^{-2}$]
$U^2_{T\text{-}A}$	attachment turbulent kinetic energy [$m^2 \cdot s^{-2}$]
$U^2_{T\text{-}D}$	detachment turbulent kinetic energy [$m^2 \cdot s^{-2}$]
$\sqrt{\overline{U_i}^2}$	root-mean-squared velocity of i – turbulent velocity [$m \cdot s^{-1}$]
V_D	dispersion free energy of interaction [J]
V_E	electrostatic free energy of interaction [J]
V_g	superficial air flow rate [$m \cdot s^{-1}$]
V_H	hydrophobic free energy of interaction [J]
V_T	total free energy of interaction [J]
w	relative velocity between colliding particles – may be due to shear and/or accelerative mechanisms [$m \cdot s^{-1}$]
W_A	work of adhesion [J]
Z_{12}	collision frequency between particle and bubble [$m^{-3} \cdot s^{-1}$]
Z_C	total possible collisions [$m^{-3} \cdot s^{-1}$]

β	collision kernel [$m^3 \cdot s^{-1}$]
ε	average energy dissipation [$m^2 \cdot s^{-3}$]
γ	turbulence constant [-]
κ	wave number [m^{-1}]
κ_{avg}	average attachment wave number [m^{-1}]
κ_I	impeller wave number [m^{-1}]
κ_K	Kolmogorov wave number [m^{-1}]
$\kappa_{P/B}$	particle/bubble wave number [m^{-1}]
θ_i	dimensionless relaxation time [-]
ν	kinematic viscosity [$m^2 \cdot s^{-1}$]
ρ_f	density of fluid [$kg \cdot m^{-3}$]
ρ_p	density of particle [$kg \cdot m^{-3}$]
τ_i	particle/bubble relaxation time [s]
τ_η	Kolmogorov timescale [s]
ω	impeller radial velocity [rpm]

References

Abrahamson, J. (1975). "Collision rates of small particles in a vigorously turbulent fluid." Chemical Engineering Science **30**(11): 1371-9.

Batchelor, G. K. (1951). "Pressure fluctuations in isotropic turbulence." Proc. Cambridge Phil. Soc. **47**: 359-374.

Bloom, F. and T. J. Heindel (2002). "On the structure of collision and detachment frequencies in flotation models." Chemical Engineering Science **57**(13): 2467-2473.

Bourloutski, E. and M. Sommerfeld (2002). "Parameter studies on the effect of boundary conditions in three-dimensional calculations of bubble column." FED (American Society of Mechanical Engineers) **[257-2]**(A, Proceedings of the 2002 ASME Joint U.S.-European Fluids Engineering Conference): 355-364.

Brady, M., D. P. Telionis, et al. (2004). Three-phase, particle image velocimetry measurements in a model flotation cell. 2004 ASME Heat Transfer/Fluids Engineering Summer Conference.

Buurman, C. (1990). "Stirring of concentrated slurries: a semi-empirical model for complete suspension at high solids concentrations and 5 m3 verification experiments." Institution of Chemical Engineers Symposium Series - Fluid Mixing 4 **121**: 343-350.

Camp, T. R. and P. C. Stein (1943). "Velocity gradients and integral work in fluid motion." J. Boston Soc. Civ. Engrs. **30**(4): 219.

Ceylan, K., A. Altunbas, et al. (2001). "A new model for estimation of drag force in the flow of Newtonian fluids around rigid or deformable particles." Powder Technology **119**(2-3): 250-256.

Chahine, G. L. (1995). Bubble interactions with vortices. Fluid Vortices. S. I. Green.

Crowe, C. T. and T. R. Trout (1995). Particle interactions with vortices. Fluid Vortices. S. I. Green.

Dai, Z., D. Fornasiero, et al. (2000). "Particle-bubble collision models -- a review." Advances in Colloid and Interface Science **85**(2-3): 231-256.

Gore, R. A. and C. T. Crowe (1991). "Modulation of turbulence by a dispersed phase." Transactions of the ASME **113**: 304-307.
Govan, A. H. (1989). "A simple equation for the diffusion coefficient of large particles in a turbulent gas flow." International Journal of Multiphase Flow **15**(2): 287-94.
Kruis, F. E. and K. A. Kusters (1997). "The collision rate of particles in turbulent flow." Chemical Engineering Communications **158**: 201-230.
Lee, C. H., L. E. Erickson, et al. (1987). "Bubble breakup and coalescence in turbulent gas-liquid dispersions." Chemical Engineering Communications **59**(1-6): 65-84.
Levins, D. M. and J. R. Glastonbury (1972). "Particle-liquid hydrodynamics and mass transfer in a stirred vessel." Trans. Inst. Chem. Engrs. **50**: 32-41.
Liepe, F. and H. O. Moeckel (1976). "Studies of the combination of substances in liquid phase. Part 6: The influence of the turbulence on the mass transfer of suspended particles." Chemische Technik (Leipzig, Germany) **28**(4): 205-209.
Lu, S.-c. (2000). "Bubble-particle interaction in flotation cell." Trans. Nonferrous Met. Soc. China **10**(Special Issue): 40-44.
Luttrell, G. H. and R. H. Yoon (1992). "A hydrodynamic model for bubble-particle attachment." Journal of Colloid and Interface Science **154**(1): 129-137.
Mao, L. and R.-H. Yoon (1997). "Predicting flotation rates using a rate equation derived from first principles." International Journal of Mineral Processing **51**(1-4): 171-181.
Pyke, B., D. Fornasiero, et al. (2003). "Bubble particle heterocoagulation under turbulent conditions." Journal of Colloid and Interface Science **265**(1): 141-151.
Reade, W. C. and L. R. Collins (1998). "Collision and coagulation in the infinite-stokes number regime." Aerosol Science and Technology **29**: 493-509.
Saffman, P. G. and J. S. Turner (1956). "On the collision of drops in turbulent clouds." Journal of Fluid Mechanics **1**: 16-30.
Schubert, H. (1999). "On the turbulence-controlled microprocesses in flotation machines." International Journal of Mineral Processing **56**: 257-276.
Schulze, H. J. (1993). Flotation as a heterocoagulation process: Possibilities of calculating the probability of flotation. Coagulation and Flocculation. B. Dobias, Marcel Dekker.
Smoluchowski, M. (1917). "Versuch einer mathematischen theorie der koagulations-kinetik kollöider losungen." Z. Phys. Chem **92**: 129.
Sundaram, S. and L. R. Collins (1997). "Collision statistics in an isotropic particle-laden turbulent suspension. Part 1. Direct numerical simulations." Journal of Fluid Mechanics **335**: 75-109.
Wang, S. K., S. J. Lee, et al. (1990). "Statistical analysis of turbulent two-phase pipe flow." Journal of Fluids Engineering **112**(1): 89-95.
Yoon, R.-H. and L. Mao (1996). "Application of extended DLVO theory, IV. Derivation of flotation rate equation from first principles." Journal of Colloid and Interface Science **181**(2): 613-626.
Yuu, S. (1984). "Homogeneous and isotropic turbulence." American Institute of Chemical Engineers Journal **30**(5): 802-807.

Developing a Turbulent Flotation Model from First Principles

I. M. Sherrell

Abstract

A new flotation model has been developed for use in a turbulent environment and is the first proposed to take into account all three surface forces (electrostatic, van der Waals, and hydrophobic). Previous models that account for turbulence do not take into account all surface forces while the one model that does take into account all surface forces (Yoon and Mao 1996) is only applicable in quiescent conditions. Since most flotation occurs in a turbulent environment, these previous models cannot be applied. The new model includes attachment, detachment, and froth recovery probabilities. The effects of each individual process are shown. Simulations using this model show trends seen in industrial flotation systems.

Introduction

Flotation is widely used throughout the mining industry as well as the chemical, petroleum, and recycling industries. It is the most efficient process, to date, for solid-solid separation of minerals. It is now more diverse in its application, with uses such as separation of ink from paper, plastics separation in recycling, soil contamination separation, and separation of carbon from fly ash. The industry is growing along with knowledge of the process and sub-processes. With this increased knowledge, a more reliable flotation model has been derived from first principles. This results in a general flotation model, and allows its use in the mining industry, regardless of machine type and material being recovered.

Flotation is a three-phase process, which uses a medium of water (liquid) to separate various particles (solid) by the addition of air bubbles (gas). Hydrophobic particles attach to the bubbles and rise to the top of the flotation cell where they are extracted while hydrophilic (or less hydrophobic) particles remain in the slurry. All three phases are found in flotation machines, which produce a turbulent environment. To enhance the separation, surfactants may be added that alter surface properties. The combination of a three-phase turbulent environment with a modified surface chemistry makes modeling of the process very complex.

Surface forces play a crucial role in the attachment and detachment processes between a particle and bubble. Proper modeling of these forces is vital to having a general flotation model. The DLVO theory models some of the surface forces seen in flotation. This theory combines the van der Waals force and the electrostatic force into a total surface force. The main problem with the DLVO theory is the lack of any hydrophobic force parameter, which is known to be a major contributor to surface forces between particles and bubbles in a water medium (Yoon and Mao 1996; Yoon 2000). The extended DLVO theory incorporates this third force (hydrophobic) into the DLVO theory.

The most rigorous flotation model, to date, dealing with all three surface forces (electrostatic, van der Waals, and hydrophobic) was proposed by Mao and Yoon (1997).

$$k = \frac{1}{4} S_b \left[\frac{3}{2} + \frac{4 \mathrm{Re}_b^{0.72}}{15} \right] \left(\frac{r_1}{r_2} \right)^2 \exp\left(-\frac{E_1}{E_{k-A}} \right) \left[1 - \exp\left(-\frac{W_A + E_1}{E_{k-D}} \right) \right] \qquad [1]$$

The model is based upon first principles in a quiescent environment and agrees well with experimental data. The problem of this model is its applicability to industrial applications. Turbulence is encountered in almost all flotation systems, including mineral and coal flotation. Since this is a quiescent model, the results predicted do not match industrial flotation systems. This model did provide a key basis for the current model by the use of the extended DLVO theory and its relationship to the energies of the system.

Model

Due to the turbulent environment experienced inside a flotation cell, particle-bubble collisions are modeled far differently than in a quiescent environment. For laminar flows, the collision frequency may be modeled using the volume that the bubble travels through and the percent solids of the slurry (Mao and Yoon 1997). A collision efficiency would then be applied that would account for streamline effects. On the other hand, particles and bubbles in turbulent flows generally do not follow the path of the fluid and are modeled based upon their deviation from the fluid path. The Stokes number, a ratio of the particle relaxation (response) time to the smallest fluid relaxation time (Kolmogorov timescale), represents how well a particle follows the fluid flow and is a way to measure this deviation. If a particle's relaxation time is equal to or less than the Kolmogorov timescale then the lag time between the fluid movement and the particle movement will be zero and the particle will follow the fluid completely. Any particles with relaxation times above the Kolmogorov timescale will have some departure from the fluid path.

$$St = \frac{\tau_i}{\tau_\eta} = \tau_i \Big/ \left(\frac{\nu}{\varepsilon} \right)^{1/2} \qquad [2]$$

Particle and bubble relaxation times are given by various authors throughout the literature (Govan 1989; Ceylan, Altunbas et al. 2001; Bourloutski and Sommerfeld 2002).

There are two mechanisms involved in turbulent collisions. The shear mechanism accounts for relative motions of particles (fluid, solid, or gas) in a shear field. These collisions always occur in a turbulent field, even among fluid particles. Collisions between particles with Stokes numbers less than 1 occur by shear only. The second mechanism, the accelerative mechanism, accounts for inertial effects due to large and/or heavy particles. Collisions due to the accelerative mechanism occur above a Stokes number of 1 where there is some lag between the particle and fluid.

Saffman and Turner (1956) proposed a collision model based upon the shear mechanism, where the Stokes number is zero, while Abrahamson (1975) proposed a model based entirely on the accelerative mechanism, where the Stokes number is infinity. There are collision models that combine the shear and accelerative mechanisms (Williams and Crane 1983; Kruis and Kusters 1997), but nothing to date accounts for bubble-particle collisions in a liquid environment. This is complicated due to the fact that bubbles are lighter than the surrounding fluid, while particles are heavier. Since Abrahamson's model more closely predicts real world collisions when Stokes numbers are greater than 1 (Sundaram and Collins 1997) combined with the fact that most particles in flotation are within this range, leads to the current use of Abrahamson's model.

Abrahamson's model

$$Z_{12} = 2^{3/2}\pi^{1/2}N_1N_2d_{12}^2\sqrt{\left(\overline{U_1^2}+\overline{U_2^2}\right)} \quad [3]$$

incorporates the number densities, N_i, of both the particles (1) and bubbles (2), the average diameter of the collision, d_{12} (= r_1+r_2), and the turbulent root-mean-squared velocities of the particles and bubbles, $\sqrt{\overline{U_i^2}}$. The particle turbulent root-mean-squared velocity is given by Liepe and Moeckel (1976) in Equation [4].

$$\sqrt{\overline{U_1^2}} = 0.4\frac{\varepsilon^{4/9}d_1^{7/9}}{\nu^{1/3}}\left(\frac{\rho_1-\rho_3}{\rho_3}\right)^{2/3} \quad [4]$$

The bubble turbulent mean-squared velocity is given by Lee et al. (1987) in Equation [5].

$$\overline{U_2^2} = C_0\left(\varepsilon d_2\right)^{2/3} \quad [5]$$

Rate Constant

Knowing the collision frequency and the corresponding probability of collection, the change in particle concentration within the entire flotation cell can be calculated as the number of collisions between particles and bubbles that occur (Z_{12}) that lead to attachment (P_A), once attached do not detach (1-P_D), and are able to rise within the froth (R_F).

$$\frac{dN_1}{dt} = -Z_{12}P_A\left(1-P_D\right)R_F \quad [6]$$

Comparing equation [6] with a first order rate equation [7], that most researchers believe model flotation (Kelsall 1961; Arbiter and Harris 1962; Mao and Yoon 1997),

$$\frac{dN_1}{dt} = -kN_1 \quad [7]$$

results in an equation for the rate constant that is dependent on hydrodynamics of the flotation cell as well as surface forces of the particles and bubbles.

$$k = \frac{Z_{12}P_A\left(1-P_D\right)R_F}{N_1} \quad [8]$$

Reducing the collision frequency to its individual components

$$Z_{12} = \beta N_1N_2 \quad [9]$$

produces the final rate constant equation.

$$k = \beta N_2P_A\left(1-P_D\right)R_F \quad [10]$$

Particle Collection

The probability of collection is dependent on the attachment and detachment processes and is a combination of their probabilities. These are both influenced by surface properties of the particles and bubbles as well as hydrodynamics of the system. Surface energies are modeled based upon the Extended DLVO theory. This incorporates the electrostatic, V_E, van der Waals (dispersion), V_D, and hydrophobic, V_H, surface forces (Rabinovich and Churaev 1979; Shaw 1992; Mao and Yoon 1997). V_H is a function of K_{131} and K_{232}, which can be obtained from experimental results (Rabinovich and Yoon 1994; Yoon and Ravishankar 1994; Yoon and Mao 1996; Yoon and Ravishankar 1996; Yoon, Flinn et al. 1997; Vivek 1998; Pazhianur 1999; Yoon

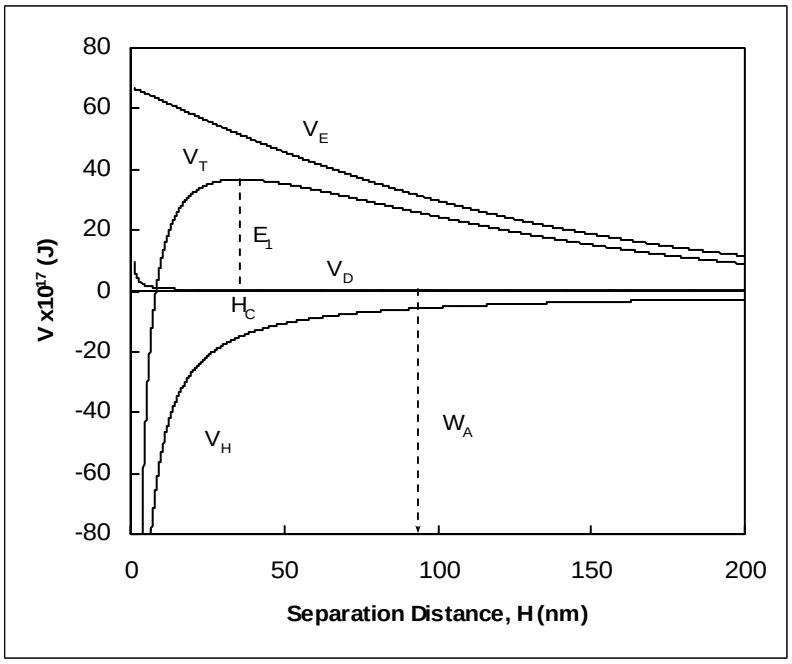

Figure 1. Surface energy vs. distance of separation between two particles (i.e. particle-bubble).

and Aksoy 1999). The surface forces are additive and combine to form the total energy of interaction, V_T, as shown in Figure 1.

For attachment there exists a maximum repulsive (positive) energy, E_1, that must be overcome. This maximum energy occurs at the critical rupture thickness, H_c. For separation distances less than H_c, the free energy continuously drops. Therefore, nothing will prevent the particle and bubble from coming together once H_c is overcome.

The probability of attachment is dependent on the energy barrier that must be overcome and the kinetic energy of attachment, $E_{k\text{-}A}$.

$$P_A = \exp\left(-\frac{E_1}{E_{k-A}}\right) \qquad [11]$$

The probability of detachment is dependent on the kinetic energy of detachment, $E_{k\text{-}D}$, and the work of adhesion, W_A, that must be overcome for detachment to occur (Figure 1).

$$P_D = \exp\left(-\frac{W_A}{E_{k-D}}\right) \qquad [12]$$

The work of adhesion is the energy needed to return the free energy of interaction to a zero value. It is assumed, that when detachment occurs, the equilibrium edge of the bubble will be past the critical rupture thickness. This is due to the small critical rupture thickness (approximately 100 nm) as compared to the deformation that a bubble goes through (tens to hundreds of microns) (Schimann 2004). Since the bubble edge will already be past the critical rupture thickness, E_1 does not need to be overcome and therefore is not used in detachment. The work of adhesion is the energy required to take apart a bubble-particle aggregate into a separate bubble and particle. This energy is obtained by surface tensions (gas-solid, gas-liquid, solid-liquid) and their respective areas. A well known model used by Mao (1997)

$$W_A = \gamma_{lv}\pi r_1^2 \left(1-\cos\theta\right)^2 \qquad [13]$$

assumes that the bubble surface is completely flat. Since the bubble and particle sizes are within two orders of magnitude of each other, a more accurate way to calculate W_A would be to assume a spherical bubble attached to a spherical particle. With simple geometry, this can be easily worked out and the current model uses this approach.

It is known that the contact angle for spherical particles is smaller than flat plate measurements (Preuss and Butt 1998). There can be up to a 10 degree contact angle reduction for colloidal sized particles. The contact angle used in the work of adhesion equation is usually obtained by measurements upon flat plates. Since it is assumed that this reduction is a function of particle size and that particles in flotation are much larger than colloidal sized particles, a constant 5 degree reduction is included in this model.

Energies

The main source of energy within a flotation cell comes from the motion of the impeller. The impeller motion produces the turbulent environment within the flotation cell. The impeller itself creates the largest eddies within the cell, roughly equal to the impeller size. The energy input into the cell (through the impeller) is transferred from the largest turbulent scale (corresponding to the impeller size) to the smallest turbulent scale (Kolmogorov microscale). A certain range of these eddy sizes will have an effect on the particles and give them their turbulent kinetic energies.

The wave number ($\kappa=2\pi/d$) equivalent to the largest eddy size (impeller) gives a kinetic energy equal to the tip-velocity of the impeller squared.

$$U_{T-large}^2 = \left(R_{Imp}\omega\right)^2 \qquad [14]$$

The kinetic energy then cascades, at a slope of -8/3 on a log-log scale, to the Kolmogorov microscale. In a pure liquid system the slope is theoretically -5/3, but with the introduction of bubbles, the slope is reduced to -8/3 (Wang, Lee et al. 1990). Particles are also found to reduce the theoretically predicted single-phase slope (Buurman 1990). In these dispersed phase systems, the energy is dissipated much more quickly, due to the fact that a portion of the energy is transferred to the particles and bubbles (Gore and Crowe 1991). Because of this, at each wave number there is less energy with particles and bubbles than without. It is assumed that with a combination of all three phases the slope will follow the -8/3 two-phase prediction. The energy spectrum is shown in Figure 2.

Eddies corresponding to the particle/bubble size through the Kolmogorov microscale will allow the particle/bubble to deviate from the fluid flow. The fluid within this range will have a different relaxation time than the particles and bubbles, as opposed to large eddies, where bubbles and particles follow their movement. This out of phase motion allows the particles and bubbles to move independent of each other and will produce collisions. It is assumed that the average amount of this energy ($U^2_{T\text{-}A}$) over the associated wave numbers ($\kappa_{P/B}$ to κ_K) directly corresponds to the particle and bubble attachment energy.

$$E_{k-A} = \frac{1}{2}\left(m_1 + m_2\right)\mathrm{U}_{T-A}^2 \qquad [15]$$

Large eddies, on the other hand, provide the energy for detachment. For detachment, bubbles and particles are already combined and, therefore, do not need a corresponding relaxation time as they do in the attachment process. Since all aggregates are subjected to large eddies, and these eddies contain the largest energies within the system, they provide the greatest

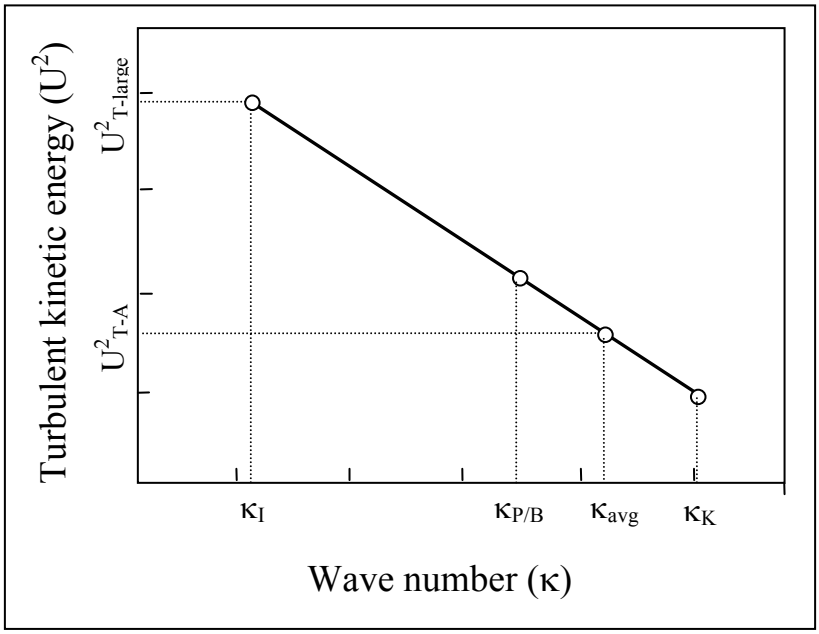

Figure 2. Turbulent kinetic energy spectrum

energy for detachment. Detachment follows from the centrifugal motion of these eddies, in which bubbles travel in towards the center of vortices and particles travel outward (Chahine 1995; Crowe and Trout 1995).

$$E_{k-D} = \frac{1}{2}\left(m_1 + m_2\right)\mathrm{U}_{T-D}^2 \qquad [16]$$

The turbulent energy corresponding to the largest eddy, $U_{T-large}^2$, is equal to the turbulent detachment energy, U_{T-D}^2.

Froth Recovery

Froth behavior can be very complex. The coalescence of bubbles and the subsequent loss of surface area, and the drainage of liquid between bubbles, to name a few, can affect the recovery of particles attached to bubble surfaces and particles entrained within the froth liquid. Froth recovery, R_f, is the percentage of particles which enter the froth, subsequently pass through the froth and are collected. All particles not recovered from the froth are returned to the slurry or never truly enter the froth phase. A simple approach to modeling this is to consider only the particles attached to the bubble surface. The only factor affecting the bubble surface would then be the coalescence of bubbles and loss of surface area. Once bubbles coalesce, a portion of their carrying capacity, for that volume of air, is lost. Once that carrying capacity is lost, it is assumed that those particles that were attached will drain back into the slurry.

This loss of surface area must be calculated with respect to the volume flow rate of air through the cell, which is assumed to be uniform throughout the slurry and froth section. A way to account for the loss of surface area is to calculate the surface area rates at both the initial (S_0) and final (S_f) stages of the froth. The fraction of surface area that is still useful for particle recovery would then be the ratio of these two surface area rates (Equation [17]).

$$R_F = \frac{S_f}{S_0} = \left(\frac{3V_g}{r_{2-f}}\right) \Big/ \left(\frac{3V_g}{r_{2-0}}\right) = \frac{r_{2-0}}{r_{2-f}} \quad [17]$$

V_g is the volumetric air flow rate divided by the cross-sectional area of the flotation cell, and is usually referred to as the superficial air flow rate. The froth recovery then becomes a ratio of the initial to final bubble sizes. This recovery assumes that the same percentage of particles adhere to the bubble surface at the initial and final stages of the froth. This recovery then becomes the maximum recovery allowed for a given froth.

Three-phase froths are highly complex. Aside from liquid and gas effects; particle size, shape, smoothness, hydrophobicity, contact angle, and concentration can affect froth behavior (Harris 1982; Knapp 1990; Johansson and Pugh 1992; Aveyard, Binks et al. 1999). Froth recovery is also thought to be a function of these variables, with particle size having a large effect. An empirical model proposed by Gorain et al. (1998) is thought to give the best results for froth recovery, to date (Equation [18]).

$$R_F = \exp\left(-\alpha \tau_f\right) \quad [18]$$

This model formulates the froth recovery as a function of the froth retention time, τ_f, and a parameter, α, that incorporates both physical and chemical properties of the froth (Mathe, Harris et al. 1998). Froth retention time is usually defined as the ratio of the froth height to superficial air flow rate, V_g. α is an empirical parameter that must be determined by experiments, for each system. α usually ranges, in industrial flotation cells, between 0.1 and 0.5 (Gorain, Harris et al. 1998).

Given the fact that there is a maximum recovery that can not be overcome, a modification of Gorain's model is proposed. All recoveries calculated using Equation [18] must be scaled using the maximum froth recovery. This is shown in Equation [19].

$$R_F = R_{\max} \exp\left(-\alpha \tau_f\right) \quad [19]$$

Assuming that the maximum froth recovery is given by Equation [17], and substituting this into Equation [19], gives the following formula for the froth recovery within a flotation cell.

$$R_F = \frac{r_{2-0}}{r_{2-f}} \exp\left(-\alpha \tau_f\right) \quad [20]$$

It is also known that particles within a flotation froth have varying retention times, due to, in large part, particle size (Mathe, Harris et al. 1998). Average retention time within a froth is given by the following formula (Equation [21]) where h_f is the froth height (Gorain, Harris et al. 1998).

$$\tau_{avg-f} = \frac{h_f}{V_g} \quad [21]$$

Superficial airflow rate is constant throughout the froth, as long as there is no diversion of the froth (secondary product output such as lower froth diversion) and steady state has been reached. Knowing that small particles within a liquid environment follow the flow, small particles are thought to have a froth retention time equal to the average retention time within the froth. It is also known that larger particles have a more difficult time traveling upward in the froth (Bikerman 1973). It is assumed that particles take longer to travel through the froth, due to their density and/or size. Knowing this, a froth retention time model is proposed

$$\tau_f\left(d_p\right)=\frac{h_f}{V_g}P_{fr} \qquad [22]$$

that is a function of particle size, d_p, and takes this into account by the addition of a froth particle effect, P_{fr}.

The particle effect on the retention time is given the functional form

$$P_{fr}=\exp\left(B\frac{d_p}{d_{p-n}}\right) \qquad [23]$$

where B is a constant and $d_{p\text{-}n}$ is the particle diameter whose bubble-particle aggregate mass is equal to the fluid mass as shown in Equation [24].

$$d_{p-n}=\left(\frac{\rho_3-\rho_2}{\rho_1-\rho_3}\right)^{1/3}d_2 \qquad [24]$$

$d_{p\text{-}n}$ takes into account the density of the particle as well as the size of the attached bubble.

A graphical representation of P_{fr} and its effect on froth recovery can be seen in Figure 3. The neutrally buoyant particle, $d_{p\text{-}n}$, affecting Equation [23] is used to take into account the buoyancy of the bubble with an attached particle. Smaller or less dense particles allow the bubble to travel upward within the froth more quickly. The smaller a particle is compared to the neutrally buoyant particle, the closer the particle effect is to 1. Therefore, the closer the particle is to following the fluid flow the closer the particle retention time is to the average retention time within the froth. The larger or more dense the particle is compared to the neutrally buoyant particle, the greater the particle effect becomes. Large particles will take longer to travel through the froth, if at all. Particle effect, using this functional form, must always be greater than 1 and therefore, particle froth retention time must always be equal to or greater than average froth retention time. B is thought to be a function of frother type and cell-dynamics and is found empirically for each system. The effect of B can be seen in Figure 3.

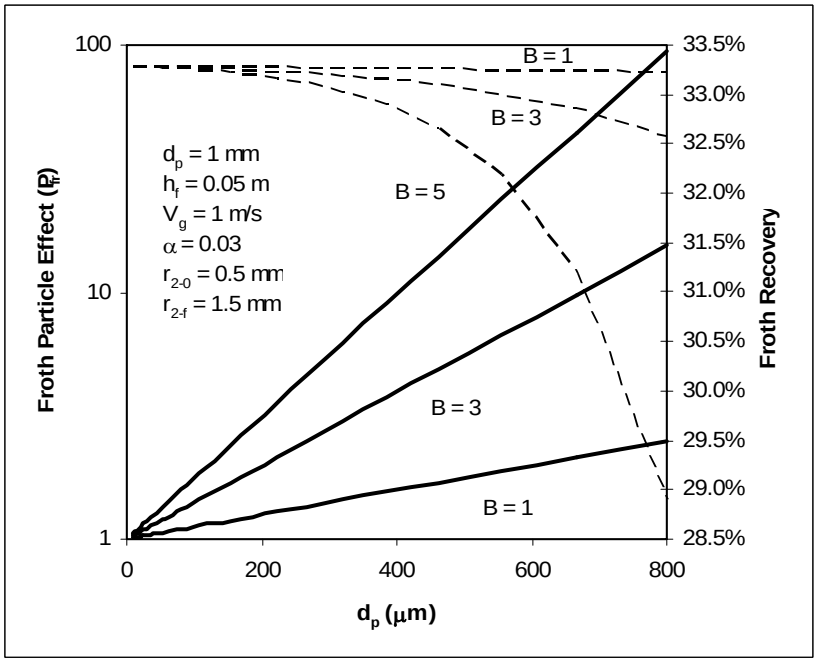

Figure 3. Particle size effect on froth particle effect, P_{fr}, (—) and froth recovery (- -)

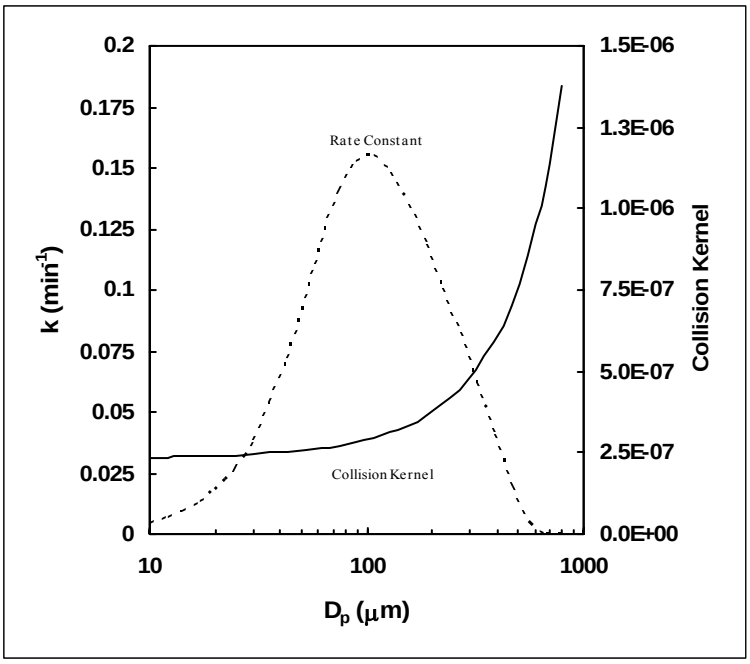

Figure 4. Effect of the collision kernel (—) on the rate constant (- -). Same conditions shown in Figure 9, contact angle 60 degrees.

Results

The effect of the individual components on the theoretical rate constant can be determined using Equation [10]. The importance of each individual process on the overall flotation process can be shown. These processes include the collision frequency, which is a function of the collision kernel (Figure 4), the froth recovery (Figure 5) and the probability of attachment and detachment (Figure 6).

Figure 4 through Figure 6 reveal a great deal of information about the entire flotation process. The overall magnitude of the rate constant is determined by the collision kernel, as well as the number density of the bubbles as shown in Figure 4. As the particle size increases, the collision kernel exponentially increases. This would result in greater and greater rate constants as particle size increases. This is not seen in flotation due to the combined effect of froth recovery and detachment. As shown in Figure 5, as particle size increases, the froth recovery decreases. Depending on the constant *B* being used (Equation [23]), the effect of particle size can be increased or reduced. Therefore, froth is a limiting factor to large particle flotation. Detachment also plays a roll in lowering the rate constant as shown in Figure 6. As particle size increases, detachment increases, until eventually no particle can stay attached to a bubble. The drop in probability of detachment corresponding to the maximum rate constant particle size is due to the combined effect of work of adhesion and turbulent detachment energy. Both increase as particle size increases. Because the relationship between the work of adhesion and turbulent detachment energy to particle size is not linear, initially work of adhesion increases much slower than turbulent detachment energy, until a certain particle size is reached. After this particle size is reached turbulent detachment energy increases more rapidly than work of adhesion which

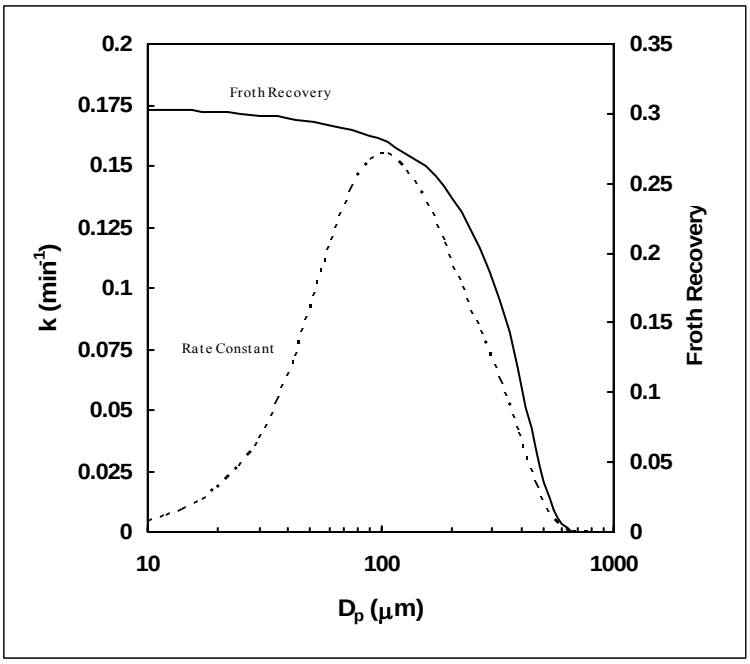

Figure 5. Effect of froth recovery (—) on the rate constant (- -). Same conditions shown in Figure 9, contact angle 60 degrees.

leads to higher detachment probabilities. Attachment does not have an affect on the rate constant due to the fact that everything attaches under the conditions shown.

Simulations were also run to show the effect of individual variables on the flotation rate constant. These variables include the particle diameter, bubble diameter, surface tension, contact

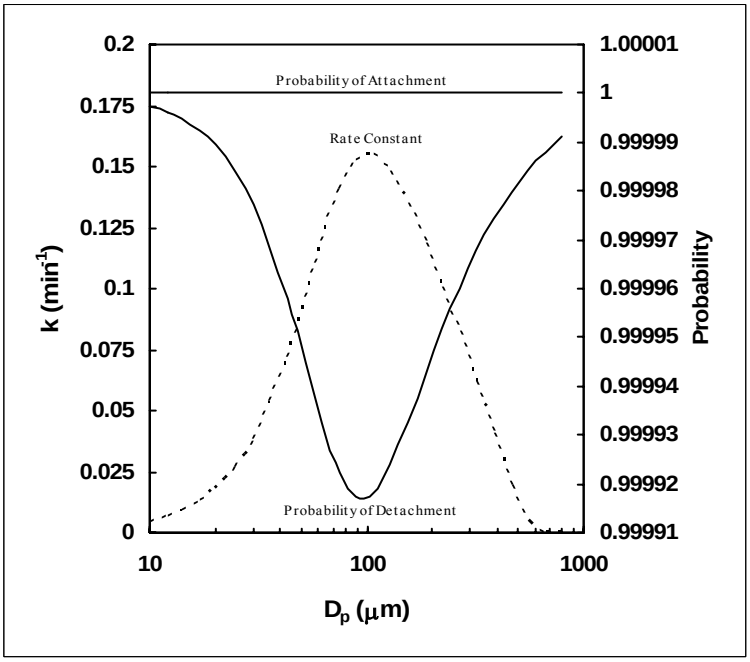

Figure 6. Effect of attachment and detachment probabilities (—) on the rate constant (- -). Same conditions shown in Figure 9, contact angle 60 degrees.

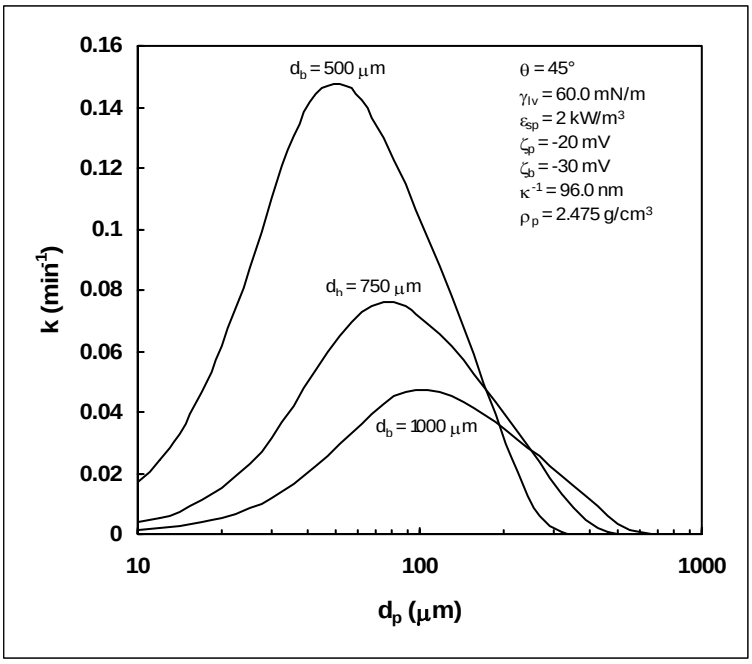

Figure 7. Effect of bubble size on the flotation rate constant. Smaller bubbles are more beneficial to small particle flotation while large particles may benefit more from bigger bubbles. This is due to a combination of specific surface area, kinetic energies, and surface forces.

angle, and specific energy input.

Figure 7 and Figure 8 show the effect of physical variables on the rate constant. The outcome from varying the bubble diameter, along with the particle diameter, can be found in Figure 7. As the bubble diameter decreases, the rate constant increases. In addition, when the bubble diameter is decreased, the particle diameter, where the maximum rate constant occurs, is decreased. This affirms the phenomenon found in column flotation, where smaller bubbles are more beneficial to small particle flotation. The first phenomenon (increased small particle rate constant) is mainly due to the fact that bigger bubbles have lower specific surface area (surface area per unit volume of air flow). This results in a lower amount of sites for potential particles to adhere to. The smaller the bubble, the greater the specific surface area, and therefore the greater potential for particles to become attached. For the same volume of air, smaller bubbles have the potential to float more particles.

The second phenomenon (shift where maximum rate constant occurs) is due, mainly, to kinetic energies, as well as surface forces. As a bubble becomes smaller, its kinetic energy decreases. The energy difference between smaller and larger bubbles is more greatly felt, in interactions, by smaller particles, because of the small particles' already low kinetic energies. Surface forces are also affected by the smaller bubbles but more so in the energy barrier than in the work of adhesion. The energy barrier will decrease, like kinetic energy, when the bubble size is reduced. Since both main variables (energy barrier and attachment kinetic energy) are reduced for the probability of attachment, it is not thought that the attachment process is affecting this movement. Probability of detachment, on the other hand, has only one variable greatly affected by bubble size. It is thought that the detachment process of smaller bubbles will lower the maximum rate constant particle size.

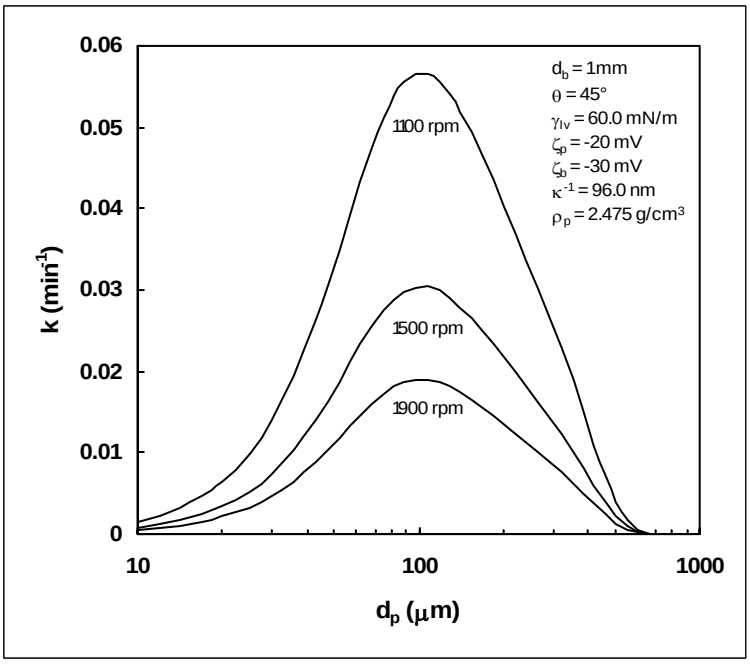

Figure 8. Effect of energy input, in the form of impeller rpm, on the flotation rate constant. Higher energy inputs decrease rate constant due to higher probabilities of detachment from higher kinetic energies of detachment. Bubble size changes due to increased impeller speeds are not taken into account.

It should also be noted that as bubble size decreases, large particles become more difficult to float. This is due to the froth recovery factor, R_F. The neutral density particle size, $d_{p\text{-}n}$, decreases with decreasing bubble size, which makes recovery of large particles more difficult. The smaller the bubble size becomes in the froth, the greater the difficulty large particles have in traveling upward within the froth.

The outcome from varying the energy input, in the form of impeller speed, along with the particle diameter, is shown in Figure 8. Although not much difference is seen in the particle size where the maximum rate constant occurs, there is a meaningful difference in the magnitude of the rate constant. As the specific energy input increases, the rate constant decreases. At first, this seems counter-intuitive, and the opposite effect is seen in industrial machines. It was thought that as the energy input into the system increases the rate constant would also increase. This is true up to a point after which the potential for detachment increases substantially more than the potential for attachment. Lower energy input values, which reverse the effect on the rate constant, are not shown, since most industrial flotation machines are run with much higher impeller speeds. Actual industrial flotation machines see an opposite effect because of the production of bubbles. As the energy input into a system is increased, the bubble size is decreased. The reduced bubble size is what causes the increase in the rate constant. There is no relationship between bubble size and energy input in the present flotation model. The bubble size is constant throughout this simulation. When the bubble production model given by Johansen et al. (1997) is input into the current model, the opposite effect is shown. Higher energy inputs produce higher rate constants because of smaller bubbles. Johansen's model is not used to calculate flotation rate constants due it's applicability to flotation systems. It was derived for bubble formation in a liquid metal environment. It was input here only to state that there can

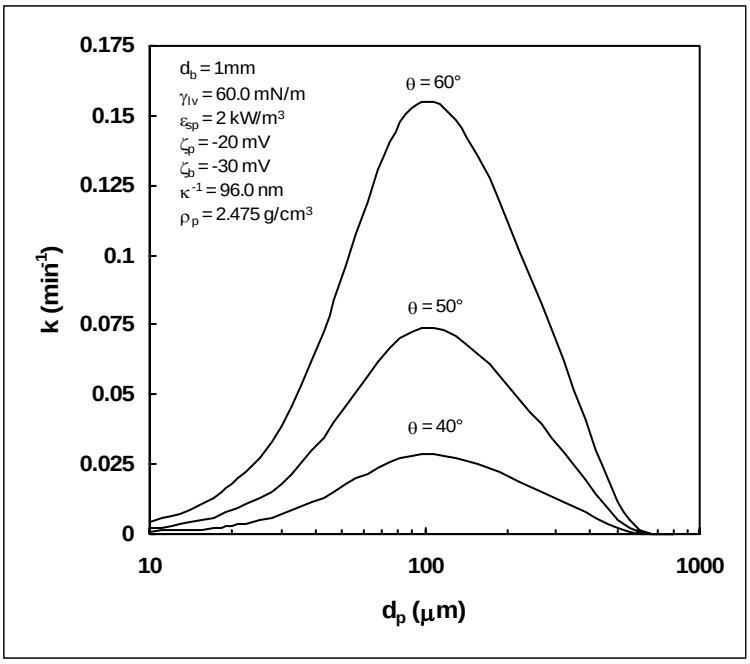

Figure 9. Effect of contact angle on the flotation rate constant. Higher contact angles increase the work of adhesion, which decreases the probability of detachment. This increases the rate constant. It should be noted that contact angles and hydrophobic force constants are directly related. Both increase or decrease the rate constant in tandem.

be a combined effect of bubble size and energy input on the rate constant that shows the same effect as industrial machines.

Figure 9 and Figure 10 show the effects of surface chemistry parameters. The outcome of varying the contact angle, along with the particle diameter, can be found in Figure 9. As the angle increases, the rate constant increases. This is due, mostly, to the work of adhesion. A higher contact angle increases the work of adhesion, which in turn makes a greater "energy barrier" for detachment. This greater "energy barrier" decreases the probability of detachment and increases the rate constant. It should also be noted that the contact angle and hydrophobic force constant are related (Rabinovich and Yoon 1994; Yoon and Ravishankar 1994; Yoon and Ravishankar 1996; Vivek 1998; Pazhianur 1999). The contact angle and hydrophobic force constant, which are directly proportional, will both increase or decrease the rate constant in tandem.

The final surface force parameter that was varied is the surface tension. This is shown in Figure 10, along with the effect of particle diameter. Similar to the contact angle, the effects shown here are entirely due to the work of adhesion. A higher surface tension increases the work of adhesion, which makes it harder for particles to become detached. Therefore, the probability of detachment decreases, with increasing surface tension, and the rate constant increases.

It should be noted that all simulations that were run show a maximum, of the rate constant at, approximately, a particle diameter of 100 microns. This is seen in industrial flotation cells and is a good sign as to the validity of the model and the assumptions used to derive the model.

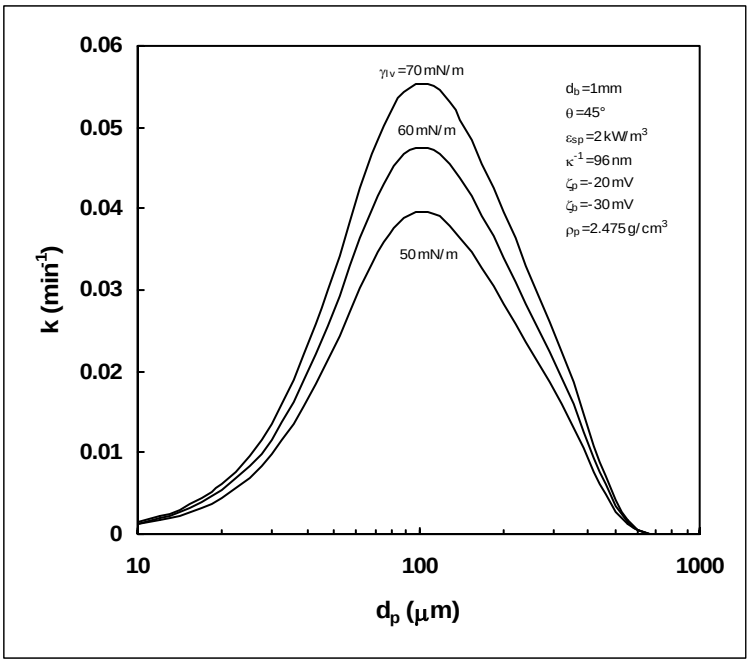

Figure 10. Effect of liquid-vapor surface tension on the flotation rate constant. Higher surface tensions increase the work of adhesion and decrease the probability of detachment. This increases the overall rate constant.

These simulations show that surface chemistry parameters play as important a role in flotation as physical parameters. An analysis of flotation cannot be conducted while only looking at the physical characteristics of the flotation machinery and the feed to that machinery. The chemical interactions between all aspects of flotation must be considered. This includes water chemistry and surface chemistry. A big determining factor in flotation is the hydrophobic force. This manifests itself in the hydrophobic force constant and contact angle. If this force is omitted, a flotation equation cannot be considered universal and will only be valid in a very few situations. The current equation incorporates all current surface chemistry as well as hydrodynamic knowledge. Although the current model does predict trends that are seen in industry, a more precise knowledge of the effect of froth on the rate constant will provide a more robust and applicable model.

Conclusions

A flotation model was developed that can predict trends in the flotation of solid particles. The model incorporates hydrodynamic as well as surface chemistry parameters in a turbulent environment. A collision frequency is used, along with a probability of collection and a froth recovery factor to calculate the rate of particles that are recovered per unit volume per unit time. The collision frequency is calculated using a model proposed by Abrahamson. Both probability of attachment and probability of detachment, which combine to form the probability of collection, compare surface energy values with the kinetic energies of the particles and bubbles to determine their respective probabilities. The kinetic energies of the particles and bubbles come from the turbulent energies of eddies directly affecting the attachment and detachment of the particles and bubbles. The froth recovery factor is calculated using a modification of a model

given by Gorain el al. (1998). The modification takes into account the particle size as well as a maximum froth recovery determined by bubble size.

Simulations were run that found phenomena similar to those found in industrial flotation cells. From these simulations, the surface chemistry parameters were deemed as important as the physical parameters of the flotation system. One of the most important of the surface chemistry parameters was the hydrophobic force. This influences both the hydrophobic force constant, which in turn influences the contact angle; the contact angle having a large impact on the rate constant. Further refinement of the model is necessary to incorporate a better understanding of the froth section of flotation. The current model can predict trends found in the flotation industry.

Nomenclature

1	subscript – refers to particle
2	subscript – refers to bubble
3	subscript – refers to liquid
B	constant
C_0	constant equal to 2.0
d_{12}	diameter of collision [m]
d_i	diameter of i [m]
d_p	diameter of particle [m]
$d_{p\text{-}n}$	diameter of neutrally buoyant particle [m]
E_1	surface energy barrier [J]
$E_{k\text{-}D}$	kinetic energy of detachment [J]
$E_{k\text{-}A}$	kinetic energy of attachment [J]
H_c	critical rupture thickness [m]
h_f	froth height [m]
k	rate constant [min^{-1}]
m_i	mass of particle or bubble [kg]
N_i	number density of i – number per unit volume [m^{-3}]
P_A	probability of attachment [-]
P_D	probability of detachment [-]
P_{fr}	particle effect – retention time [-]
$r_{2\text{-}0}$	radius of bubble – slurry-froth interface [m]
$r_{2\text{-}f}$	radius of bubble – top of froth [m]
Re_b	Reynolds number of bubble [-]
R_F	froth recovery factor [-]
r_i	radius of subscript i [m]
R_{Imp}	radius of impeller [m]
R_{max}	maximum froth recovery [-]
S_0	surface area rate – slurry-froth interface [s^{-1}]
S_b	surface area rate – within slurry [s^{-1}]
S_f	surface area rate – top of froth [s^{-1}]
St	Stokes number [-]
$U^2_{T\text{-large}}$	large scale turbulent kinetic energy [$m^2 \cdot s^{-2}$]
$U^2_{T\text{-}A}$	attachment turbulent kinetic energy [$m^2 \cdot s^{-2}$]

$U^2_{T\text{-}D}$	detachment turbulent kinetic energy [$m^2 \cdot s^{-2}$]
$\sqrt{\overline{U_i^2}}$	root-mean-squared velocity of i – turbulent velocity [$m \cdot s^{-1}$]
V_D	dispersion free energy of interaction [J]
V_E	electrostatic free energy of interaction [J]
V_g	superficial air flow rate [$m \cdot s^{-1}$]
V_H	hydrophobic free energy of interaction [J]
V_T	total free energy of interaction [J]
W_A	work of adhesion [J]
Z_{12}	collision frequency between particle and bubble [$m^{-3} \cdot s^{-1}$]
α	froth recovery parameter [s^{-1}]
β	collision kernel [$m^3 \cdot s^{-1}$]
γ_{lv}	liquid-vapor surface tension [$N \cdot m^{-1}$]
ε	average energy dissipation [$m^2 \cdot s^{-3}$]
κ	wave number [m^{-1}]
κ_{avg}	average attachment wave number [m^{-1}]
κ_I	impeller wave number [m^{-1}]
κ_K	Kolmogorov wave number [m^{-1}]
$\kappa_{P/B}$	particle/bubble wave number [m^{-1}]
θ	contact angle [rad] – measured through liquid
ν	kinematic viscosity [$m^2 \cdot s^{-1}$]
ρ_i	density of i [$kg \cdot m^{-3}$]
$\tau_{avg\text{-}f}$	average froth retention time [s]
τ_f	froth retention time [s]
τ_i	particle/bubble relaxation time [s]
τ_η	Kolmogorov timescale [s]
ω	impeller radial velocity [rpm]

References

Abrahamson, J. (1975). "Collision rates of small particles in a vigorously turbulent fluid." Chemical Engineering Science **30**(11): 1371-9.

Arbiter, N. and C. C. Harris (1962). Flotation Kinetics. Froth flotation - 50th anniversary volume. D. W. Fuerstenau, American Institute of Mining, Metallurgical, and Petroleum Engineers.

Aveyard, R., B. P. Binks, et al. (1999). "Foams and emulsions. Their stability and breakdown by solid particles and liquid droplets. The colloid chemistry of a dog's breakfast." NATO ASI Series, Series E: Applied Sciences **354**(Foams and Emulsions): 21-44.

Bikerman, J. J. (1973). Applied Physics and Engineering, No. 10: Foams. [Physicochemical Aspects].

Bourloutski, E. and M. Sommerfeld (2002). "Parameter studies on the effect of boundary conditions in three-dimensional calculations of bubble column." FED (American Society of Mechanical Engineers) **[257-2]**(A, Proceedings of the 2002 ASME Joint U.S.-European Fluids Engineering Conference): 355-364.

Buurman, C. (1990). "Stirring of concentrated slurries: a semi-empirical model for complete suspension at high solids concentrations and 5 m3 verification experiments." Institution of Chemical Engineers Symposium Series - Fluid Mixing 4 **121**: 343-350.

Ceylan, K., A. Altunbas, et al. (2001). "A new model for estimation of drag force in the flow of Newtonian fluids around rigid or deformable particles." Powder Technology **119**(2-3): 250-256.

Chahine, G. L. (1995). Bubble interactions with vortices. Fluid Vortices. S. I. Green.

Crowe, C. T. and T. R. Trout (1995). Particle interactions with vortices. Fluid Vortices. S. I. Green.

Gorain, B. K., M. C. Harris, et al. (1998). "The effect of froth residence time on the kinetics of flotation." Minerals Engineering **11**(7): 627-638.

Gore, R. A. and C. T. Crowe (1991). "Modulation of turbulence by a dispersed phase." Transactions of the ASME **113**: 304-307.

Govan, A. H. (1989). "A simple equation for the diffusion coefficient of large particles in a turbulent gas flow." International Journal of Multiphase Flow **15**(2): 287-94.

Harris, P. J. (1982). Frothing phenomena and frothers. Principles of Flotation. R. P. King. Johannesburg, South African Institute of Mining and Metallurgy**:** 237-251.

Johansen, S. T., S. Gradahl, et al. (1997). "The bubble size and mass transfer mechanisms in rotor stirred reactors." Light Metals (Warrendale, Pennsylvania): 663-666.

Johansson, G. and R. J. Pugh (1992). "The influence of particle size and hydrophobicity on the stability of mineralized froths." International Journal of Mineral Processing **34**(1-2): 1-21.

Kelsall, D. F. (1961). "Application of probability in the assessment of flotation systems." Bull. Instn. Min. Metall. **650**: 191-204.

Knapp, J. M. S. (1990). A study of flotation froth behavior. Mining and Minerals Engineering, Virginia Polytechnic Institute and State University.

Kruis, F. E. and K. A. Kusters (1997). "The collision rate of particles in turbulent flow." Chemical Engineering Communications **158**: 201-230.

Lee, C. H., L. E. Erickson, et al. (1987). "Bubble breakup and coalescence in turbulent gas-liquid dispersions." Chemical Engineering Communications **59**(1-6): 65-84.

Liepe, F. and H. O. Moeckel (1976). "Studies of the combination of substances in liquid phase. Part 6: The influence of the turbulence on the mass transfer of suspended particles." Chemische Technik (Leipzig, Germany) **28**(4): 205-209.

Mao, L. and R.-H. Yoon (1997). "Predicting flotation rates using a rate equation derived from first principles." International Journal of Mineral Processing **51**(1-4): 171-181.

Mathe, Z. T., M. C. Harris, et al. (1998). "Review of froth modeling in steady state flotation systems." Minerals Engineering **11**(5): 397-421.

Pazhianur, R. (1999). Hydrophobic force in flotation, Virginia Polytechnic Institute and State University.

Preuss, M. and H.-J. Butt (1998). "Measuring the contact angle of individual colloidal particles." Journal of Colloid and Interface Science **208**(2): 468-477.

Rabinovich, Y. I. and N. V. Churaev (1979). "Effect of electromagnetic delay on the forces of molecular attraction." Kolloidnyi Zhurnal **41**(3): 468-74.

Rabinovich, Y. I. and R. H. Yoon (1994). "Use of atomic force microscope for the measurements of hydrophobic forces." Colloids and Surfaces, A: Physicochemical and Engineering Aspects **93**: 263-73.

Saffman, P. G. and J. S. Turner (1956). "On the collision of drops in turbulent clouds." Journal of Fluid Mechanics **1**: 16-30.
Schimann, H. C. R. (2004). "Detachment force and energy of a cetyltrymethylammonium bromide coated silica sphere from a flat bubble." pending publication.
Shaw, D. J. (1992). Introduction to colloid and surface chemistry. Boston, Butterworth-Heinemann.
Sundaram, S. and L. R. Collins (1997). "Collision statistics in an isotropic particle-laden turbulent suspension. Part 1. Direct numerical simulations." Journal of Fluid Mechanics **335**: 75-109.
Vivek, S. (1998). Effects of long-chain surfactants, short-chain alcohols and hydrolysable cations on the hydrophobic and hydration forces, Virginia Polytechnic Institute and State University.
Wang, S. K., S. J. Lee, et al. (1990). "Statistical analysis of turbulent two-phase pipe flow." Journal of Fluids Engineering **112**(1): 89-95.
Williams, J. J. E. and R. I. Crane (1983). "Particle collision rate in turbulent flow." International Journal of Multiphase Flow **9**(4): 421-35.
Yoon, R. H. (2000). "The role of hydrodynamic and surface forces in bubble-particle interaction." International Journal of Mineral Processing **58**(1-4): 129-143.
Yoon, R. H. and S. B. Aksoy (1999). "Hydrophobic forces in thin water films stabilized by dodecylammonium chloride." Journal of Colloid and Interface Science **211**(1): 1-10.
Yoon, R.-H., D. H. Flinn, et al. (1997). "Hydrophobic interactions between dissimilar surfaces." Journal of Colloid and Interface Science **185**(2): 363-370.
Yoon, R.-H. and L. Mao (1996). "Application of extended DLVO theory, IV. Derivation of flotation rate equation from first principles." Journal of Colloid and Interface Science **181**(2): 613-626.
Yoon, R.-H. and S. A. Ravishankar (1994). "Application of extended DLVO theory III. Effect of octanol on the long-range hydrophobic forces between dodecylamine-coated mica surfaces." Journal of Colloid and Interface Science **166**(1): 215-24.
Yoon, R.-H. and S. A. Ravishankar (1996). "Long-range hydrophobic forces between mica surfaces in alkaline dodecylammonium chloride solutions." Journal of Colloid and Interface Science **179**(2): 403-411.

A Comprehensive Model for Flotation under Turbulent Flow Conditions: Verification

I. M. Sherrell

Abstract

A flotation model has been proposed that is applicable in a turbulent environment. The model takes into account hydrodynamics of the flotation cell as well as all relevant surface forces (van der Waals, electrostatic, and hydrophobic) by use of the Extended DLVO theory. The flotation model includes probabilities for attachment, detachment, and froth recovery as well as a collision frequency. Flotation experiments have been conducted to verify this model. Model results are close to experimental values, which lead to the conclusion that the model can predict the flotation rate constant in other circumstances, such as industrial (e.g., coal and mineral) flotation.

Introduction

Industrial flotation is a turbulent process that separates one material from another. In most cases, this includes one solid particle from another solid particle. The process is used, among others, to separate plastics in the recycling industry, decontaminate soil, separate carbon from fly ash, etc. Most importantly, it is used to upgrade minerals in the mining industry.

Flotation begins with the introduction of air into a slurry. Certain particles (hydrophobic) are able to attach to bubbles formed from this air. The bubbles then travel vertically and are collected, while the slurry continues to travel horizontally. The process, essentially, separates material based on its ability to attach to air bubbles. This is the driving factor in flotation.

Modeling of this process, which would be beneficial in the application of flotation as well as the design of the flotation process, is very complex due to the three phases found in the flotation machines as well as the turbulent environment in which flotation occurs. To complicate matters, surface forces must be taken into account. Modification of these forces, by the addition of surfactants, allows the process to be more efficient and in some cases is the only mechanism allowing the process to take place.

Surface forces play a crucial role in the attachment and detachment processes between a particle and bubble. Proper modeling of these forces is vital to having a general flotation model. The DLVO theory models some of the surface forces seen in flotation. This theory combines the van der Waals force and the electrostatic force into a total surface force. The problem with the DLVO theory is the lack of any hydrophobic force parameter, which is known to be a major contributor to surface forces between particles and bubbles in a water medium (Yoon and Mao 1996; Yoon 2000). The extended DLVO theory incorporates this third force (hydrophobic) into the DLVO theory.

The most rigorous flotation model, to date, dealing with all three surface forces (electrostatic, van der Waals, and hydrophobic) was proposed by Mao and Yoon (1997).

$$k = \frac{1}{4} S_b \left[\frac{3}{2} + \frac{4 \mathrm{Re}_b^{0.72}}{15} \right] \left(\frac{r_1}{r_2} \right)^2 \exp\left(-\frac{E_1}{E_{k-A}} \right) \left[1 - \exp\left(-\frac{W_A + E_1}{E_{k-D}} \right) \right] \quad [1]$$

The model is based upon first principles in a quiescent environment and agrees well with experimental data. The problem of this model is its applicability to industrial applications where turbulence is encountered. This model did provide a key basis for the current model by the use of the extended DLVO theory and its relationship to the energies of the system.

Model

The current flotation model was first proposed by Sherrell and Yoon (To be submitted - summer 2004). Assuming that the rate process is first order (Kelsall 1961; Arbiter and Harris 1962; Mao and Yoon 1997) and that the rate is equal to the number of collisions between particles and bubbles ($\beta N_1 N_2$) that lead to attachment (P_A), once attached do not detach ($1\text{-}P_D$), and are able to rise within the froth (R_F), leads to Equation [2].

$$k = \beta N_2 P_A \left(1 - P_D\right) R_F \quad [2]$$

Equation [2] gives the rate constant for the turbulent flotation process and is a function of both the hydrodynamics of the flotation cell and surface forces of the particles and bubbles by the inclusion of the collision frequency kernel, β, probability of attachment, P_A, probability of detachment, P_D, and the froth recovery, R_F.

Collision Frequency

Knowing that the environment within a flotation cell is highly turbulent, collisions that occur within this environment occur for reasons far different than ones that occur in laminar flows. Mao and Yoon (1997) modeled laminar collisions using the volume that the bubble travels through and the percent solids of the slurry. A collision efficiency was then applied that accounted for streamline effects. In turbulent flows, particles and bubbles deviate from the fluid path. This deviation is measured by the Stokes number; a ratio of the particle relaxation (response) time to the smallest fluid relaxation time (Kolmogorov timescale).

Two mechanisms account for turbulent collisions; the shear and accelerative mechanisms. The shear mechanism accounts for relative motions of particles (fluid, solid, or gas) in a shear field. These collisions always occur in a turbulent field, even among fluid particles. Collisions between particles with Stokes numbers less than 1 occur by shear only. The accelerative mechanism accounts for inertial effects due to large and/or heavy particles. Collisions due to the accelerative mechanism occur above a Stokes number of 1 where there is some lag between the particle and fluid.

Sundaram and Collins (1997) ran a numerical simulation of real world collisions and found that for Stokes numbers above 1, a model proposed by Abrahamson (1975) provided more reliable results. Abrahamson's model is based entirely on the accelerative mechanism of collision and assumes a Stokes number of infinity. A combination of shear and accelerative mechanisms (Williams and Crane 1983; Kruis and Kusters 1997) is assumed to provide the best results for flotation collisions, but no current shear/accelerative models can account for both heavier and lighter than the surrounding fluid particle collisions. Since most particles in flotation have a Stokes number greater than 1, Abrahamson's model is currently used (Equation [3]).

$$Z_{12} = 2^{3/2} \pi^{1/2} N_1 N_2 d_{12}^2 \sqrt{\left(\overline{U_1^2} + \overline{U_2^2} \right)} \quad [3]$$

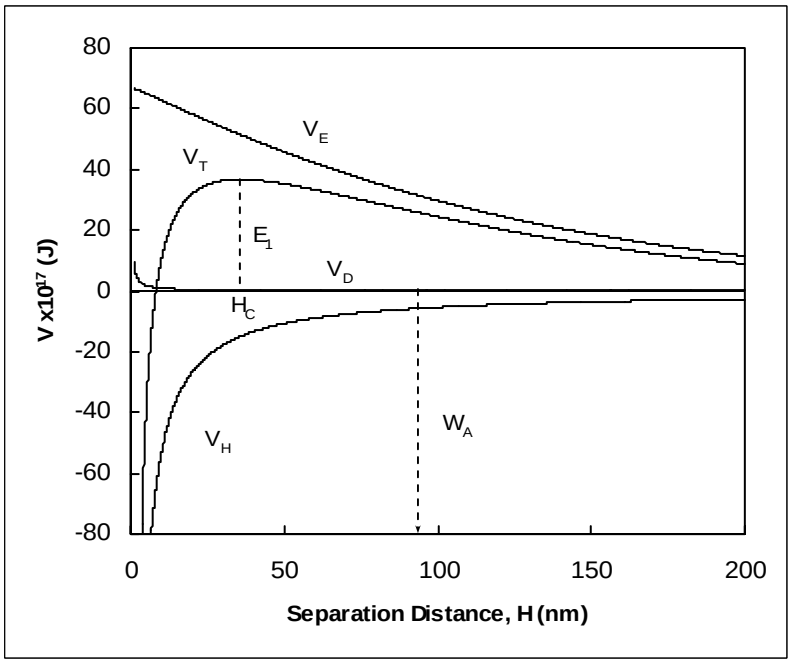

Figure 1. Surface energy vs. distance of separation between two particles (i.e. particle-bubble)

The particle turbulent root-mean-squared velocity, $\sqrt{\overline{U_i^2}}$, within this model is given by Liepe and Moeckel (1976). The bubble turbulent mean-squared velocity is given by Lee et al. (1987).

Particle Collection

The attachment and detachment processes are both influenced by surface properties of the particles and bubbles as well as hydrodynamics of the system. Surface energies are modeled based upon the Extended DLVO theory. This incorporates the electrostatic, V_E, van der Waals (dispersion), V_D, and hydrophobic, V_H, surface forces (Rabinovich and Churaev 1979; Shaw 1992; Mao and Yoon 1997). V_H is a function of hydrophobic force constants (K_{131} and K_{232}), which can be obtained from experimental results (Rabinovich and Yoon 1994; Yoon and Ravishankar 1994; Yoon and Mao 1996; Yoon and Ravishankar 1996; Yoon, Flinn et al. 1997; Vivek 1998; Pazhianur 1999; Yoon and Aksoy 1999). The surface forces are additive and combine to form the total energy of interaction, V_T, as shown in Figure 1.

The probability of attachment is dependent on the energy barrier that must be overcome and the kinetic energy of attachment, $E_{k\text{-}A}$.

$$P_A = \exp\left(-\frac{E_1}{E_{k-A}}\right) \qquad [4]$$

For attachment there exists a maximum repulsive (positive) energy, E_1, that must be overcome. This maximum energy occurs at the critical rupture thickness, H_c. Nothing prevents the particle and bubble from adhering once H_c is overcome due to the continuous drop in surface energy at smaller separation distances.

The probability of detachment is dependent on the kinetic energy of detachment, $E_{k\text{-}D}$, and the work of adhesion, W_A, which must be overcome for detachment to occur (Figure 1).

$$P_D = \exp\left(-\frac{W_A}{E_{k-D}}\right) \quad [5]$$

The work of adhesion is the energy required to return the free energy of interaction to a zero value, which, in turn, is the energy needed to take apart a bubble-particle aggregate into a separate bubble and particle. This energy is obtained thermodynamically by surface tensions (gas-solid, gas-liquid, solid-liquid) and their respective areas. A well known model used by Mao (1997)

$$W_A = \gamma_{lv}\pi r_1^2 \left(1-\cos\theta\right)^2 \quad [6]$$

assumes that the bubble surface is completely flat. Since the bubble and particle sizes are within two orders of magnitude of each other, a more accurate approach to calculate W_A would be to assume a spherical bubble attached to a spherical particle. With simple geometry, this can easily be worked out and the current model uses this approach.

Contact angles, used within Equation [6], are known to be smaller for spherical particles than corresponding flat plate measurements (Preuss and Butt 1998). There can be up to a 10 degree contact angle reduction for colloidal sized particles. The contact angle used in Equation [6] is usually obtained by measurements upon flat plates. Since it is assumed that this reduction is a function of particle size and that particles in flotation are much larger than colloidal sized particles, a constant 5 degree reduction is included in this model.

The energies for the attachment and detachment processes that will overcome these energy barriers are provided by the turbulence within the flotation cell. Energy input into the cell (through the impeller) is transferred from the largest turbulent scale (corresponding to the impeller size) to the smallest turbulent scale (Kolmogorov microscale). A certain range of these eddy sizes will have an effect on the particles and give them their turbulent kinetic energies.

Kolmogorov theory predicts, for homogenous turbulence, that energy will cascade from the largest scales to the smallest scales. The largest scale (impeller) produces the largest energy which then is transferred (at a slope of -5/3 on log-log scale) to the small scale where it is dissipated. With the addition of bubbles the slope is found to be -8/3 (Wang, Lee et al. 1990). Particles are also found to reduce the theoretically predicted slope (Buurman 1990). It is assumed that with a combination of all three phases, the slope will follow the -8/3 prediction for a two-phase flow.

Eddies corresponding to the particle/bubble size through the Kolmogorov microscale will allow the particle and bubble to deviate from the fluid flow. The fluid within this range will have a different relaxation time than the particles and bubbles, as opposed to large eddies, where bubbles and particles follow their movement. This out of phase motion allows the particles and bubbles to move independent of each other and will produce collisions. It is assumed that the average amount of this energy ($U^2_{T\text{-}A}$) over the associated wave numbers directly corresponds to the particle and bubble attachment energy as shown in Equation [7], where m_1 and m_2 are the particle and bubble masses respectively.

$$E_{k-A} = \frac{1}{2}\left(m_1 + m_2\right)\mathrm{U}^2_{T-A} \quad [7]$$

Large eddies, on the other hand, provide the energy for detachment. For detachment, bubbles and particles are already combined and, therefore, do not need a corresponding relaxation time as they do in the attachment process. Since all aggregates are subjected to large eddies, and these eddies contain the largest energies within the system, they provide the greatest energy for detachment. Detachment follows from the centrifugal motion of these eddies, in

which bubbles travel in towards the center of vortices while particles travel outward (Chahine 1995; Crowe and Trout 1995).

$$E_{k-D} = \frac{1}{2}\left(m_1 + m_2\right)\mathrm{U}_{T-D}^2 \qquad [8]$$

The turbulent energy corresponding to the largest eddy is equal to the turbulent detachment kinetic energy, U_{T-D}^2.

Froth Recovery

Froth recovery, R_f, is the percentage of particles that enter the froth and subsequently pass through the froth and are collected. All particles not recovered from the froth are returned to the slurry or never truly enter the froth phase. A simple approach of modeling this is to consider only the particles attached to the bubble surface. The only factor affecting the bubble surface would then be the coalescence of bubbles and loss of surface area. Once bubbles coalesce, a portion of their carrying capacity, for that volume of air, is lost. Once that carrying capacity is lost, it is assumed that those particles that were attached will drain back into the slurry. This provides a maximum froth recovery barrier that can not be overcome. It should be noted that this does not take into account entrainment, but only accounts for attached particles. This loss of surface area is equal to the ratio of the final and initial froth bubble sizes.

$$R_{\max} = \frac{S_f}{S_0} = \left(\frac{3V_g}{r_{2-f}}\right) \Bigg/ \left(\frac{3V_g}{r_{2-0}}\right) = \frac{r_{2-0}}{r_{2-f}} \qquad [9]$$

To theoretically model three-phase froths liquid and gas effects as well as particle size, shape, smoothness, hydrophobicity, contact angle, and concentration must be taken into account (Harris 1982; Knapp 1990; Johansson and Pugh 1992; Aveyard, Binks et al. 1999). Froth recovery is also thought to be a function of these variables, with particle size having a large effect. An empirical model proposed by Gorain et al. (1998) is thought to give the best results for froth recovery, to date.

$$R_F = \exp\left(-\alpha\tau_f\right) \qquad [10]$$

Equation [10] is a function of the froth retention time, τ_f, and a parameter, α, that incorporates both physical and chemical properties of the froth (Mathe, Harris et al. 1998). Froth retention time is usually defined as the ratio of the froth height to superficial air flow rate, V_g. α is an empirical parameter that must be determined by experiments, for each system. α usually ranges, in industrial flotation cells, between 0.1 and 0.5 (Gorain, Harris et al. 1998).

Given the fact that there is a maximum recovery that can not be overcome, a modification of Gorain's model is proposed. All recoveries calculated using equation [10] must then be scaled using the maximum froth recovery (Equation [9]).

$$R_F = \frac{r_{2-0}}{r_{2-f}}\exp\left(-\alpha\tau_f\right) \qquad [11]$$

It is also known that particles within a flotation froth have varying retention times, due to, in large part, particle size (Mathe, Harris et al. 1998). Average retention time within a froth is the ratio of froth height, h_f, to superficial air flow rate (Gorain, Harris et al. 1998). Knowing that small particles within a liquid environment follow the flow, small particles are thought to have a froth retention time equal to the average retention time within the froth. It is also known that larger particles have a more difficult time traveling upward in the froth (Bikerman 1973). It is

proposed that certain particles take longer to travel through the froth due to their size and density. Knowing this, a froth retention time model is proposed

$$\tau_f\left(d_p\right)=\frac{h_f}{V_g}P_{fr} \qquad [12]$$

that is a function of particle size, d_p, and takes this into account by the addition of a froth particle effect, P_{fr}.

The particle effect on the retention time is given the functional form

$$P_{fr}=\exp\left(B\frac{d_p}{d_{p-n}}\right) \qquad [13]$$

where B is a constant and $d_{p\text{-}n}$ is the particle diameter that, when attached to a given bubble size, the bubble-particle aggregate has a neutral buoyancy. The neutrally buoyant particle, $d_{p\text{-}n}$, affecting Equation [13] is used to take into account the buoyancy of the bubble with an attached particle. Smaller or less dense particles allow the bubble to travel upward within the froth more quickly. The smaller a given particle is compared to the neutrally buoyant particle size, the closer the particle effect is to 1. Therefore, the closer the particle is to following the fluid (or bubble) flow the closer the particle retention time is to the average retention time within the froth. The larger or more dense the particle is compared to the neutrally buoyant particle, the greater the particle effect becomes. Large particles will take longer to travel through the froth, if they travel through the froth at all. Particle effect, using this functional form, must always be greater than 1 and therefore, particle froth retention time must always be equal to or greater than the average froth retention time. B is thought to be a function of frother type and cell-dynamics and is found empirically for each system.

Experimental

Sample

Model verification was carried out by continuous flotation experiments. These experiments were performed using samples obtained from Potters Industries Inc. The samples were Ballotini impact beads which are ground soda-lime glass used in sandblasting. These were already sized and at least 80% spherical. Three different sizes were obtained: 40x70 mesh (Potters spec AA), 70x140 mesh (Potters spec AD), and 170x325 mesh (Potters spec AH). No preparation of the sample was required, beyond what the experimental procedure entails.

To measure contact angle of the particles, a flat surface was desired. A representative portion of the glass particles was melted in an oven at 800ºC. These large glass pieces (approximately 12mm x 12mm) were then ground flat on two sides. One side was polished, eventually using a 2400 grit polishing cloth. Contact angles were easily measured using these polished surfaces.

Surfactants

Cetyl (hexadecyl) trimethyl ammonium bromide (C_{16}TAB) was used as a collector due to the wide Ph fluctuations it can encounter and still perform satisfactorily, as well as ease of use. This was obtained from Sigma-Aldrich. Polypropylene glycol with an average molecular weight of 425 (PPG-425) was used as a frother. This was also obtained from Sigma-Aldrich.

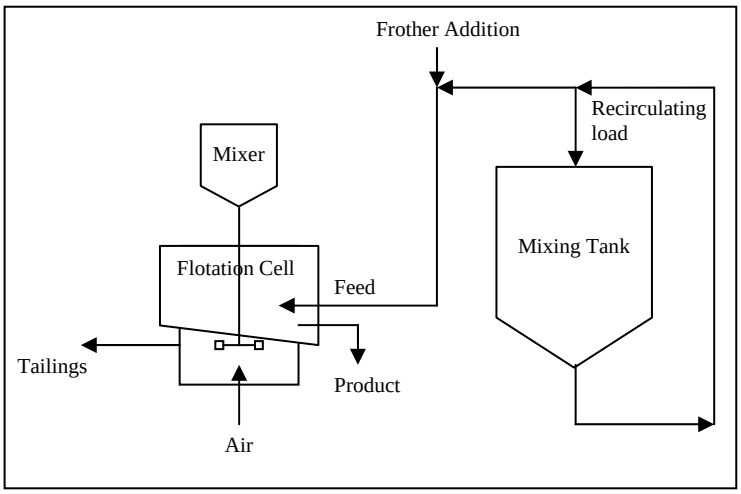

Figure 2. Flotation circuit schematic

Continuous Testing

Testing was run on a continuous flotation circuit. This produces steady-state conditions in which the flotation environment is not constantly changing and a flotation rate constant is not arbitrarily set, as in batch tests (De Bruyn and Modi 1956; Jowett and Safvi 1960; Mehrotra and Padmanabhan 1990). Continuous testing is both more difficult to setup and takes longer than batch testing to perform, but results in more representative and reproducible data. Batch testing data is difficult to collect because it must be collected in a short period of time, with steady state never being reached. This brings into question what conditions are affecting the batch flotation tests. Rate constants are constantly changing, while some believe that the flotation rate order may also change (Brown and Smith 1953-54). This is not the case with a continuous flotation circuit.

Experimental Setup

A diagram of the flotation circuit is shown in Figure 2. All feed to the flotation cell comes from the mixing tank. The contents of the mixing tank are recirculated from the bottom of the tank to the top. The combination of the mixer, within the tank, and the recirculating load provides a well mixed environment in the mixing tank. This allows ideal conditioning, where collector adsorption on particles is as equal as possible, as well as constant feed grade to the flotation cell. A constant feed grade is needed to reach steady state in the continuous cell. The contact angle samples are also placed within the conditioning tank so that they are conditioned along with the sample being tested. They were held in the mixing tank within a perforated plexiglass container which was retrieved after each flotation test was complete.

Feed is pumped out of the recirculating load using a variable speed Masterflex peristaltic pump. This rate is approximately 1.33 L/min, which gives an average residence time (before the introduction of air) within the 2L cell of 1.5 minutes. Before the feed enters the cell, frother is introduced to obtain a dosage of 10ppm.

The flotation cell is modeled after the Rushton flotation cell (Rushton, Costich et al. 1950; Deglon, O'Connor et al. 1997; Armenante, Mazzarotta et al. 1999; Jenne and Reuss 1999) as shown in Figure 3, where $H/D = 1$, $d/D = 1/3$, and $w/D = 1/10$. The height of the impeller off the bottom of the cell, h, was set at 4mm for these tests. The h/D ratio in a typical Rushton cell

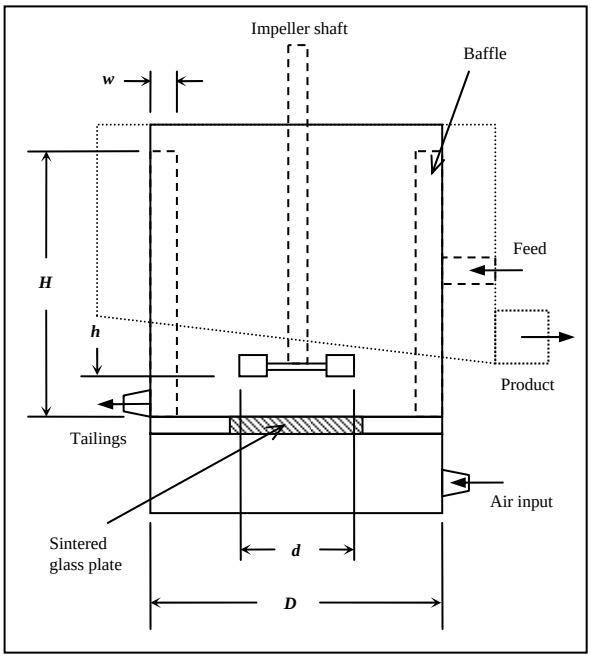

Figure 3. Flotation cell dimensions.

is 1/2, however *h* needed to be smaller than in a typical Rushton cell for the impeller to create small bubbles, from the air coming through the sintered plate, as well as mix large particles, which settle on the bottom of the cell. The height of the impeller still provided excellent mixing as shown by a dye tracer. Four baffles were evenly spaced within the cell, at a height 0.5 inches above the slurry level. A Rushton impeller was used with a diameter of 2.0 inches, which is slightly larger than the desired *d* diameter of 1.83 inches given from the above ratios. The actual dimensions of the flotation cell are as follows; D = 5.5 inches, H = 6.0 inches, d = 2.0 inches, w = 0.55 inches, h = 0.16 inches. H given here is the height of the baffles, while the liquid was kept below this height.

Feed entered the flotation cell mid-way up one side. On the opposite side, tailings were pumped from the bottom of the cell with a variable speed peristaltic pump. The pump speed was adjusted so that froth height was minimized and constant. Air was introduced through the bottom of the cell using compressed gas and a flow meter. All tests were kept at the same constant air rate. Air entered a chamber below the cell which was connected to the main cell by a plexiglass partition which contained a sintered glass plate. The sintered glass plate (porosity C) was obtained from Ace Glass. Air flowed through the plate and was broken up by the plate itself and the action of the impeller situated directly over top of the plate. Mixing within the cell was accomplished by a Lightnin Labmaster L1U10F mixer using a R100 Rushton impeller.

Sampling positions were located as shown in Figure 4 for the feed, product, and tailings. The feed sample was situated where there was a direct drop in the material so that a flow diverter was not needed. Any diversion of a contained flow might cause pressure differences which would lead to different flow rates. The design of the system accommodated this so that correct rates could be measured for the feed as well as the tailings and product. The product was measured at the output of the launder around the cell, which collected the freely overflowing product from the cell. Tailings were collected at the output of the tailings pump.

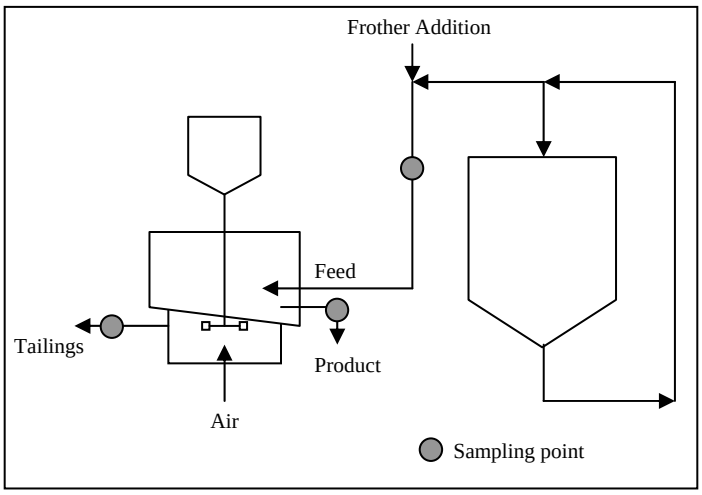

Figure 4. Sampling points around flotation cell.

Experimental Procedure

All samples were reused for subsequent tests so that particle size, as well as particle surface chemistry did not drastically change between tests. This required the cleaning of samples between tests. All glass samples were placed in an H_2SO_4 bath overnight. The acid was then drained using a glass fiber filter and rinsed three times. The sample was then placed in a bucket and filled with water to dilute any leftover acid. The bucket was then drained, making sure particles had settled to the bottom, and the process was repeated until a natural pH reading was obtained (usually 5 repetitions). The glass particles were then placed within the mixing tank and water was added until the correct percent solids (by volume) was reached.

Contact angle samples were rinsed with deionized water, after being cleaned in the acid bath, and a deionized water contact angle was measured to determine if all samples were properly cleaned. The samples were then placed within a plexiglass holder which was subsequently placed within the mixing tank.

Once all samples were within the mixing tank, the mixer and recirculating pump were turned on. C_{16}TAB was then added, at the desired concentration, and left to condition for at least 10 minutes. When conditioning was complete, the feed and frother pump were turned on, airflow was set to the desired flow reading and the Lightnin mixer was turned on to the desired speed setting.

Once steady state was reached, all desired measurements were taken. Torque and rpm measurements, used to calculate energy input, were taken directly from the Lightnin mixer. A pressure differential reading, used for air holdup calculations, was taken between two points within the cell using a Comark C9553 pressure meter. Three full data sets were taken for each test.

Once the test was complete, the contact angle samples were removed from the mixing tank along with a representative sample of the solids and liquid from the tank, for zeta potential and contact angle measurements.

Table 1. Flotation test variables

Test #	Particle Category	Particle Size – approx. (mm)	Contact Angle - approx. (deg)	Impeller RPM	% Solids (by volume)
1	AA	300	25	1200	8.5
2	AD	140	25	1200	8.5
3	AH	65	25	1200	8.5
4	AA	300	33	1200	8.5
5	AD	140	33	1200	8.5
6	AH	65	33	1200	8.5
7	AA	300	40	1200	8.5
8	AD	140	40	1200	8.5
9	AH	65	40	1200	8.5
10	AA	300	33	900	8.5
11	AD	140	33	900	8.5
12	AH	65	33	900	8.5
13	AA	300	33	1500	8.5
14	AD	140	33	1500	8.5
15	AH	65	33	1500	8.5
16	AA	300	33	1200	5
17	AD	140	33	1200	5
18	AH	65	33	1200	5
19	AA	300	33	1200	12
20	AD	140	33	1200	12
21	AH	65	33	1200	12

Sample Analysis

Variables

The effects of 4 different variables were examined during these tests. These include particle size, contact angle, energy input, and feed concentration. A layout of the tests is shown in Table 1. Some tests were run twice due to variations in the measured and desired contact angles. A high, medium and low value for each variable was desired, with a medium baseline comparable for all tests.

Rate Constant

After mass balancing all flow rate data, the rate constant was determined. The typical formula used in flotation is

$$R = \frac{k\tau}{1 + k\tau} \qquad [14]$$

where R is recovery and τ is average retention time within the cell. This formula assumes perfect mixing and can be rewritten by substituting $R=Pp/Ff$ for the recovery.

$$k = \frac{Pp}{\tau(Ff - Pp)} \qquad [15]$$

P and F are the flow rates of the product and feed respectively while p and f are the grades of those flow rates. By assuming that steady state has been reached and substituting in the tailings mass flow rate (Tt), the rate constant is then given by Equation [16].

$$k = \frac{Pp}{\tau Tt} \qquad [16]$$

This formula is valid only for single input and single output processes. Within an industrial flotation process, the flow rate of the froth is much less than the tailings flow rate, and the above

Table 2. Experimental Data

Test #	Part. Size (μm)	Cont. Angle	Imp. RPM	Specific Energy Input (W/m3)	Feed % Solids (by Vol.)	Exp. Rate Constant (min^{-1})	Theo. Rate Constant (min^{-1})
1	294.8	21.7	1200	17615	4.1%	2.2E-3	1.2E-3
				14886	7.7%	1.1E-3	7.6E-3
				13211	7.7%	1.1E-3	3.4E-2
2	139.5	26.4	1200	13534	8.5%	3.0E-2	4.3E-1
				13762	9.3%	1.7E-2	4.2E-1
				13244	8.5%	1.5E-2	3.9E-1
3	63.5	26.8	1200	13980	9.4%	5.1E+0	3.6E+0
				13980	8.9%	3.8E+0	3.5E+0
				12582	9.1%	3.2E+0	1.7E+0
4	297.9	32.4	1200	16514	7.5%	6.5E-3	1.2E-3
				18997	6.9%	5.4E-4	8.6E-4
				22729	7.7%	9.3E-4	7.4E-4
5	140.2	34.3	1200	14591	9.1%	1.5E+0	3.5E+0
				13840	9.0%	1.4E+0	3.8E+0
				13907	8.3%	1.6E+0	4.4E+0
6-a	64.4	32.8	1200	16147	8.9%	3.8E+0	7.1E+0
				16147	9.2%	3.7E+0	7.5E+0
				13550	8.4%	3.7E+0	5.6E+0
6-b	66.4	33.9	1200	13980	8.1%	5.6E+0	8.6E+0
				13980	6.3%	5.4E+0	5.4E+0
				14679	5.9%	5.6E+0	7.9E+0
7-a	295.7	41.2	1200	15378	7.6%	1.0E-2	4.5E-2
				13840	7.1%	7.0E-3	1.9E-1
				15091	7.6%	9.0E-3	2.9E-2
7-b	294.1	50.3	1200	15626	6.8%	1.3E-1	1.0E-1
				15378	7.2%	9.5E-2	3.4E-2
				16147	7.0%	9.3E-2	4.1E-2
8	139.5	40.0	1200	15185	8.9%	4.4E+0	6.8E+0
				13762	8.4%	3.5E+0	4.6E+0
				13426	8.2%	3.2E+0	7.7E+0
9	66.9	38.0	1200	14679	3.4%	7.1E+0	1.7E+1
				16494	3.5%	6.6E+0	1.3E+1
				14928	4.2%	6.9E+0	1.3E+1
10	295.2	37.9	900	11513	6.9%	3.8E-2	1.8E-2
				9813	7.0%	2.3E-2	7.5E-2
				9496	7.1%	2.7E-2	1.7E-1
11	140.2	30.9	900	13294	9.0%	5.1E+0	5.2E+0
				13345	8.7%	3.9E+0	2.8E+0
				12952	8.5%	4.1E+0	3.9E+0
12	66.8	30.5	900	12045	8.4%	7.8E+0	5.7E+0
				12233	7.1%	7.4E+0	5.2E+0
				11627	6.9%	5.8E+0	2.4E+0
13	295.6	39.6	1500	20301	7.3%	3.2E-2	7.1E-3
				20446	7.4%	2.8E-2	5.1E-3
				20668	7.4%	2.8E-2	5.5E-3
14	140.5	32.8	1500	18922	9.4%	2.3E+0	2.8E+0
				17400	9.2%	2.0E+0	1.9E+0
				17809	8.9%	1.7E+0	2.5E+0
15	65.2	31.1	1500	16235	8.6%	4.1E+0	3.9E+0
				14547	7.6%	3.4E+0	2.0E+0
				14769	7.3%	4.2E+0	4.1E+0
16	296.5	43.5	1200	15882	3.7%	5.0E-2	1.7E-2
				14547	4.2%	2.2E-2	7.9E-2
				16533	4.4%	2.4E-2	1.7E-2
17	140.2	39.5	1200	14728	4.9%	4.6E+0	5.9E+0
				14206	4.8%	3.0E+0	4.5E+0
				13892	4.7%	3.5E+0	7.6E+0
18	67.2	32.6	1200	15869	5.0%	6.0E+0	6.7E+0
				15056	4.1%	4.7E+0	6.7E+0
				14534	3.8%	4.8E+0	6.7E+0
19-a	296.1	47.5	1200	13392	12.0%	8.4E-2	2.1E+0
				12024	10.6%	8.0E-2	2.4E+0
				13534	10.1%	5.1E-2	2.3E+0
19-b	293.1	46.7	1200	13696	10.7%	2.2E-2	1.7E+0
				12176	10.4%	3.2E-2	3.3E+0
				13729	9.9%	1.8E-2	5.2E+0
20-a	139.5	33.9	1200	12050	13.3%	1.5E+0	3.4E+0
				12050	11.4%	1.3E+0	4.1E+0
				12485	11.2%	1.4E+0	3.6E+0
20-b	138.8	35.3	1200	16421	12.6%	3.8E+0	5.9E+0
				15728	11.4%	5.0E+0	3.4E+0
				15378	10.4%	5.4E+0	3.5E+0
21	62.6	37.9	1200	17941	13.3%	6.0E+0	1.1E+1
				17941	11.8%	3.9E+0	5.0E+0
				18454	11.5%	3.9E+0	6.6E+0

equation is relatively accurate. Within these flotation experiments, the froth rate is relatively much higher than in industrial flotation practices. The process is actually one input stream with two output streams. Equation [16] is not valid for the current process. A more accurate way of determining the rate constant is to take the mass rate of particle flotation (*Pp*) divided by the mass of that particle within the flotation cell (*Vv*) (Schuhmann 1942; Feteris 1987). If the cell is assumed to be perfectly mixed, the particle concentration within the cell is equal to the particle concentration within the tailings. The rate constant then becomes

$$k = \frac{Pp}{Vv} = \frac{Pp}{Vt} = \frac{Pp}{\tau Ft} \qquad [17]$$

As can be seen, the only difference between Equation [16] and [17] are the flow rates *T* and *F*. If a single output stream at steady state is assumed, Equation [17] reduces to [16]. Since this is not the case for these experiments, the more general form of the equation ([17]) is being used. Rate constants are shown in Table 2.

Air Fraction

Air fraction was determined from the difference between the two pressure differential readings taken during the flotation tests. One reading was obtained with air in the system, while the other was taken without. Knowing the percent solids (*%S*) within the cell (before the addition of air), as well as the densities of the solid (ρ_1), liquid (ρ_3) and air (ρ_2), the air fraction (*%A*) can be calculated using Equation [18].

$$\%A = \frac{\Delta P_A - \Delta P_S}{gh\rho_2\left(\rho_1 \%S + \rho_3\left(1 - \%S\right)\right)} \qquad [18]$$

The percent solids within the cell was assumed to be the tailings percent solids. If the cell is perfectly mixed, the tailings concentration is equal to the cell concentration.

Surface Tension

Surface tension was determined with a KSV Sigma 70 tensiometer using the Du Nouy ring method. Since surface tension is temperature sensitive, the liquid samples were stored in a refrigerator until a measurement could be performed. They were then taken from the refrigerator and allowed to reach their corresponding experimental temperature. A 25 mL sample was placed within a plastic container which was positioned within the machine. C_{16}TAB is surface active on the liquid-vapor interface and therefore affects surface tension. C_{16}TAB also adheres to glass. To keep the amount of C_{16}TAB in solution constant throughout the test and therefore have a constant surface tension, a plastic container was used.

Contact Angle

Contact angle measurements were performed using a Rame-Hart Model 100 goniometer which employs the sessile drop method. The glass samples were rinsed to clear particles from the surface, dried with nitrogen and then placed upon the viewing stage. A sample of the liquid from the mixing tank was used to determine the contact angle. The average of, at least, 5 measurements were obtained for each glass particle. Three glass particles were used per flotation test. All three glass particle values were then averaged together to get one contact angle per test. The average contact angle values can be found in Table 2.

Zeta Potential

The zeta potential of the particles were measured using a Lazer Zee model 501 zeta potential meter. A representative sample from the mixing tank was set within an ultrasonic bath for 10 minutes to break up any particle aggregates. The sample container was then shaken up, let to sit for one minute so that large particles would settle, and a sample was taken near the top of the container. This procedure reduced the particle size being measured, which results in a better measurement from this zeta potential meter. The sample was then measured at least 5 times, with the voltage being applied for, at most, 2 seconds per measurement. This reduced the amount of sample heating which leads to false measurements. One sample was used per test.

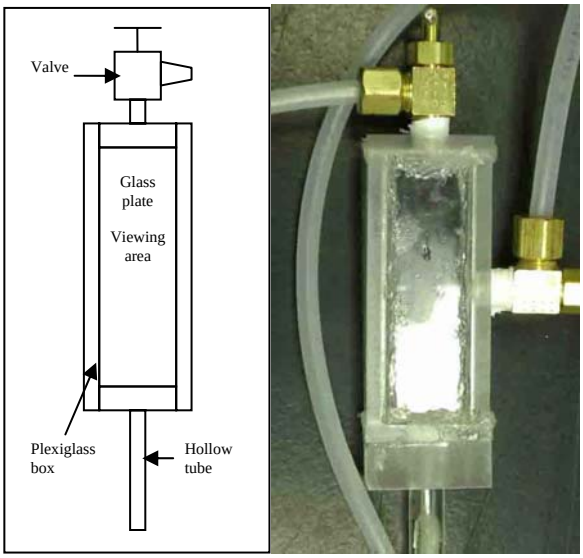

Figure 5. Bubble sampling device.

Particle Size

Particle size is very important for model prediction as well as data representation. This measurement was taken using a Microtrac X100 which employs a laser diffraction analysis and light scattering technique. This technique gives a very reliable measurement for spherical particles and the analyzer measures well within the tested particles' size range.

The sauter mean size was the desired output from this machine. The particle measuring program could not do this automatically, so a number distribution of particle sizes was measured per sample. The number distribution was then converted into the sauter mean size.

The sauter mean size is the particle size that has the same surface area to volume ratio as the entire sample's surface area to volume ratio. This is commonly used in fluid dynamic modeling as well as froth modeling. The sauter particle size for each test can be found in Table 2.

Bubble Size

A representative bubble size was determined for the frother dosage used (10ppm), as well as sintered plate porosity, impeller type and diameter, and air flow rate. This was found by running the flotation setup in exactly the same way as it was in the flotation tests, with the exception of particles. This data was not recorded during the flotation tests because of the time consumed in taking the measurements as well as the fact that particles would have blocked the measuring device. The long time of this test would have resulted in the sample being exhausted mid-way through the bubble size test. A pure water test, with only the addition of frother, could be run continuously, with out a mixing tank. For these reasons, it was thought best to run these tests without particles so that a more reproducible as well as feasible experiment could be performed. The bubble size determined in this test is assumed to be the bubble size within the flotation tests, although it is known that particles can affect the formation of bubbles and therefore bubble size.

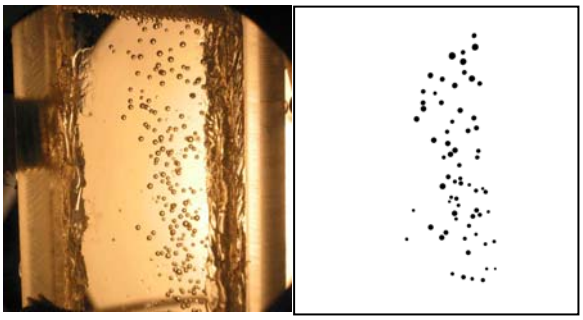

Figure 6. Original and modified bubble pictures.

Once steady state was reached, a sampling device (Figure 5) was lowered into the flotation cell. The device is comprised of two glass plates held in place by a plexiglass box. This provides bubble and liquid containment as well as a viewing area for the bubbles. A hollow plexiglass tube is attached to one end of the box while the other end has a valve. When the valve is opened, and at the bottom of the device, water can be introduced, through the valve end, until water completely fills the device. The valve can then be closed, the device inverted, and the tube can be inserted into the flotation cell. The sealed, liquid-filled container allows bubbles to travel upward, through the plexiglass tubing into the glass-plate viewing area. Pressure measuring positions were made available in the middle of the viewing area and at the bottom of the hollow tube.

Following this procedure, to view bubbles within the flotation cell, digital pictures were taken of those bubbles so that a size analysis could be performed. These digital pictures were imported into Photoshop where they were manipulated into black and white clearly discernible

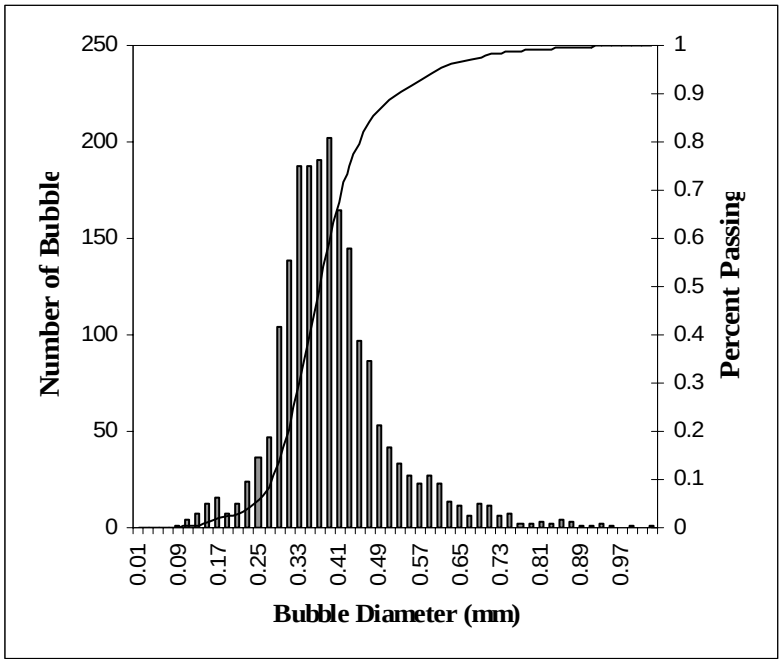

Figure 7. Bubble size population distribution with a Sauter mean size of 467.4 microns

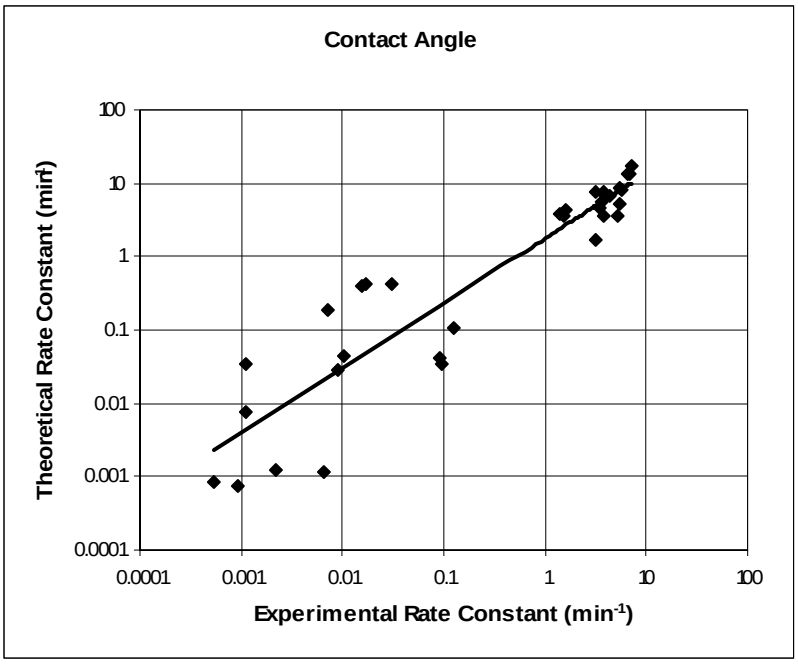

Figure 8. Relationship between experimental and theoretical rate constants with variations in contact angle.

bubble images. An example of this is shown in Figure 6. Bubbles that were indistinct or overlapping were deleted from the picture.

After the clear bubble images were prepared, they were imported into a Matlab program which determined the size of each bubble. Knowing the size of each bubble, under those operating conditions, the sauter size was determined. A graphical representation of the population distribution of the bubble size is shown in Figure 7.

The pressure differential between the inlet of the tube and the viewing area was also recorded. This gives the pressure difference between the measuring area, where the bubble size is now known, and within the cell, where the actual bubble size is desired. The pressure difference was found to be negligible and did not affect the bubble size.

Results

Once all parameters for the model were determined, the rate constants were calculated using Equation [2] and can be found in Table 2. A fit was done for the variable *B* in the froth recovery section of the model. *B* is 4.7 for this machine and frother type. The relationship between experimental and theoretical rate constants is shown in Figure 8 through Figure 11.

Figure 8 shows the relationship between the experimental and theoretical rate constants with variations in contact angle. Overall there is good agreement between the two. As can be seen, as contact angle increases (corresponding to high rate constants) there is excellent agreement between experimental and theoretical rate constants. With lower rate constants, and therefore lower contact angles, more scattering of the data is apparent. This shows the sensitivity of the rate constant to contact angle. With slight variations between measured and actual contact angles, great differences are seen in values of rate constants. These variations may be due to incomplete collector adsorption due to conditioning time or mixing as well as errors in measurement. It should be noted that other input variables will have errors which may cause

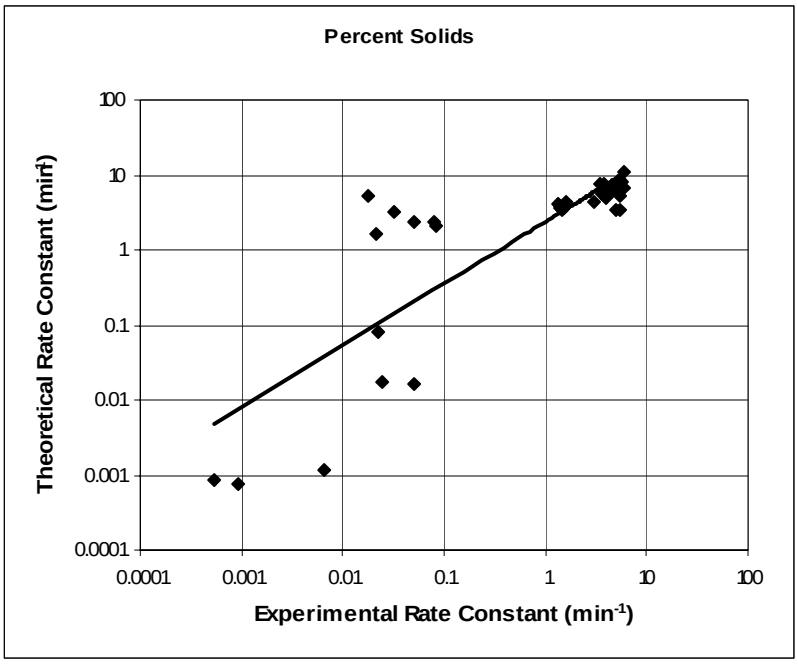

Figure 9. Relationship between experimental and theoretical rate constants with variations in percent solids. Entire data set.

and/or add to this scattering. These errors may only become apparent at low contact angles when particle detachment, in the slurry or froth, becomes an issue. This shows the great importance of reliable input data as well as constant steady state conditions. It was noted that there were fluctuations within the system, while experiments were run, mostly within percent solids. Fluctuations may also have been present for contact angles. The experimental procedure

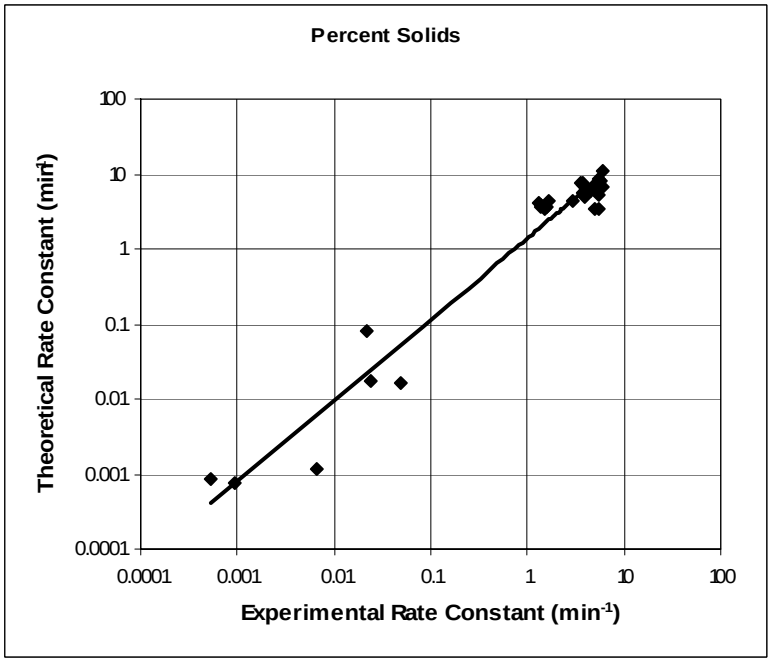

Figure 10. Relationship between experimental and theoretical rate constants with variations in percent solids. Excluding large particle – high percent solids data set.

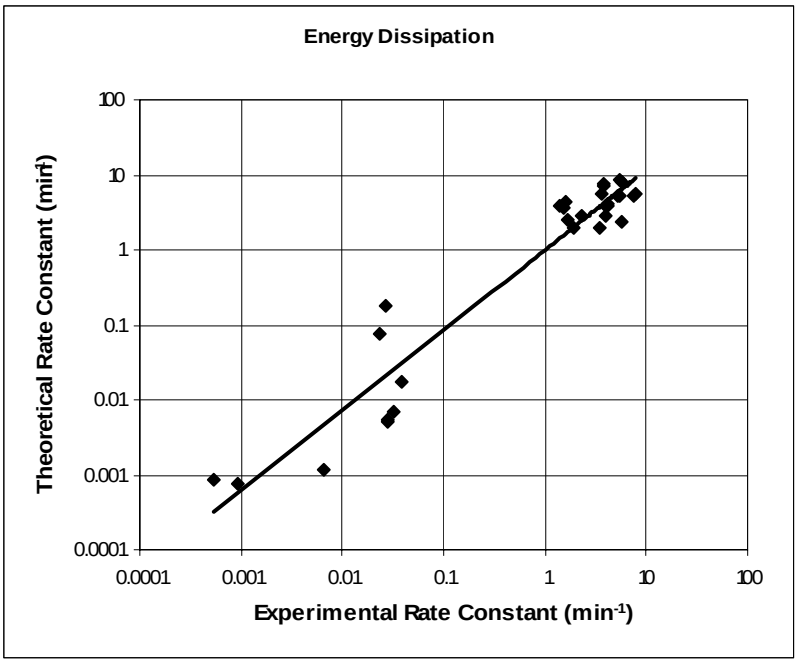

Figure 11. Relationship between experimental and theoretical rate constants with variations in energy dissipation.

available for measuring contact angle would not have perceived these fluctuations.

The effect of percent solids can be seen in Figure 9 and Figure 10. Figure 9 shows wide variations between theoretical and experimental rate constants. This is mostly due to 2 data sets; 19-a and 19-b from Table 2. These data sets are the high percent solids, large particle size tests. Two full tests were run for test number 19 because the particles were difficult to keep in suspension. With this particle size and percent solids, the mixing action of the impeller was inadequate. This is the reason for the discrepancy between the experimental and theoretical rate constants. The model predictions are based upon the assumption that there is complete mixing. Other effects may become noticeable when mixing is not adequate.

Knowing that there was error in these 2 tests, they were removed from the analysis. This is shown in Figure 10, which displays excellent agreement between theoretical and experimental rate constants. Knowing that removal of incomplete mixing data resulted in agreement between experiment and theory tells a great deal about the assumption of mixing for model use. Adequate mixing must be present for the model to predict rate constants accurately.

Figure 11 shows the relationship between theoretical and experimental rate constants while energy input was varied. The energy was varied by increasing or reducing the speed of the mixer within the flotation cell. Overall there is good agreement between the experimental and theoretical values.

Overall, there is good agreement between the experimental and theoretical data, although there are fluctuations within data sets. This is mostly due to errors in measuring input data. Reliable input data is seen to be a problem in these tests, with errors compounding due to the many variables measured. For the model to be useful in real world applications many data sets must be taken, to average out this error, or very reliable input data must be obtained.

Conclusions

A first order turbulent flotation rate equation has been proposed and verified experimentally. The rate model encompasses both hydrodynamic and surface force effects, which are incorporated into the collision frequency, probability of attachment, probability of detachment, and froth recovery sections of the model. The model is semi-empirical in nature due to the inclusion of the froth recovery. No froth recovery model has been proposed that is purely theoretical, so a well known and reliable empirical model has been incorporated into the present rate model.

Experimental verification has been performed with good results. Model calculations are similar to experimental data. A result of the rate calculations was the understanding that input data must be very reliable to use this model. Also, adequate mixing must be observed for the model to be reliable. With this knowledge, the current rate equation can be used to predict output from an industrial flotation process. The model can be very helpful in the optimization of plant performance and flotation equipment design.

Nomenclature

%A	air fraction [-]
%S	percent solids without air - by vol. [-]
1	subscript – refers to particle
2	subscript – refers to bubble
3	subscript – refers to liquid
B	constant [-]
d_{12}	diameter of collision [m]
d_p	diameter of particle [m]
d_{p-n}	diameter of neutrally buoyant particle [m]
E_1	surface energy barrier [J]
E_{k-A}	kinetic energy of attachment [J]
E_{k-D}	kinetic energy of detachment [J]
F	feed flow rate [$m^3 \cdot s^{-1}$]
f	feed grade [-]
g	gravity [$m \cdot s^{-2}$]
h	distance between pressure readings [m]
h_f	froth height [m]
k	rate constant [min^{-1}]
m_i	mass of particle or bubble [kg]
N_i	number density of i – number per unit volume [m^{-3}]
P	product flow rate [$m^3 \cdot s^{-1}$]
p	product grade [-]
P_A	probability of attachment [-]
P_D	probability of detachment [-]
P_{fr}	particle effect – retention time [-]
R	recovery [-]
r_{2-0}	radius of bubble – slurry-froth interface [m]
r_{2-f}	radius of bubble – top of froth [m]

Re_b	Reynolds number of bubble [-]
R_F	froth recovery factor [-]
r_i	radius of subscript i [m]
S_0	surface area rate – slurry-froth interface [s^{-1}]
S_b	surface area rate – within slurry [s^{-1}]
S_f	surface area rate – top of froth [s^{-1}]
T	tailings flow rate [$m^3 \cdot s^{-1}$]
t	tailings grade [-]
$U^2_{T\text{-}A}$	attachment turbulent kinetic energy [$m^2 \cdot s^{-2}$]
$U^2_{T\text{-}D}$	detachment turbulent kinetic energy [$m^2 \cdot s^{-2}$]
$\sqrt{\overline{U_i}^2}$	root-mean-squared velocity of i – turbulent velocity [$m \cdot s^{-1}$]
V	effective volume of cell [m^3]
v	grade within cell [-]
V_g	superficial air flow rate [$m \cdot s^{-1}$]
W_A	work of adhesion [J]
Z_{12}	collision frequency between particle and bubble [$m^{-3} \cdot s^{-1}$]
α	froth recovery parameter [s^{-1}]
β	collision kernel [$m^3 \cdot s^{-1}$]
γ_{lv}	liquid-vapor surface tension [$N \cdot m^{-1}$]
ΔP_A	pressure differential – with air [Pa]
ΔP_S	pressure differential – without air [Pa]
θ	contact angle [rad] – measured through liquid
ρ_i	density of i [$kg \cdot m^{-3}$]
τ	average retention time [s]
τ_f	froth retention time [s]

References

Abrahamson, J. (1975). "Collision rates of small particles in a vigorously turbulent fluid." Chemical Engineering Science **30**(11): 1371-9.

Arbiter, N. and C. C. Harris (1962). Flotation Kinetics. Froth flotation - 50th anniversary volume. D. W. Fuerstenau, American Institute of Mining, Metallurgical, and Petroleum Engineers.

Armenante, P. M., B. Mazzarotta, et al. (1999). "Power Consumption in Stirred Tanks Provided with Multiple Pitched-Blade Turbines." Industrial & Engineering Chemistry Research **38**(7): 2809-2816.

Aveyard, R., B. P. Binks, et al. (1999). "Foams and emulsions. Their stability and breakdown by solid particles and liquid droplets. The colloid chemistry of a dog's breakfast." NATO ASI Series, Series E: Applied Sciences **354**(Foams and Emulsions): 21-44.

Bikerman, J. J. (1973). Applied Physics and Engineering, No. 10: Foams. [Physicochemical Aspects].

Brown, D. J. and H. G. Smith (1953-54). "The flotation of coal as a rate process." Transactions - the Insitution of Mining Engineers **113**: 1001-1020.

Buurman, C. (1990). "Stirring of concentrated slurries: a semi-empirical model for complete suspension at high solids concentrations and 5 m3 verification experiments." Institution of Chemical Engineers Symposium Series - Fluid Mixing 4 **121**: 343-350.

Chahine, G. L. (1995). Bubble interactions with vortices. Fluid Vortices. S. I. Green.

Crowe, C. T. and T. R. Trout (1995). Particle interactions with vortices. Fluid Vortices. S. I. Green.

De Bruyn, P. L. and H. J. Modi (1956). "Particle size and flotation rate of quartz." Transactions of the American Institute of Mining, Metallurgical and Petroleum Engineers **205**(Tech. Publ. 4210-B).

Deglon, D. A., C. T. O'Connor, et al. (1997). "Efficacy of a spinning disk as a bubble break-up devices." Chemical Engineering Science **53**(1): 59-70.

Feteris, S. M. F., J.A.; Jowett, A. (1987). "Modelling the effect of froth detph in flotation." International Journal of Mineral Processing **20**: 121-135.

Gorain, B. K., M. C. Harris, et al. (1998). "The effect of froth residence time on the kinetics of flotation." Minerals Engineering **11**(7): 627-638.

Harris, P. J. (1982). Frothing phenomena and frothers. Principles of Flotation. R. P. King. Johannesburg, South African Institute of Mining and Metallurgy**:** 237-251.

Jenne, M. and M. Reuss (1999). "A critical assessment on the use of k-e turbulence models for simulation of the turbulent liquid flow induced by a Rushton-turbine in baffled stirred-tank reactors." Chemical Engineering Science **54**(17): 3921-3941.

Johansson, G. and R. J. Pugh (1992). "The influence of particle size and hydrophobicity on the stability of mineralized froths." International Journal of Mineral Processing **34**(1-2): 1-21.

Jowett, A. and S. M. M. Safvi (1960). "Refinements in methods of determining flotation rates." Transactions of the American Institute of Mining, Metallurgical and Petroleum Engineers **217**(Tech. Publ. 59B244): 351-7.

Kelsall, D. F. (1961). "Application of probability in the assessment of flotation systems." Bull. Instn. Min. Metall. **650**: 191-204.

Knapp, J. M. S. (1990). A study of flotation froth behavior. Mining and Minerals Engineering, Virginia Polytechnic Institute and State University.

Kruis, F. E. and K. A. Kusters (1997). "The collision rate of particles in turbulent flow." Chemical Engineering Communications **158**: 201-230.

Lee, C. H., L. E. Erickson, et al. (1987). "Bubble breakup and coalescence in turbulent gas-liquid dispersions." Chemical Engineering Communications **59**(1-6): 65-84.

Liepe, F. and H. O. Moeckel (1976). "Studies of the combination of substances in liquid phase. Part 6: The influence of the turbulence on the mass transfer of suspended particles." Chemische Technik (Leipzig, Germany) **28**(4): 205-209.

Mao, L. and R.-H. Yoon (1997). "Predicting flotation rates using a rate equation derived from first principles." International Journal of Mineral Processing **51**(1-4): 171-181.

Mathe, Z. T., M. C. Harris, et al. (1998). "Review of froth modeling in steady state flotation systems." Minerals Engineering **11**(5): 397-421.

Mehrotra, S. P. and N. P. H. Padmanabhan (1990). "Flotation kinetics - a review." Transactions of the Indian Institute of Metals **43**(1): 9-21.

Pazhianur, R. (1999). Hydrophobic force in flotation, Virginia Polytechnic Institute and State University.

Preuss, M. and H.-J. Butt (1998). "Measuring the contact angle of individual colloidal particles." Journal of Colloid and Interface Science **208**(2): 468-477.
Rabinovich, Y. I. and N. V. Churaev (1979). "Effect of electromagnetic delay on the forces of molecular attraction." Kolloidnyi Zhurnal **41**(3): 468-74.
Rabinovich, Y. I. and R. H. Yoon (1994). "Use of atomic force microscope for the measurements of hydrophobic forces." Colloids and Surfaces, A: Physicochemical and Engineering Aspects **93**: 263-73.
Rushton, J. H., E. W. Costich, et al. (1950). "Power characteristics of mixing impellers. I." Chem. Eng. Progress **46**: 395-404.
Schuhmann, R. J. (1942). "Flotation Kinetics: I. Methods for steady state study of flotation problems." Journal of Physical Chemistry **46**: 891-902.
Shaw, D. J. (1992). Introduction to colloid and surface chemistry. Boston, Butterworth-Heinemann.
Sherrell, I. M. and R. H. Yoon (To be submitted - summer 2004). "Developing a turbulent flotation model from first principles." Journal of Colloid and Interface Science.
Sundaram, S. and L. R. Collins (1997). "Collision statistics in an isotropic particle-laden turbulent suspension. Part 1. Direct numerical simulations." Journal of Fluid Mechanics **335**: 75-109.
Vivek, S. (1998). Effects of long-chain surfactants, short-chain alcohols and hydrolysable cations on the hydrophobic and hydration forces, Virginia Polytechnic Institute and State University.
Wang, S. K., S. J. Lee, et al. (1990). "Statistical analysis of turbulent two-phase pipe flow." Journal of Fluids Engineering **112**(1): 89-95.
Williams, J. J. E. and R. I. Crane (1983). "Particle collision rate in turbulent flow." International Journal of Multiphase Flow **9**(4): 421-35.
Yoon, R. H. (2000). "The role of hydrodynamic and surface forces in bubble-particle interaction." International Journal of Mineral Processing **58**(1-4): 129-143.
Yoon, R. H. and S. B. Aksoy (1999). "Hydrophobic forces in thin water films stabilized by dodecylammonium chloride." Journal of Colloid and Interface Science **211**(1): 1-10.
Yoon, R.-H., D. H. Flinn, et al. (1997). "Hydrophobic interactions between dissimilar surfaces." Journal of Colloid and Interface Science **185**(2): 363-370.
Yoon, R.-H. and L. Mao (1996). "Application of extended DLVO theory, IV. Derivation of flotation rate equation from first principles." Journal of Colloid and Interface Science **181**(2): 613-626.
Yoon, R.-H. and S. A. Ravishankar (1994). "Application of extended DLVO theory III. Effect of octanol on the long-range hydrophobic forces between dodecylamine-coated mica surfaces." Journal of Colloid and Interface Science **166**(1): 215-24.
Yoon, R.-H. and S. A. Ravishankar (1996). "Long-range hydrophobic forces between mica surfaces in alkaline dodecylammonium chloride solutions." Journal of Colloid and Interface Science **179**(2): 403-411.

Summary

The primary objective of this research was to derive a generic turbulent flotation model based as much as possible upon first principles. This was accomplished by incorporating models of the collision frequency, probability of attachment, probability of detachment, and froth recovery into one model for the rate constant of the entire flotation process.

Collision frequency - The collision frequency model used is typical to other flotation models in existence. It assumes a Stokes number of infinity, which is not true in flotation for either particles or bubbles, but has been shown to be close to real world situations for much lower Stokes numbers. This was based upon numerical simulations performed by previous researchers.

A review of the collision frequency models relating to flotation, existing in the literature to date, was also given. The most relevant, current model available for flotation was presented with all applicable assumptions. An area that has not been studied within the fluid mechanics profession was pointed out. This included the collision of particles and bubbles within a liquid environment. No present model can account for the differing densities between these three phases.

Probability of attachment - The probability of attachment related the surface forces of interaction, based upon the extended DLVO theory, to the turbulent energy of attachment. The energy of attachment was assumed to be that of an average vortex between the kolmogorov microscale and the particle/bubble scale.

Probability of detachment – The probability of detachment relates the work of adhesion to the maximum turbulent energy available within the system for detachment. The work of adhesion was calculated by the thermodynamic change in energy based upon the change in area between the final and initial conditions of detachment and the respective surface tensions of those areas. The maximum scale for the detachment turbulent energy was given as the impeller size with the detachment energy equal to the turbulent energy at this scale.

Froth recovery - Once the particle has intersected the froth, there is a certain probability that the particle will travel through the froth and exit into the product as

opposed to re-entering the slurry or never truly entering the froth. A form of a well known empirical model was used for this probability which is a function of average residence time within the froth. A function of the particle residence time was proposed as well as a maximum froth recovery.

The flotation model was verified by experiments performed in an idealized flotation cell. The cell was based upon a typical Rushton flotation cell with slight modifications to dimensional ratios due to mixing effects. Ground silica particles were floated using cetyl trimethyl ammonium bromide as the collector and polypropylene glycol (M_N = 425) as the frother. Once the froth recovery parameter was fit to the experimental data, there was good agreement between the theoretical and experimental rate constants across the entire range of variables tested, which includes particle diameter, contact angle, percent solids, and energy input.

Theoretical trends were predicted using the derived flotation rate equation. The effects of particle size, bubble size, energy input, contact angle, and liquid-vapor surface tension were shown. Trends and values predicted by the model were similar to those seen in industrial situations. This shows the usefulness of the model with control and prediction capabilities for running industrial processes as well as the design of those processes.

Recommendations for Future Work

Based upon the knowledge gained from this investigation, the following are considered excellent areas for further research.

(1) **Froth recovery (particle froth residence time)** – The development of a non-empirical froth recovery model will greatly benefit the proposed flotation equation. The current equation is empirical with no theoretical basis. Also, the one parameter that must be fit in the current flotation equation is included within the froth recovery model. This parameter is used to calculate the particle residence time within the forth. When this parameter can be replaced by known input variables and a theoretical froth recovery model can be derived, a truly universal slurry and froth flotation model will be available. The current model is only universal within the slurry.

(2) **Collision frequencies of particles and bubbles** – The derivation of a collision frequency that can account for particles and bubbles is needed for future flotation models. Currently, only two phases are accounted for in collision frequencies. This is not the case in flotation, where three phases are encountered. The effect of all three phases on the collision frequency must be accounted for, as well as the full range of Stokes numbers encountered in flotation.

(3) **Combined effect of particles and bubbles on turbulence** – The individual effects of particles and bubbles on the turbulent energy spectrum have been previously predicted and verified. The combined effect of two phases on a third has not. Since a similar relationship exists between air and water and solid and water, the assumption was made that the combined air-solid effects on water are equal. This may not be the case. Further research into this will verify or disprove this assumption.

(4) **Attachment and detachment energies** – The proposed attachment and detachment energies are based upon the turbulent energy spectrum and what that spectrum can affect. Although the scales given can affect the particles and bubbles, the exact magnitude of the energy imparted to them might vary from the

assumed magnitude. Further research and verification into this should be performed.

(5) **Bubble turbulent velocity** – The bubble turbulent slip velocity used within the current flotation model has not been found to be verified within the literature. It was input into the current model solely on the basis of its stated prediction for bubble turbulent slip velocity. No other bubble turbulent slip velocity has been found within the literature. Verification of the current velocity should be performed.

Appendix A

Experimental Data and Model Predictions

Date performed	2/19/2004
Test number	1

Constants

solids density	2475	kg/m3
pressure differential distance	0.0994	m
cell diameter	13.97	cm

Experimental

		Run			
		1	2	3	units
experimental data	tailings wet weight - total	124.4	112.1	133.3	g
	tailings wet tare	26.077	25.982	26.387	g
	tailings dry weight - total	47.8	59.0	68.6	g
	tailings dry tare	8.3	8.3	8.3	g
	tailings time	30.21	11.43	13.71	sec
	product wet weight - total	148.8	133.3	147.7	g
	product wet tare	25.387	25.422	25.035	g
	product dry weight - total	8.6	8.3	8.4	g
	product dry tare	8.4	8.2	8.2	g
	product time	7.02	6.55	7.03	sec
	feed wet weight - total	146.9	147.9	127.2	g
	feed wet tare	18.871	18.429	18.360	g
	feed dry weight - total	30.3	29.7	26.8	g
	feed dry tare	8.3	8.3	8.2	g
	feed time	5.10	5.17	4.24	sec
	pressure differential - no air	0.129	0.139	0.176	psi
		0.125	0.140	0.172	psi
		0.123	0.139	0.171	psi
	pressure differential - with air	0.103	0.143	0.143	psi
		0.102	0.142	0.145	psi
		0.103	0.149	0.145	psi
	liquid height	10.0	12.0	13.2	cm
		0.0	11.5	13.5	cm
		0.0	12.0	13.3	cm
calculated	avg pressure dif. - no air	0.126	0.139	0.173	psi
	avg pressure dif. - with air	0.103	0.145	0.144	psi
	avg liquid height	10.0	11.8	13.3	cm
	air fraction	0.118	-0.025	0.135	-
	active volume	1352	1585	1769	ml
	retention time	72.0	72.1	77.5	sec
mass balanced	feed percent solids	0.041	0.077	0.077	by vol
	feed flow rate	18.77	21.99	22.83	ml/sec
	tailings percent solids	0.257	0.352	0.341	by vol
	tailings flow rate	2.95	4.77	5.15	ml/sec
	product percent solids	0.001	0.001	0.001	by vol
	product flow rate	15.83	17.21	17.68	ml/sec
	exp. rate constant	**2.17E-03**	**1.10E-03**	**1.09E-03**	**min^{-1}**

Misc experimental data

	Run			
	1	2	3	units
temp	42	44	46	F
pH	4.15	4.24	4.38	

Particle Size Data

particle size passing - (μm)	percent in channel - by number		
704	0.13	0.09	0.06
592	0.73	0.55	0.34
497.8	3.16	2.74	1.90
418.6	10.96	10.79	8.71
352	27.11	28.81	26.88
296	36.26	38.28	39.92
248.9	18.43	16.67	19.40
209.3	3.22	2.07	2.79
176	0.00	0.00	0.00
148	0.00	0.00	0.00
124.5	0.00	0.00	0.00
104.7	0.00	0.00	0.00
88	0.00	0.00	0.00
74	0.00	0.00	0.00
62.23	0.00	0.00	0.00
52.33	0.00	0.00	0.00
44	0.00	0.00	0.00
37	0.00	0.00	0.00
31.11	0.00	0.00	0.00
26.16	0.00	0.00	0.00
22	0.00	0.00	0.00

Model

		Run			
		1	2	3	units
additional experimental data	torque	12	12	12	in-lb
	impeller speed	1200			rpm
	contact angle	23	16	20	deg
	contact angle	21	20	19	deg
	contact angle	21	25	21	deg
	contact angle	26	21	21	deg
	contact angle	28	23	21	deg
	contact angle	-	-	-	deg
	contact angle	-	-	-	deg
	contact angle	-	-	-	deg
	surface tension	59.06	59.83	60.08	N/m
	zeta potential	6.1			mV
calculated data	power	27.12	27.12	27.12	Watt
	avg contact angle	23.80	21.00	20.40	deg
	overall contact angle	21.73			deg
	overall surface tension	59.66			N/m
	sauter particle diameter	296.6	297.5	290.2	μm
	avg sauter part diameter	294.8			μm
	avg bub. sauter diameter	467.4			μm
	model rate constant	**1.24E-03**	**7.51E-03**	**3.40E-02**	**min^{-1}**

Date performed	2/24/2004
Test number	2

Constants

solids density	2475	kg/m3
pressure differential distance	0.0994	m
cell diameter	13.97	cm

Experimental

		Run			
		1	2	3	units
experimental data	tailings wet weight - total	128.9	163.2	131.7	g
	tailings wet tare	25.455	25.843	25.663	g
	tailings dry weight - total	39.7	53.2	40.3	g
	tailings dry tare	8.3	8.2	8.2	g
	tailings time	8.67	8.78	6.88	sec
	product wet weight - total	177.3	146.4	131.7	g
	product wet tare	26.396	25.840	25.814	g
	product dry weight - total	13.6	10.7	9.9	g
	product dry tare	8.3	8.2	8.1	g
	product time	12.89	10.99	9.49	sec
	feed wet weight - total	145.4	164.3	165.7	g
	feed wet tare	18.676	18.623	18.825	g
	feed dry weight - total	34.4	37.6	36.9	g
	feed dry tare	8.4	8.1	8.8	g
	feed time	4.95	5.70	5.84	sec
	pressure differential - no air	0.132	0.129	0.141	psi
		0.133	0.130	0.142	psi
		0.131	0.132	0.139	psi
	pressure differential - with air	0.129	0.130	0.129	psi
		0.130	0.129	0.131	psi
		0.129	0.130	0.127	psi
	liquid height	14.0	13.8	13.2	cm
		14.1	13.8	13.3	cm
		14.2	14.0	13.4	cm
calculated	avg pressure dif. - no air	0.132	0.130	0.141	psi
	avg pressure dif. - with air	0.129	0.130	0.129	psi
	avg liquid height	14.1	13.9	13.3	cm
	air fraction	0.015	0.004	0.067	-
	active volume	2016	1983	1902	ml
	retention time	93.5	85.9	82.1	sec
mass balanced	feed percent solids	0.085	0.093	0.085	by vol
	feed flow rate	21.55	23.09	23.18	ml/sec
	tailings percent solids	0.161	0.165	0.153	by vol
	tailings flow rate	10.32	12.41	12.46	ml/sec
	product percent solids	0.015	0.009	0.007	by vol
	product flow rate	11.23	10.67	10.71	ml/sec
	exp. rate constant	**3.02E-02**	**1.69E-02**	**1.54E-02**	**min^{-1}**

Misc experimental data

	Run			
	1	2	3	units
temp	42	44	44	F
pH	3.4	3.43	3.49	

Particle Size Data

particle size passing - (μm)	percent in channel - by number		
704	0.00		0.00
592	0.00		0.00
497.8	0.00		0.00
418.6	0.01		0.00
352	0.06		0.06
296	0.30		0.28
248.9	1.50		1.41
209.3	6.92		6.55
176	22.45		21.64
148	37.60		37.43
124.5	24.79		25.75
104.7	6.37		6.88
88	0.00		0.00
74	0.00		0.00
62.23	0.00		0.00
52.33	0.00		0.00
44	0.00		0.00
37	0.00		0.00
31.11	0.00		0.00
26.16	0.00		0.00
22	0.00		0.00

Model

		Run			
		1	2	3	units
additional experimental data	torque	13	13	12	in-lb
	impeller speed	1200			rpm
	contact angle	23	27	27	deg
	contact angle	25	28	25	deg
	contact angle	25	27	27	deg
	contact angle	27	29	26	deg
	contact angle	-	28	-	deg
	contact angle	-	-	-	deg
	contact angle	-	-	-	deg
	contact angle	-	-	-	deg
	surface tension	60.07	60.77	60.62	N/m
	zeta potential	17.0			mV
calculated data	power	29.38	29.38	27.12	Watt
	avg contact angle	25.00	27.80	26.25	deg
	overall contact angle	26.35			deg
	overall surface tension	60.49			N/m
	sauter particle diameter	140.0		139.0	μm
	avg sauter part diameter	139.5			μm
	avg bub. sauter diameter	467.4			μm
	model rate constant	**4.27E-01**	**4.15E-01**	**3.84E-01**	**min^{-1}**

Date performed	2/25/2004
Test number	3

Constants

solids density	2475	kg/m3
pressure differential distance	0.0994	m
cell diameter	13.97	cm

Experimental

		Run			
		1	2	3	units
experimental data	tailings wet weight - total	98.3	114.2	128.0	g
	tailings wet tare	26.733	25.830	26.569	g
	tailings dry weight - total	12.1	13.8	14.6	g
	tailings dry tare	8.3	8.1	8.2	g
	tailings time	13.57	12.62	14.56	sec
	product wet weight - total	146.0	156.0	140.0	g
	product wet tare	26.455	26.544	25.937	g
	product dry weight - total	37.0	39.4	36.8	g
	product dry tare	8.2	8.4	8.1	g
	product time	5.60	6.95	6.35	sec
	feed wet weight - total	154.6	149.5	160.6	g
	feed wet tare	18.574	18.685	18.806	g
	feed dry weight - total	36.1	34.4	36.5	g
	feed dry tare	8.3	8.2	8.3	g
	feed time	5.28	5.16	5.44	sec
	pressure differential - no air	0.127	0.125	0.122	psi
		0.124	0.125	0.121	psi
		0.125	0.127	0.121	psi
	pressure differential - with air	0.078	0.078	0.099	psi
		0.076	0.077	0.095	psi
		0.076	0.077	0.093	psi
	liquid height	11.0	10.0	10.0	cm
		10.0	10.5	11.0	cm
		0.0	11.0	0.0	cm
calculated	avg pressure dif. - no air	0.125	0.126	0.121	psi
	avg pressure dif. - with air	0.077	0.077	0.096	psi
	avg liquid height	10.5	10.5	10.5	cm
	air fraction	0.332	0.328	0.174	-
	active volume	1074	1082	1329	ml
	retention time	46.5	47.9	59.6	sec
mass balanced	feed percent solids	0.094	0.089	0.091	by vol
	feed flow rate	23.08	22.60	22.31	ml/sec
	tailings percent solids	0.022	0.027	0.026	by vol
	tailings flow rate	5.08	6.67	6.76	ml/sec
	product percent solids	0.114	0.116	0.120	by vol
	product flow rate	18.00	15.92	15.55	ml/sec
	exp. rate constant	**5.14E+00**	**3.79E+00**	**3.17E+00**	**min^{-1}**

Misc experimental data

	Run			
	1	2	3	units
temp	42	42	44	F
pH	7.29	7.37	7.42	

Particle Size Data

particle size passing - (μm)	percent in channel - by number		
704	0.00	0.00	0.00
592	0.00	0.00	0.00
497.8	0.00	0.00	0.00
418.6	0.00	0.00	0.00
352	0.00	0.00	0.00
296	0.00	0.00	0.00
248.9	0.00	0.00	0.00
209.3	0.02	0.01	0.02
176	0.06	0.05	0.06
148	0.23	0.21	0.26
124.5	0.94	0.90	1.12
104.7	3.81	3.71	4.61
88	12.55	12.35	14.90
74	27.25	27.00	30.12
62.23	31.43	31.41	30.47
52.33	17.88	18.21	14.50
44	5.83	6.15	3.94
37	0.00	0.00	0.00
31.11	0.00	0.00	0.00
26.16	0.00	0.00	0.00
22	0.00	0.00	0.00

Model

		Run			
		1	2	3	units
additional experimental data	torque	10	10	9	in-lb
	impeller speed	1200			rpm
	contact angle	24	26	27	deg
	contact angle	28	21	25	deg
	contact angle	29	25	28	deg
	contact angle	32	27	31	deg
	contact angle	27	-	#REF!	deg
	contact angle	-	-	#REF!	deg
	contact angle	-	-	#REF!	deg
	contact angle	-	-	#REF!	deg
	surface tension	59.4	60.69	60.6	N/m
	zeta potential	-20.5			mV
calculated data	power	22.60	22.60	20.34	Watt
	avg contact angle	28.00	24.75	27.75	deg
	overall contact angle	26.83			deg
	overall surface tension	60.23			N/m
	sauter particle diameter	62.9	62.6	64.8	μm
	avg sauter part diameter	63.5			μm
	avg bub. sauter diameter	467.4			μm
	model rate constant	**3.54E+00**	**3.48E+00**	**1.67E+00**	**min^{-1}**

Date performed	2/26/2004
Test number	4

Constants

solids density	2475	kg/m3
pressure differential distance	0.0994	m
cell diameter	13.97	cm

Experimental

		Run			
		1	2	3	units
experimental data	tailings wet weight - total	181.1	142.9	167.1	g
	tailings wet tare	26.077	25.982	26.387	g
	tailings dry weight - total	58.0	66.5	87.3	g
	tailings dry tare	8.3	8.3	8.2	g
	tailings time	13.30	18.11	19.00	sec
	product wet weight - total	103.4	127.6	114.6	g
	product wet tare	25.387	25.422	25.035	g
	product dry weight - total	8.6	8.2	8.2	g
	product dry tare	8.3	8.2	8.1	g
	product time	6.42	5.53	5.01	sec
	feed wet weight - total	207.7	168.6	159.4	g
	feed wet tare	18.871	18.429	18.360	g
	feed dry weight - total	40.9	34.2	32.4	g
	feed dry tare	8.3	8.3	8.2	g
	feed time	8.10	6.26	6.00	sec
	pressure differential - no air	0.108	0.120	0.128	psi
		0.112	0.121	0.130	psi
		0.108	0.122	0.133	psi
	pressure differential - with air	0.079	0.103	0.105	psi
		0.077	0.105	0.100	psi
		0.076	0.106	0.100	psi
	liquid height	8.0	8.5	7.5	cm
		0.0	0.0	8.0	cm
		0.0	0.0	0.0	cm
calculated	avg pressure dif. - no air	0.109	0.121	0.130	psi
	avg pressure dif. - with air	0.077	0.105	0.102	psi
	avg liquid height	8.0	8.5	7.8	cm
	air fraction	0.181	0.079	0.134	-
	active volume	1004	1200	1028	ml
	retention time	47.1	55.3	46.7	sec
mass balanced	feed percent solids	0.075	0.069	0.077	by vol
	feed flow rate	21.29	21.71	22.02	ml/sec
	tailings percent solids	0.165	0.310	0.343	by vol
	tailings flow rate	9.53	4.85	4.90	ml/sec
	product percent solids	0.002	0.000	0.000	by vol
	product flow rate	11.76	16.86	17.13	ml/sec
	exp. rate constant	**6.53E-03**	**5.37E-04**	**9.33E-04**	**min^{-1}**

Misc experimental data

	Run			
	1	2	3	units
temp	41	42	44	F
pH	3.94	3.97	4.03	

Particle Size Data

particle size passing - (μm)	percent in channel - by number		
704	0.15		0.12
592	0.81		0.67
497.8	3.37		3.06
418.6	11.25		11.14
352	27.20		28.13
296	36.05		36.87
248.9	18.07		17.36
209.3	3.10		2.65
176	0.00		0.00
148	0.00		0.00
124.5	0.00		0.00
104.7	0.00		0.00
88	0.00		0.00
74	0.00		0.00
62.23	0.00		0.00
52.33	0.00		0.00
44	0.00		0.00
37	0.00		0.00
31.11	0.00		0.00
26.16	0.00		0.00
22	0.00		0.00

Model

		Run			
		1	2	3	units
additional experimental data	torque	9	11	12	in-lb
	impeller speed	1200			rpm
	contact angle	30	31	30	deg
	contact angle	33	32	34	deg
	contact angle	38	34	31	deg
	contact angle	34	32	33	deg
	contact angle	27	32	35	deg
	contact angle	-	-	33	deg
	contact angle	-	-	-	deg
	contact angle	-	-	-	deg
	surface tension	51.65	56.29	51.31	N/m
	zeta potential	26.5			mV
calculated data	power	20.34	24.86	27.12	Watt
	avg contact angle	32.40	32.20	32.67	deg
	overall contact angle	32.42			deg
	overall surface tension	53.08			N/m
	sauter particle diameter	297.9		297.8	μm
	avg sauter part diameter	297.9			μm
	avg bub. sauter diameter	467.4			μm
	model rate constant	**1.14E-03**	**8.53E-04**	**7.30E-04**	**min^{-1}**

Date performed	2/20/2004
Test number	5

Constants

solids density	2475	kg/m3
pressure differential distance	0.0994	m
cell diameter	13.97	cm

Experimental

		Run			
		1	2	3	units
experimental data	tailings wet weight - total	126.0	125.0	130.1	g
	tailings wet tare	26.733	25.830	7.667	g
	tailings dry weight - total	20.0	20.7	20.0	g
	tailings dry tare	8.3	8.2	8.2	g
	tailings time	15.90	15.24	15.66	sec
	product wet weight - total	146.0	129.1	140.5	g
	product wet tare	26.455	26.544	25.937	g
	product dry weight - total	35.2	30.7	31.8	g
	product dry tare	8.4	8.3	8.2	g
	product time	6.31	5.13	5.68	sec
	feed wet weight - total	143.1	151.1	142.9	g
	feed wet tare	18.574	18.713	18.778	g
	feed dry weight - total	33.2	34.7	32.6	g
	feed dry tare	8.3	8.3	8.2	g
	feed time	4.77	4.98	4.83	sec
	pressure differential - no air	0.126	0.123	0.121	psi
		0.125	0.122	0.119	psi
		0.124	0.124	0.119	psi
	pressure differential - with air	0.095	0.088	0.087	psi
		0.091	0.090	0.085	psi
		0.089	0.088	0.085	psi
	liquid height	11.0	11.2	12.5	cm
		11.0	12.0	12.7	cm
		11.2	11.8	12.8	cm
calculated	avg pressure dif. - no air	0.125	0.123	0.120	psi
	avg pressure dif. - with air	0.092	0.089	0.086	psi
	avg liquid height	11.1	11.7	12.7	cm
	air fraction	0.219	0.224	0.226	-
	active volume	1325	1388	1503	ml
	retention time	58.9	59.3	62.3	sec
mass balanced	feed percent solids	0.091	0.090	0.083	by vol
	feed flow rate	22.50	23.41	24.12	ml/sec
	tailings percent solids	0.051	0.055	0.042	by vol
	tailings flow rate	5.83	6.01	7.14	ml/sec
	product percent solids	0.105	0.102	0.100	by vol
	product flow rate	16.67	17.40	16.98	ml/sec
	exp. rate constant	**1.55E+00**	**1.40E+00**	**1.63E+00**	**min^{-1}**

Misc experimental data

	Run			
	1	2	3	units
temp	41	41	42	F
pH	5.98	6.09	6.28	

Particle Size Data

particle size passing - (μm)	percent in channel - by number		
704	0.00		0.00
592	0.00		0.00
497.8	0.00		0.00
418.6	0.01		0.00
352	0.08		0.07
296	0.36		0.31
248.9	1.71		1.54
209.3	7.33		6.90
176	22.62		22.04
148	37.14		37.25
124.5	24.47		25.24
104.7	6.28		6.65
88	0.00		0.00
74	0.00		0.00
62.23	0.00		0.00
52.33	0.00		0.00
44	0.00		0.00
37	0.00		0.00
31.11	0.00		0.00
26.16	0.00		0.00
22	0.00		0.00

Model

		Run			
		1	2	3	units
additional experimental data	torque	11	11	12	in-lb
	impeller speed	1200			rpm
	contact angle	31	39	30	deg
	contact angle	30	37	34	deg
	contact angle	32	36	33	deg
	contact angle	33	38	34	deg
	contact angle	37	41	31	deg
	contact angle	33	-	31	deg
	contact angle	-	-	-	deg
	contact angle	-	-	-	deg
	surface tension	60.72	55.05	60.45	N/m
	zeta potential	-13.6			mV
calculated data	power	24.86	24.86	27.12	Watt
	avg contact angle	32.67	38.20	32.17	deg
	overall contact angle	34.34			deg
	overall surface tension	58.74			N/m
	sauter particle diameter	140.7		139.7	μm
	avg sauter part diameter	140.2			μm
	avg bub. sauter diameter	467.4			μm
	model rate constant	**3.51E+00**	**3.80E+00**	**4.35E+00**	**min^{-1}**

Date performed	2/21/2004
Test number	6-a

Constants

solids density	2475	kg/m3
pressure differential distance	0.0994	m
cell diameter	13.97	cm

Experimental

		Run			
		1	2	3	units
experimental data	tailings wet weight - total	111.6	139.5	153.6	g
	tailings wet tare	26.733	25.830	26.569	g
	tailings dry weight - total	13.4	15.2	14.8	g
	tailings dry tare	8.2	8.2	8.2	g
	tailings time	15.24	17.46	16.29	sec
	product wet weight - total	136.9	134.6	137.5	g
	product wet tare	26.455	26.544	25.937	g
	product dry weight - total	34.0	36.4	34.6	g
	product dry tare	8.3	8.1	8.2	g
	product time	5.80	6.15	6.26	sec
	feed wet weight - total	156.9	136.2	148.2	g
	feed wet tare	18.574	18.713	18.778	g
	feed dry weight - total	35.6	30.9	32.5	g
	feed dry tare	8.2	8.2	8.1	g
	feed time	5.63	4.79	5.16	sec
	pressure differential - no air	0.140	0.124	0.101	psi
		0.131	0.131	0.099	psi
		0.124	0.126	0.104	psi
	pressure differential - with air	0.095	0.088	0.070	psi
		0.093	0.087	0.069	psi
		0.000	0.087	0.072	psi
	liquid height	10.0	10.0	10.5	cm
		0.0	0.0	11.0	cm
		0.0	0.0	11.0	cm
calculated	avg pressure dif. - no air	0.132	0.127	0.101	psi
	avg pressure dif. - with air	0.094	0.087	0.070	psi
	avg liquid height	10.0	10.0	10.8	cm
	air fraction	0.256	0.270	0.212	-
	active volume	1140	1119	1309	ml
	retention time	52.4	52.6	57.7	sec
mass balanced	feed percent solids	0.089	0.092	0.084	by vol
	feed flow rate	21.75	21.27	22.67	ml/sec
	tailings percent solids	0.025	0.026	0.022	by vol
	tailings flow rate	5.35	6.36	7.46	ml/sec
	product percent solids	0.110	0.120	0.114	by vol
	product flow rate	16.39	14.90	15.21	ml/sec
	exp. rate constant	**3.75E+00**	**3.73E+00**	**3.65E+00**	**min^{-1}**

Misc experimental data

	Run			
	1	2	3	units
temp	42	42	44	F
pH	5.91	6.18	6.28	

Particle Size Data

particle size passing - (μm)	percent in channel - by number		
704	0.00	0.00	0.00
592	0.00	0.00	0.00
497.8	0.00	0.00	0.00
418.6	0.00	0.00	0.00
352	0.00	0.00	0.00
296	0.00	0.00	0.00
248.9	0.00	0.00	0.00
209.3	0.02	0.00	0.01
176	0.09	0.00	0.04
148	0.35	0.10	0.18
124.5	1.47	0.77	0.76
104.7	5.78	4.37	3.17
88	17.44	15.78	10.98
74	31.92	31.61	25.74
62.23	28.31	30.21	32.49
52.33	11.73	13.65	19.94
44	2.89	3.51	6.69
37	0.00	0.00	0.00
31.11	0.00	0.00	0.00
26.16	0.00	0.00	0.00
22	0.00	0.00	0.00

Model

		Run			
		1	2	3	units
additional experimental data	torque	11	11	10	in-lb
	impeller speed	1200			rpm
	contact angle	36	34	22	deg
	contact angle	36	31	34	deg
	contact angle	34	35	30	deg
	contact angle	37	34	30	deg
	contact angle	35	31	33	deg
	contact angle	-	-	-	deg
	contact angle	-	-	-	deg
	contact angle	-	-	-	deg
	surface tension	60.43	61.2	61.05	N/m
	zeta potential	-15.8			mV
calculated data	power	24.86	24.86	22.60	Watt
	avg contact angle	35.60	33.00	29.80	deg
	overall contact angle	32.80			deg
	overall surface tension	60.89			N/m
	sauter particle diameter	66.8	64.8	61.6	μm
	avg sauter part diameter	64.4			μm
	avg bub. sauter diameter	467.4			μm
	model rate constant	**7.01E+00**	**7.40E+00**	**5.55E+00**	**min^{-1}**

Date performed	3/5/2004
Test number	6-b

Constants

solids density	2475	kg/m3
pressure differential distance	0.0994	m
cell diameter	13.97	cm

Experimental

		Run			
		1	2	3	units
experimental data	tailings wet weight - total	118.6	89.3	104.7	g
	tailings wet tare	26.077	25.982	26.387	g
	tailings dry weight - total	6.9	5.1	5.5	g
	tailings dry tare	3.3	3.3	3.3	g
	tailings time	15.18	13.37	16.49	sec
	product wet weight - total	130.1	146.9	130.1	g
	product wet tare	25.387	25.422	25.035	g
	product dry weight - total	26.6	24.0	19.9	g
	product dry tare	3.3	3.3	3.3	g
	product time	5.45	6.01	5.56	sec
	feed wet weight - total	184.5	161.0	161.8	g
	feed wet tare	18.871	18.429	18.360	g
	feed dry weight - total	33.0	23.7	22.7	g
	feed dry tare	3.3	3.3	3.3	g
	feed time	6.59	5.72	6.09	sec
	pressure differential - no air	0.119	0.117	0.122	psi
		0.121	0.116	0.128	psi
		0.118	0.113	0.125	psi
	pressure differential - with air	0.078	0.090	0.090	psi
		0.079	0.089	0.087	psi
		0.080	0.089	0.086	psi
	liquid height	10.5	10.5	10.0	cm
		0.0	0.0	0.0	cm
		0.0	0.0	0.0	cm
calculated	avg pressure dif. - no air	0.119	0.115	0.125	psi
	avg pressure dif. - with air	0.079	0.089	0.088	psi
	avg liquid height	10.5	10.5	10.0	cm
	air fraction	0.278	0.180	0.259	-
	active volume	1162	1319	1136	ml
	retention time	51.5	57.9	52.2	sec
mass balanced	feed percent solids	0.081	0.063	0.059	by vol
	feed flow rate	22.55	22.80	21.74	ml/sec
	tailings percent solids	0.016	0.012	0.012	by vol
	tailings flow rate	5.94	4.66	4.66	ml/sec
	product percent solids	0.104	0.077	0.072	by vol
	product flow rate	16.61	18.15	17.09	ml/sec
	exp. rate constant	**5.58E+00**	**5.37E+00**	**5.62E+00**	**min^{-1}**

Misc experimental data

	Run			
	1	2	3	units
temp	46	51	55	F
pH	7.25	7.42	7.48	

Particle Size Data

particle size passing - (μm)	percent in channel - by number		
704	0.00		0.00
592	0.00		0.00
497.8	0.00		0.00
418.6	0.00		0.00
352	0.00		0.00
296	0.00		0.00
248.9	0.00		0.00
209.3	0.02		0.02
176	0.09		0.07
148	0.37		0.31
124.5	1.54		1.37
104.7	5.89		5.51
88	17.19		16.70
74	31.02		31.15
62.23	28.20		28.94
52.33	12.43		12.71
44	3.25		3.22
37	0.00		0.00
31.11	0.00		0.00
26.16	0.00		0.00
22	0.00		0.00

Model

		Run			
		1	2	3	units
additional experimental data	torque	10	10	10	in-lb
	impeller speed	1200			rpm
	contact angle	35	32	31	deg
	contact angle	41	29	32	deg
	contact angle	36	32	34	deg
	contact angle	37	32	34	deg
	contact angle	38	31	35	deg
	contact angle	-	30	-	deg
	contact angle	-	-	-	deg
	contact angle	-	-	-	deg
	surface tension	60.73	60.88	59.7	N/m
	zeta potential	-15.6			mV
calculated data	power	22.60	22.60	22.60	Watt
	avg contact angle	37.40	31.00	33.20	deg
	overall contact angle	33.87			deg
	overall surface tension	60.44			N/m
	sauter particle diameter	66.6		66.2	μm
	avg sauter part diameter	66.4			μm
	avg bub. sauter diameter	467.4			μm
	model rate constant	**8.47E+00**	**5.33E+00**	**7.88E+00**	**min^{-1}**

Date performed	2/23/2004
Test number	7-a

Constants

solids density	2475	kg/m3
pressure differential distance	0.0994	m
cell diameter	13.97	cm

Experimental

		Run			
		1	2	3	units
experimental data	tailings wet weight - total	151.8	167.3	178.9	g
	tailings wet tare	25.455	25.843	25.663	g
	tailings dry weight - total	58.0	58.0	67.1	g
	tailings dry tare	8.3	8.3	8.2	g
	tailings time	11.41	14.00	14.54	sec
	product wet weight - total	150.7	138.2	132.3	g
	product wet tare	26.396	25.840	25.814	g
	product dry weight - total	9.4	8.9	9.1	g
	product dry tare	8.4	8.3	8.3	g
	product time	8.02	6.73	7.17	sec
	feed wet weight - total	151.0	179.6	157.4	g
	feed wet tare	18.676	18.623	18.825	g
	feed dry weight - total	30.7	36.3	32.2	g
	feed dry tare	8.4	8.3	8.2	g
	feed time	5.59	6.77	5.77	sec
	pressure differential - no air	0.123	0.115	0.121	psi
		0.127	0.114	0.121	psi
		0.119	0.115	0.123	psi
	pressure differential - with air	0.097	0.079	0.108	psi
		0.096	0.080	0.107	psi
		0.095	0.081	0.106	psi
	liquid height	10.5	12.0	10.8	cm
		10.4	11.5	10.8	cm
		10.6	11.5	10.5	cm
calculated	avg pressure dif. - no air	0.123	0.115	0.122	psi
	avg pressure dif. - with air	0.096	0.080	0.107	psi
	avg liquid height	10.5	11.7	10.7	cm
	air fraction	0.146	0.190	0.079	-
	active volume	1374	1448	1510	ml
	retention time	60.0	63.2	68.1	sec
mass balanced	feed percent solids	0.076	0.071	0.076	by vol
	feed flow rate	22.91	22.93	22.19	ml/sec
	tailings percent solids	0.206	0.194	0.206	by vol
	tailings flow rate	8.27	8.17	8.00	ml/sec
	product percent solids	0.003	0.002	0.003	by vol
	product flow rate	14.64	14.76	14.19	ml/sec
	exp. rate constant	**1.02E-02**	**7.04E-03**	**9.01E-03**	**min^{-1}**

Misc experimental data

	Run			
	1	2	3	units
temp	42	42	44	F
pH	5.19	5.4	5.65	

Particle Size Data

particle size passing - (μm)	percent in channel - by number		
704	0.08		0.07
592	0.46		0.41
497.8	2.48		2.23
418.6	10.80		9.95
352	29.65		28.67
296	37.74		38.65
248.9	16.37		17.46
209.3	2.42		2.56
176	0.00		0.00
148	0.00		0.00
124.5	0.00		0.00
104.7	0.00		0.00
88	0.00		0.00
74	0.00		0.00
62.23	0.00		0.00
52.33	0.00		0.00
44	0.00		0.00
37	0.00		0.00
31.11	0.00		0.00
26.16	0.00		0.00
22	0.00		0.00

Model

		Run			
		1	2	3	units
additional experimental data	torque	11	11	11	in-lb
	impeller speed	1200			rpm
	contact angle	37	39	41	deg
	contact angle	42	41	41	deg
	contact angle	40	40	42	deg
	contact angle	38	49	42	deg
	contact angle	37	48	40	deg
	contact angle	41	45	-	deg
	contact angle	-	41	-	deg
	contact angle	-	-	-	deg
	surface tension	58.78	59.92	59.63	N/m
	zeta potential	-7.9			mV
calculated data	power	24.86	24.86	24.86	Watt
	avg contact angle	39.17	43.29	41.20	deg
	overall contact angle	41.22			deg
	overall surface tension	59.44			N/m
	sauter particle diameter	297.1		294.4	μm
	avg sauter part diameter	295.7			μm
	avg bub. sauter diameter	467.4			μm
	model rate constant	**4.46E-02**	**1.83E-01**	**2.87E-02**	**min^{-1}**

Date performed	3/1/2004
Test number	7-b

Constants

solids density	2475	kg/m3
pressure differential distance	0.0994	m
cell diameter	13.97	cm

Experimental

		Run			
		1	2	3	units
experimental data	tailings wet weight - total	111.0	122.6	132.9	g
	tailings wet tare	25.455	25.843	25.663	g
	tailings dry weight - total	32.8	40.6	42.6	g
	tailings dry tare	3.3	3.3	3.3	g
	tailings time	14.35	15.68	15.32	sec
	product wet weight - total	142.1	132.9	135.5	g
	product wet tare	26.396	25.840	25.814	g
	product dry weight - total	11.8	11.0	10.2	g
	product dry tare	3.3	3.3	3.3	g
	product time	6.58	6.17	6.63	sec
	feed wet weight - total	146.5	169.5	149.3	g
	feed wet tare	18.676	18.623	18.825	g
	feed dry weight - total	24.9	28.7	24.2	g
	feed dry tare	3.3	3.3	3.3	g
	feed time	5.29	6.28	5.55	sec
	pressure differential - no air	0.117	0.107	0.123	psi
		0.119	0.110	0.123	psi
		0.118	0.110	0.117	psi
	pressure differential - with air	0.088	0.101	0.106	psi
		0.090	0.100	0.106	psi
		0.091	0.000	0.104	psi
	liquid height	11.0	10.5	10.0	cm
		10.0	10.7	10.0	cm
		10.0	10.3	10.0	cm
calculated	avg pressure dif. - no air	0.118	0.109	0.121	psi
	avg pressure dif. - with air	0.090	0.101	0.105	psi
	avg liquid height	10.3	10.5	10.0	cm
	air fraction	0.157	0.046	0.086	-
	active volume	1335	1536	1401	ml
	retention time	62.6	72.1	65.9	sec
mass balanced	feed percent solids	0.068	0.072	0.070	by vol
	feed flow rate	21.32	21.29	21.25	ml/sec
	tailings percent solids	0.185	0.209	0.193	by vol
	tailings flow rate	4.94	4.87	5.53	ml/sec
	product percent solids	0.032	0.031	0.027	by vol
	product flow rate	16.38	16.42	15.72	ml/sec
	exp. rate constant	**1.28E-01**	**9.52E-02**	**9.33E-02**	**min^{-1}**

Misc experimental data

	Run			
	1	2	3	units
temp	42	42	44	F
pH	7.05	7.15	7.21	

Particle Size Data

particle size passing - (μm)	percent in channel - by number		
704	0.13	0.03	0.03
592	0.69	0.24	0.23
497.8	3.16	1.58	1.57
418.6	11.49	8.66	8.78
352	28.68	28.69	29.41
296	36.59	40.47	40.85
248.9	16.71	17.86	16.98
209.3	2.55	2.47	2.15
176	0.00	0.00	0.00
148	0.00	0.00	0.00
124.5	0.00	0.00	0.00
104.7	0.00	0.00	0.00
88	0.00	0.00	0.00
74	0.00	0.00	0.00
62.23	0.00	0.00	0.00
52.33	0.00	0.00	0.00
44	0.00	0.00	0.00
37	0.00	0.00	0.00
31.11	0.00	0.00	0.00
26.16	0.00	0.00	0.00
22	0.00	0.00	0.00

Model

		Run			
		1	2	3	units
additional experimental data	torque	11	11	11	in-lb
	impeller speed	1200			rpm
	contact angle	54	46	48	deg
	contact angle	53	51	46	deg
	contact angle	54	50	49	deg
	contact angle	48	51	49	deg
	contact angle	49	52	47	deg
	contact angle	52	53	49	deg
	contact angle	54	-	51	deg
	contact angle	-	-	-	deg
	surface tension	58.87	52.46	59.31	N/m
	zeta potential	-8.1			mV
calculated data	power	24.86	24.86	24.86	Watt
	avg contact angle	52.00	50.50	48.43	deg
	overall contact angle	50.31			deg
	overall surface tension	56.88			N/m
	sauter particle diameter	299.2	291.0	292.1	μm
	avg sauter part diameter	294.1			μm
	avg bub. sauter diameter	467.4			μm
	model rate constant	**1.04E-01**	**3.38E-02**	**4.03E-02**	**min^{-1}**

Date performed	2/27/2004
Test number	8

Constants

solids density	2475	kg/m3
pressure differential distance	0.0994	m
cell diameter	13.97	cm

Experimental

		Run			
		1	2	3	units
experimental data	tailings wet weight - total	125.4	111.6	140.6	g
	tailings wet tare	25.455	25.843	25.663	g
	tailings dry weight - total	13.4	12.4	15.0	g
	tailings dry tare	8.1	8.1	8.2	g
	tailings time	18.47	16.03	17.90	sec
	product wet weight - total	143.0	135.9	135.6	g
	product wet tare	26.396	25.840	25.814	g
	product dry weight - total	36.3	32.5	33.3	g
	product dry tare	8.2	8.1	8.2	g
	product time	6.20	5.92	5.97	sec
	feed wet weight - total	168.9	161.1	160.4	g
	feed wet tare	18.676	18.623	18.825	g
	feed dry weight - total	36.8	34.6	33.2	g
	feed dry tare	8.2	8.2	8.2	g
	feed time	6.15	5.84	5.81	sec
	pressure differential - no air	0.127	0.121	0.130	psi
		0.121	0.123	0.130	psi
		0.126	0.126	0.127	psi
	pressure differential - with air	0.090	0.100	0.093	psi
		0.088	0.102	0.093	psi
		0.088	0.099	0.091	psi
	liquid height	9.0	11.0	11.0	cm
		10.0	10.5	11.0	cm
		10.0	10.5	10.8	cm
calculated	avg pressure dif. - no air	0.125	0.123	0.129	psi
	avg pressure dif. - with air	0.089	0.100	0.092	psi
	avg liquid height	9.7	10.7	10.9	cm
	air fraction	0.246	0.157	0.250	-
	active volume	1117	1378	1257	ml
	retention time	52.1	64.2	57.3	sec
mass balanced	feed percent solids	0.089	0.084	0.082	by vol
	feed flow rate	21.43	21.47	21.95	ml/sec
	tailings percent solids	0.022	0.021	0.025	by vol
	tailings flow rate	5.28	5.20	6.21	ml/sec
	product percent solids	0.111	0.104	0.104	by vol
	product flow rate	16.15	16.27	15.74	ml/sec
	exp. rate constant	**4.37E+00**	**3.52E+00**	**3.18E+00**	**min^{-1}**

Misc experimental data

	Run			
	1	2	3	units
temp	41	42	42	F
pH	7.1	7.15	7.12	

Particle Size Data

particle size passing - (μm)	percent in channel - by number		
704	0.00		0.00
592	0.00		0.00
497.8	0.00		0.00
418.6	0.00		0.00
352	0.06		0.06
296	0.31		0.29
248.9	1.56		1.42
209.3	7.17		6.40
176	22.87		21.14
148	37.57		37.39
124.5	24.34		26.30
104.7	6.12		7.00
88	0.00		0.00
74	0.00		0.00
62.23	0.00		0.00
52.33	0.00		0.00
44	0.00		0.00
37	0.00		0.00
31.11	0.00		0.00
26.16	0.00		0.00
22	0.00		0.00

Model

		Run			
		1	2	3	units
additional experimental data	torque	10	10	10	in-lb
	impeller speed	1200			rpm
	contact angle	38	36	38	deg
	contact angle	39	38	41	deg
	contact angle	45	39	40	deg
	contact angle	46	41	39	deg
	contact angle	41	-	39	deg
	contact angle	43	-	40	deg
	contact angle	-	-	-	deg
	contact angle	-	-	-	deg
	surface tension	60.29	60.08	54.53	N/m
	zeta potential	-14.9			mV
calculated data	power	22.60	22.60	22.60	Watt
	avg contact angle	42.00	38.50	39.50	deg
	overall contact angle	40.00			deg
	overall surface tension	58.30			N/m
	sauter particle diameter	140.5		138.6	μm
	avg sauter part diameter	139.5			μm
	avg bub. sauter diameter	467.4			μm
	model rate constant	**6.76E+00**	**4.54E+00**	**7.66E+00**	**min^{-1}**

Date performed	3/17/2004
Test number	9

Constants

solids density	2475	kg/m3
pressure differential distance	0.0994	m
cell diameter	13.97	cm

Experimental

		Run			
		1	2	3	units
experimental data	tailings wet weight - total	102.2	99.3	100.8	g
	tailings wet tare	26.733	25.830	26.575	g
	tailings dry weight - total	5.4	5.4	5.6	g
	tailings dry tare	4.1	4.2	4.2	g
	tailings time	15.05	14.53	14.71	sec
	product wet weight - total	119.6	130.7	129.7	g
	product wet tare	26.455	26.544	25.937	g
	product dry weight - total	13.6	14.0	15.6	g
	product dry tare	4.2	4.2	4.2	g
	product time	5.17	5.40	5.96	sec
	feed wet weight - total	147.0	157.1	158.4	g
	feed wet tare	18.574	18.713	18.778	g
	feed dry weight - total	14.4	16.3	19.3	g
	feed dry tare	4.1	4.2	4.2	g
	feed time	5.63	6.07	6.11	sec
	pressure differential - no air	0.122	0.129	0.130	psi
		0.123	0.128	0.129	psi
		0.122	0.127	0.131	psi
	pressure differential - with air	0.072	0.091	0.089	psi
		0.072	0.090	0.090	psi
		0.071	0.087	0.089	psi
	liquid height	9.0	9.0	8.9	cm
		0.0	8.8	8.8	cm
		0.0	0.0	0.0	cm
calculated	avg pressure dif. - no air	0.122	0.128	0.130	psi
	avg pressure dif. - with air	0.072	0.089	0.089	psi
	avg liquid height	9.0	8.9	8.9	cm
	air fraction	0.354	0.270	0.284	-
	active volume	891	996	972	ml
	retention time	40.9	44.1	45.4	sec
mass balanced	feed percent solids	0.034	0.035	0.042	by vol
	feed flow rate	21.82	22.60	21.42	ml/sec
	tailings percent solids	0.007	0.007	0.008	by vol
	tailings flow rate	4.97	4.90	4.90	ml/sec
	product percent solids	0.043	0.043	0.052	by vol
	product flow rate	16.85	17.71	16.52	ml/sec
	exp. rate constant	**7.09E+00**	**6.62E+00**	**6.87E+00**	**min^{-1}**

Misc experimental data

	Run			
	1	2	3	units
temp	48	48	50	F
pH	7.4	7.53	7.62	

Particle Size Data

particle size passing - (μm)	percent in channel - by number		
704	0.00		0.00
592	0.00		0.00
497.8	0.00		0.00
418.6	0.00		0.00
352	0.00		0.00
296	0.00		0.00
248.9	0.00		0.00
209.3	0.02		0.00
176	0.06		0.03
148	0.28		0.21
124.5	1.29		1.30
104.7	5.40		6.16
88	16.94		19.24
74	31.85		33.42
62.23	28.99		27.17
52.33	12.21		10.24
44	2.96		2.23
37	0.00		0.00
31.11	0.00		0.00
26.16	0.00		0.00
22	0.00		0.00

Model

		Run			
		1	2	3	units
additional experimental data	torque	9	10	9	in-lb
	impeller speed	1200			rpm
	contact angle	39	38	35	deg
	contact angle	39	40	37	deg
	contact angle	40	37	36	deg
	contact angle	39	39	37	deg
	contact angle	41	36	-	deg
	contact angle	40	-	-	deg
	contact angle	41	-	-	deg
	contact angle	-	-	-	deg
	surface tension	59.34	56.55	55.34	N/m
	zeta potential	-16.3			mV
calculated data	power	20.34	22.60	20.34	Watt
	avg contact angle	39.86	38.00	36.25	deg
	overall contact angle	38.04			deg
	overall surface tension	57.08			N/m
	sauter particle diameter	66.3		67.5	μm
	avg sauter part diameter	66.9			μm
	avg bub. sauter diameter	467.4			μm
	model rate constant	**1.72E+01**	**1.31E+01**	**1.33E+01**	**min^{-1}**

Date performed	3/10/2004
Test number	10

Constants

solids density	2475	kg/m3
pressure differential distance	0.0994	m
cell diameter	13.97	cm

Experimental

		Run			
		1	2	3	units
experimental data	tailings wet weight - total	136.9	132.3	127.2	g
	tailings wet tare	25.455	25.843	25.663	g
	tailings dry weight - total	45.0	45.5	43.6	g
	tailings dry tare	4.3	4.2	4.3	g
	tailings time	13.82	11.87	12.45	sec
	product wet weight - total	165.3	149.7	148.5	g
	product wet tare	26.396	25.840	25.814	g
	product dry weight - total	8.2	6.9	7.4	g
	product dry tare	4.2	4.2	4.2	g
	product time	8.64	7.47	7.41	sec
	feed wet weight - total	150.6	153.7	160.3	g
	feed wet tare	18.676	18.623	18.825	g
	feed dry weight - total	26.2	25.9	28.2	g
	feed dry tare	4.3	4.2	4.2	g
	feed time	5.33	5.50	5.79	sec
	pressure differential - no air	0.133	0.132	0.142	psi
		0.129	0.132	0.143	psi
		0.131	0.133	0.136	psi
	pressure differential - with air	0.117	0.120	0.125	psi
		0.117	0.121	0.124	psi
		0.119	0.125	0.123	psi
	liquid height	10.2	12.0	12.4	cm
		10.1	12.0	12.4	cm
		10.3	11.9	12.3	cm
calculated	avg pressure dif. - no air	0.131	0.132	0.140	psi
	avg pressure dif. - with air	0.118	0.122	0.124	psi
	avg liquid height	10.2	12.0	12.4	cm
	air fraction	0.073	0.056	0.088	-
	active volume	1450	1732	1730	ml
	retention time	66.2	76.1	78.3	sec
mass balanced	feed percent solids	0.069	0.070	0.071	by vol
	feed flow rate	21.91	22.76	22.08	ml/sec
	tailings percent solids	0.200	0.208	0.215	by vol
	tailings flow rate	6.59	6.95	6.50	ml/sec
	product percent solids	0.012	0.009	0.011	by vol
	product flow rate	15.32	15.81	15.58	ml/sec
	exp. rate constant	**3.81E-02**	**2.34E-02**	**2.71E-02**	**min^{-1}**

Misc experimental data

	Run			
	1	2	3	units
temp	44	46	46	F
pH	6.56	6.75	7	

Particle Size Data

particle size passing - (μm)	percent in channel - by number		
704	0.07		0.09
592	0.38		0.51
497.8	2.09		2.67
418.6	9.62		11.02
352	28.44		29.08
296	38.93		36.94
248.9	17.79		16.92
209.3	2.68		2.77
176	0.00		0.00
148	0.00		0.00
124.5	0.00		0.00
104.7	0.00		0.00
88	0.00		0.00
74	0.00		0.00
62.23	0.00		0.00
52.33	0.00		0.00
44	0.00		0.00
37	0.00		0.00
31.11	0.00		0.00
26.16	0.00		0.00
22	0.00		0.00

Model

		Run			
		1	2	3	units
additional experimental data	torque	8	8	8	in-lb
	impeller speed	1200			rpm
	contact angle	34	40	37	deg
	contact angle	35	37	39	deg
	contact angle	36	36	41	deg
	contact angle	37	37	40	deg
	contact angle	36	37	38	deg
	contact angle	42	-	38	deg
	contact angle	42	-	-	deg
	contact angle	-	-	-	deg
	surface tension	59.78	59.73	53.9	N/m
	zeta potential	-14.0			mV
calculated data	power	18.08	18.08	18.08	Watt
	avg contact angle	37.43	37.40	38.83	deg
	overall contact angle	37.89			deg
	overall surface tension	57.80			N/m
	sauter particle diameter	293.3		297.0	μm
	avg sauter part diameter	295.2			μm
	avg bub. sauter diameter	467.4			μm
	model rate constant	**1.78E-02**	**7.41E-02**	**1.73E-01**	**min^{-1}**

Date performed	3/12/2004
Test number	11

Constants

solids density	2475	kg/m3
pressure differential distance	0.0994	m
cell diameter	13.97	cm

Experimental

		Run			
		1	2	3	units
experimental data	tailings wet weight - total	108.8	118.2	101.8	g
	tailings wet tare	25.455	25.843	25.663	g
	tailings dry weight - total	9.3	9.8	9.0	g
	tailings dry tare	4.2	4.1	4.2	g
	tailings time	15.01	15.97	14.46	sec
	product wet weight - total	152.6	146.3	143.0	g
	product wet tare	26.396	25.840	25.814	g
	product dry weight - total	33.9	31.4	29.5	g
	product dry tare	4.1	4.2	4.2	g
	product time	6.43	6.26	5.94	sec
	feed wet weight - total	166.9	175.2	163.6	g
	feed wet tare	18.676	18.623	18.825	g
	feed dry weight - total	33.2	34.7	32.0	g
	feed dry tare	4.2	4.1	4.2	g
	feed time	5.68	6.08	5.61	sec
	pressure differential - no air	0.140	0.128	0.138	psi
		0.139	0.133	0.138	psi
		0.135	0.129	0.139	psi
	pressure differential - with air	0.088	0.100	0.097	psi
		0.081	0.096	0.097	psi
		0.083	0.100	0.097	psi
	liquid height	9.0	9.0	9.0	cm
		9.0	8.6	9.2	cm
		8.5	8.8	9.0	cm
calculated	avg pressure dif. - no air	0.138	0.130	0.138	psi
	avg pressure dif. - with air	0.084	0.099	0.097	psi
	avg liquid height	8.8	8.8	9.1	cm
	air fraction	0.366	0.213	0.281	-
	active volume	858	1062	1000	ml
	retention time	38.1	47.3	44.4	sec
mass balanced	feed percent solids	0.090	0.087	0.085	by vol
	feed flow rate	22.52	22.45	22.51	ml/sec
	tailings percent solids	0.026	0.026	0.026	by vol
	tailings flow rate	5.39	5.57	5.07	ml/sec
	product percent solids	0.110	0.107	0.102	by vol
	product flow rate	17.13	16.88	17.45	ml/sec
	exp. rate constant	**5.11E+00**	**3.94E+00**	**4.06E+00**	**min^{-1}**

Misc experimental data

	Run			
	1	2	3	units
temp	46	48	48	F
pH	7.42	7.62	7.64	

Particle Size Data

particle size passing - (μm)	percent in channel - by number		
704	0.00		0.00
592	0.00		0.00
497.8	0.00		0.00
418.6	0.00		0.01
352	0.06		0.07
296	0.31		0.35
248.9	1.56		1.70
209.3	7.05		7.35
176	22.26		22.63
148	37.02		37.01
124.5	24.99		24.50
104.7	6.75		6.38
88	0.00		0.00
74	0.00		0.00
62.23	0.00		0.00
52.33	0.00		0.00
44	0.00		0.00
37	0.00		0.00
31.11	0.00		0.00
26.16	0.00		0.00
22	0.00		0.00

Model

		Run			
		1	2	3	units
additional experimental data	torque	8	8	8	in-lb
	impeller speed	1200			rpm
	contact angle	27	29	29	deg
	contact angle	36	31	32	deg
	contact angle	27	35	29	deg
	contact angle	32	29	30	deg
	contact angle	35	30	31	deg
	contact angle	31	32	31	deg
	contact angle	-	-	-	deg
	contact angle	-	-	-	deg
	surface tension	54.83	61.31	61.32	N/m
	zeta potential	-19.7			mV
calculated data	power	18.08	18.08	18.08	Watt
	avg contact angle	31.33	31.00	30.33	deg
	overall contact angle	30.89			deg
	overall surface tension	59.15			N/m
	sauter particle diameter	139.8		140.6	μm
	avg sauter part diameter	140.2			μm
	avg bub. sauter diameter	467.4			μm
	model rate constant	**5.12E+00**	**2.77E+00**	**3.85E+00**	**min^{-1}**

Date performed	3/11/2004
Test number	12

Constants

solids density	2475	kg/m3
pressure differential distance	0.0994	m
cell diameter	13.97	cm

Experimental

		Run			
		1	2	3	units
experimental data	tailings wet weight - total	110.1	118.2	147.3	g
	tailings wet tare	26.733	25.830	26.569	g
	tailings dry weight - total	6.6	6.6	7.4	g
	tailings dry tare	4.2	4.2	4.2	g
	tailings time	14.66	15.06	20.37	sec
	product wet weight - total	133.6	143.2	127.7	g
	product wet tare	26.455	26.544	25.937	g
	product dry weight - total	29.5	27.2	23.6	g
	product dry tare	4.2	4.1	4.2	g
	product time	5.42	6.00	5.31	sec
	feed wet weight - total	173.0	150.7	165.5	g
	feed wet tare	18.574	18.713	18.778	g
	feed dry weight - total	32.3	25.8	27.7	g
	feed dry tare	4.1	4.2	4.1	g
	feed time	6.09	5.19	5.82	sec
	pressure differential - no air	0.131	0.132	0.119	psi
		0.133	0.132	0.120	psi
		0.134	0.133	0.119	psi
	pressure differential - with air	0.105	0.106	0.107	psi
		0.105	0.107	0.107	psi
		0.104	0.107	0.108	psi
	liquid height	9.5	9.7	10.0	cm
		10.0	9.5	10.2	cm
		0.0	0.0	0.0	cm
calculated	avg pressure dif. - no air	0.133	0.132	0.119	psi
	avg pressure dif. - with air	0.105	0.107	0.107	psi
	avg liquid height	9.8	9.6	10.1	cm
	air fraction	0.194	0.178	0.083	-
	active volume	1204	1209	1419	ml
	retention time	53.4	52.3	62.1	sec
mass balanced	feed percent solids	0.084	0.071	0.069	by vol
	feed flow rate	22.56	23.13	22.85	ml/sec
	tailings percent solids	0.012	0.011	0.011	by vol
	tailings flow rate	5.62	6.00	5.79	ml/sec
	product percent solids	0.109	0.093	0.089	by vol
	product flow rate	16.94	17.14	17.06	ml/sec
	exp. rate constant	**7.84E+00**	**7.39E+00**	**5.84E+00**	**min^{-1}**

Misc experimental data

	Run			
	1	2	3	units
temp	46	46	48	F
pH	7.38	7.52	7.53	

Particle Size Data

particle size passing - (μm)	percent in channel - by number		
704	0.00		0.00
592	0.00		0.00
497.8	0.00		0.00
418.6	0.00		0.00
352	0.00		0.00
296	0.00		0.00
248.9	0.00		0.00
209.3	0.02		0.03
176	0.08		0.09
148	0.32		0.39
124.5	1.37		1.62
104.7	5.51		6.21
88	16.82		17.97
74	31.44		31.64
62.23	28.90		27.56
52.33	12.45		11.53
44	3.09		2.96
37	0.00		0.00
31.11	0.00		0.00
26.16	0.00		0.00
22	0.00		0.00

Model

		Run			
		1	2	3	units
additional experimental data	torque	8	8	8	in-lb
	impeller speed	1200			rpm
	contact angle	27	32	29	deg
	contact angle	30	30	30	deg
	contact angle	26	29	31	deg
	contact angle	30	34	31	deg
	contact angle	33	30	30	deg
	contact angle	31	36	30	deg
	contact angle	-	-	-	deg
	contact angle	-	-	-	deg
	surface tension	57.28	60.98	59.76	N/m
	zeta potential	-18.8			mV
calculated data	power	18.08	18.08	18.08	Watt
	avg contact angle	29.50	31.83	30.17	deg
	overall contact angle	30.50			deg
	overall surface tension	59.34			N/m
	sauter particle diameter	66.3		67.2	μm
	avg sauter part diameter	66.8			μm
	avg bub. sauter diameter	467.4			μm
	model rate constant	**5.63E+00**	**5.16E+00**	**2.34E+00**	**min^{-1}**

Date performed	3/8/2004
Test number	13

Constants

solids density	2475	kg/m3
pressure differential distance	0.0994	m
cell diameter	13.97	cm

Experimental

		Run			
		1	2	3	units
experimental data	tailings wet weight - total	131.2	142.9	143.2	g
	tailings wet tare	26.077	26.182	26.387	g
	tailings dry weight - total	46.8	53.5	53.5	g
	tailings dry tare	3.3	3.3	3.3	g
	tailings time	13.03	14.27	14.17	sec
	product wet weight - total	158.5	163.9	163.2	g
	product wet tare	25.387	25.422	25.035	g
	product dry weight - total	6.5	6.3	6.2	g
	product dry tare	3.3	3.3	3.2	g
	product time	8.26	8.58	8.66	sec
	feed wet weight - total	151.9	159.6	164.8	g
	feed wet tare	18.871	18.429	18.360	g
	feed dry weight - total	25.8	26.9	27.9	g
	feed dry tare	3.3	3.3	3.3	g
	feed time	5.35	5.78	5.93	sec
	pressure differential - no air	0.116	0.117	0.122	psi
		0.118	0.117	0.120	psi
		0.117	0.115	0.121	psi
	pressure differential - with air	0.094	0.099	0.099	psi
		0.095	0.099	0.104	psi
		0.094	0.098	0.097	psi
	liquid height	9.0	9.0	9.2	cm
		9.7	9.5	9.4	cm
		9.5	9.5	9.1	cm
calculated	avg pressure dif. - no air	0.117	0.116	0.121	psi
	avg pressure dif. - with air	0.094	0.099	0.100	psi
	avg liquid height	9.4	9.3	9.2	cm
	air fraction	0.119	0.092	0.110	-
	active volume	1269	1299	1260	ml
	retention time	57.8	59.3	57.5	sec
mass balanced	feed percent solids	0.073	0.074	0.074	by vol
	feed flow rate	21.94	21.92	21.92	ml/sec
	tailings percent solids	0.230	0.238	0.238	by vol
	tailings flow rate	6.26	6.16	6.23	ml/sec
	product percent solids	0.010	0.009	0.009	by vol
	product flow rate	15.68	15.76	15.69	ml/sec
	exp. rate constant	**3.21E-02**	**2.77E-02**	**2.78E-02**	**min^{-1}**

Misc experimental data

	Run			
	1	2	3	units
temp	46	46	48	F
pH	7.18	7.34	7.39	

Particle Size Data

particle size passing - (μm)	percent in channel - by number		
704	0.17		0.07
592	0.89		0.42
497.8	3.53		2.21
418.6	11.21		9.82
352	26.51		28.28
296	35.74		38.26
248.9	18.67		18.00
209.3	3.28		2.94
176	0.00		0.00
148	0.00		0.00
124.5	0.00		0.00
104.7	0.00		0.00
88	0.00		0.00
74	0.00		0.00
62.23	0.00		0.00
52.33	0.00		0.00
44	0.00		0.00
37	0.00		0.00
31.11	0.00		0.00
26.16	0.00		0.00
22	0.00		0.00

Model

		Run			
		1	2	3	units
additional experimental data	torque	13	13	13	in-lb
	impeller speed	1200			rpm
	contact angle	37	39	39	deg
	contact angle	37	38	39	deg
	contact angle	41	39	39	deg
	contact angle	41	40	40	deg
	contact angle	42	43	40	deg
	contact angle	-	-	-	deg
	contact angle	-	-	-	deg
	contact angle	-	-	-	deg
	surface tension	60.44	54.52	57.64	N/m
	zeta potential	-11.3			mV
calculated data	power	29.38	29.38	29.38	Watt
	avg contact angle	39.60	39.80	39.40	deg
	overall contact angle	39.60			deg
	overall surface tension	57.53			N/m
	sauter particle diameter	297.7		293.5	μm
	avg sauter part diameter	295.6			μm
	avg bub. sauter diameter	467.4			μm
	model rate constant	**7.05E-03**	**5.05E-03**	**5.49E-03**	**min^{-1}**

Date performed	3/4/2004
Test number	14

Constants

solids density	2475	kg/m3
pressure differential distance	0.0994	m
cell diameter	13.97	cm

Experimental

		Run			
		1	2	3	units
experimental data	tailings wet weight - total	95.0	101.8	101.2	g
	tailings wet tare	25.455	25.843	25.663	g
	tailings dry weight - total	10.3	10.7	11.7	g
	tailings dry tare	3.2	3.3	3.2	g
	tailings time	14.07	14.68	15.04	sec
	product wet weight - total	157.6	159.2	159.1	g
	product wet tare	26.396	25.840	25.814	g
	product dry weight - total	33.4	33.3	32.1	g
	product dry tare	3.3	3.2	3.3	g
	product time	6.24	6.18	6.36	sec
	feed wet weight - total	159.3	170.1	168.9	g
	feed wet tare	18.676	18.623	18.825	g
	feed dry weight - total	32.1	33.7	32.1	g
	feed dry tare	3.2	3.3	3.3	g
	feed time	5.36	5.75	5.90	sec
	pressure differential - no air	0.124	0.110	0.116	psi
		0.125	0.109	0.117	psi
		0.129	0.111	0.120	psi
	pressure differential - with air	0.084	0.081	0.079	psi
		0.080	0.081	0.080	psi
		0.082	0.080	0.078	psi
	liquid height	11.0	12.0	11.5	cm
		10.5	11.8	11.3	cm
		10.5	11.0	11.2	cm
calculated	avg pressure dif. - no air	0.126	0.110	0.118	psi
	avg pressure dif. - with air	0.082	0.081	0.079	psi
	avg liquid height	10.7	11.6	11.3	cm
	air fraction	0.292	0.195	0.255	-
	active volume	1158	1431	1295	ml
	retention time	50.6	61.2	56.9	sec
mass balanced	feed percent solids	0.094	0.092	0.089	by vol
	feed flow rate	22.89	23.41	22.76	ml/sec
	tailings percent solids	0.043	0.042	0.048	by vol
	tailings flow rate	4.65	4.86	4.68	ml/sec
	product percent solids	0.107	0.105	0.099	by vol
	product flow rate	18.24	18.54	18.08	ml/sec
	exp. rate constant	**2.34E+00**	**1.96E+00**	**1.71E+00**	**min^{-1}**

Misc experimental data

	Run			
	1	2	3	units
temp	46	46	48	F
pH	7.57	7.67	7.56	

Particle Size Data

particle size passing - (μm)	percent in channel - by number		
704	0.00		0.00
592	0.00		0.00
497.8	0.00		0.00
418.6	0.01		0.00
352	0.07		0.06
296	0.35		0.30
248.9	1.73		1.51
209.3	7.60		6.89
176	23.24		22.23
148	37.09		37.52
124.5	23.84		25.08
104.7	6.07		6.41
88	0.00		0.00
74	0.00		0.00
62.23	0.00		0.00
52.33	0.00		0.00
44	0.00		0.00
37	0.00		0.00
31.11	0.00		0.00
26.16	0.00		0.00
22	0.00		0.00

Model

		Run			
		1	2	3	units
additional experimental data	torque	11	11	11	in-lb
	impeller speed	1500			rpm
	contact angle	28	35	33	deg
	contact angle	28	32	34	deg
	contact angle	28	33	34	deg
	contact angle	35	32	36	deg
	contact angle	32	-	38	deg
	contact angle	-	-	37	deg
	contact angle	-	-	-	deg
	contact angle	-	-	-	deg
	surface tension	60.84	60.65	61.59	N/m
	zeta potential	-15.8			mV
calculated data	power	31.07	31.07	31.07	Watt
	avg contact angle	30.20	33.00	35.33	deg
	overall contact angle	32.84			deg
	overall surface tension	61.03			N/m
	sauter particle diameter	141.2		139.8	μm
	avg sauter part diameter	140.5			μm
	avg bub. sauter diameter	467.4			μm
	model rate constant	**2.75E+00**	**1.91E+00**	**2.51E+00**	**min^{-1}**

Date performed	3/9/2004
Test number	15

Constants

solids density	2475	kg/m3
pressure differential distance	0.0994	m
cell diameter	13.97	cm

Experimental

		Run			
		1	2	3	units
experimental data	tailings wet weight - total	111.0	107.1	114.2	g
	tailings wet tare	26.733	25.830	26.569	g
	tailings dry weight - total	7.7	8.0	8.1	g
	tailings dry tare	3.3	4.2	4.2	g
	tailings time	16.98	14.74	15.73	sec
	product wet weight - total	139.1	137.0	156.6	g
	product wet tare	26.455	26.544	25.937	g
	product dry weight - total	29.1	26.3	29.7	g
	product dry tare	4.2	4.2	4.2	g
	product time	5.71	5.72	6.66	sec
	feed wet weight - total	156.5	166.3	169.6	g
	feed wet tare	18.574	18.713	18.778	g
	feed dry weight - total	30.3	29.6	29.0	g
	feed dry tare	4.3	4.3	4.2	g
	feed time	5.35	5.88	6.04	sec
	pressure differential - no air	0.123	0.106	0.121	psi
		0.125	0.104	0.124	psi
		0.000	0.101	0.124	psi
	pressure differential - with air	0.083	0.082	0.082	psi
		0.084	0.082	0.082	psi
		0.084	0.082	0.078	psi
	liquid height	11.0	11.0	11.5	cm
		10.7	11.2	10.5	cm
		0.0	0.0	10.8	cm
calculated	avg pressure dif. - no air	0.124	0.104	0.123	psi
	avg pressure dif. - with air	0.084	0.082	0.081	psi
	avg liquid height	10.9	11.1	10.9	cm
	air fraction	0.276	0.149	0.291	-
	active volume	1205	1449	1189	ml
	retention time	54.0	64.5	52.4	sec
mass balanced	feed percent solids	0.086	0.076	0.073	by vol
	feed flow rate	22.30	22.45	22.68	ml/sec
	tailings percent solids	0.022	0.019	0.019	by vol
	tailings flow rate	4.83	5.35	5.40	ml/sec
	product percent solids	0.103	0.094	0.090	by vol
	product flow rate	17.47	17.10	17.28	ml/sec
	exp. rate constant	**4.10E+00**	**3.41E+00**	**4.24E+00**	**min^{-1}**

Misc experimental data

	Run			
	1	2	3	units
temp	46	46	48	F
pH	7.63	7.61	7.68	

Particle Size Data

particle size passing - (μm)	percent in channel - by number		
704	0.00		0.00
592	0.00		0.00
497.8	0.00		0.00
418.6	0.00		0.00
352	0.00		0.00
296	0.00		0.00
248.9	0.00		0.00
209.3	0.02		0.02
176	0.07		0.07
148	0.29		0.27
124.5	1.26		1.19
104.7	4.99		4.82
88	15.40		15.21
74	30.05		30.08
62.23	29.83		30.06
52.33	14.21		14.34
44	3.88		3.94
37	0.00		0.00
31.11	0.00		0.00
26.16	0.00		0.00
22	0.00		0.00

Model

		Run			
		1	2	3	units
additional experimental data	torque	12	11	11	in-lb
	impeller speed	1200			rpm
	contact angle	32	32	33	deg
	contact angle	29	29	32	deg
	contact angle	31	29	30	deg
	contact angle	32	28	33	deg
	contact angle	30	30	32	deg
	contact angle	30	34	33	deg
	contact angle	-	-	-	deg
	contact angle	-	-	-	deg
	surface tension	61.08	60.65	60.3	N/m
	zeta potential	-17.6			mV
calculated data	power	27.12	24.86	24.86	Watt
	avg contact angle	30.67	30.33	32.17	deg
	overall contact angle	31.06			deg
	overall surface tension	60.68			N/m
	sauter particle diameter	65.2		65.1	μm
	avg sauter part diameter	65.2			μm
	avg bub. sauter diameter	467.4			μm
	model rate constant	**3.91E+00**	**1.95E+00**	**4.05E+00**	**min^{-1}**

Date performed	3/2/2004
Test number	16

Constants

solids density	2475	kg/m3
pressure differential distance	0.0994	m
cell diameter	13.97	cm

Experimental

		Run			
		1	2	3	units
experimental data	tailings wet weight - total	117.8	117.6	123.9	g
	tailings wet tare	26.077	25.982	26.387	g
	tailings dry weight - total	26.1	31.9	35.2	g
	tailings dry tare	3.3	3.3	3.3	g
	tailings time	14.82	14.95	15.60	sec
	product wet weight - total	160.0	151.9	141.7	g
	product wet tare	25.387	25.422	25.035	g
	product dry weight - total	6.2	4.9	4.8	g
	product dry tare	3.3	3.3	3.3	g
	product time	7.61	7.03	6.61	sec
	feed wet weight - total	154.9	149.5	162.2	g
	feed wet tare	18.871	18.429	18.360	g
	feed dry weight - total	16.2	16.9	18.7	g
	feed dry tare	3.3	3.3	3.3	g
	feed time	5.65	5.44	6.00	sec
	pressure differential - no air	0.110	0.124	0.123	psi
		0.106	0.125	0.126	psi
		0.109	0.119	0.124	psi
	pressure differential - with air	0.097	0.101	0.108	psi
		0.097	0.101	0.106	psi
		0.098	0.102	0.106	psi
	liquid height	10.0	11.5	10.0	cm
		10.0	11.0	9.8	cm
		10.5	10.8	9.5	cm
calculated	avg pressure dif. - no air	0.108	0.123	0.124	psi
	avg pressure dif. - with air	0.097	0.101	0.107	psi
	avg liquid height	10.2	11.1	9.8	cm
	air fraction	0.066	0.121	0.100	-
	active volume	1456	1495	1348	ml
	retention time	65.0	66.7	60.5	sec
mass balanced	feed percent solids	0.037	0.042	0.044	by vol
	feed flow rate	22.39	22.42	22.27	ml/sec
	tailings percent solids	0.124	0.163	0.171	by vol
	tailings flow rate	5.51	5.19	5.19	ml/sec
	product percent solids	0.009	0.005	0.005	by vol
	product flow rate	16.88	17.24	17.08	ml/sec
	exp. rate constant	**4.96E-02**	**2.18E-02**	**2.43E-02**	**min^{-1}**

Misc experimental data

	Run			
	1	2	3	units
temp	44	46	46	F
pH	7.22	7.36	7.45	

Particle Size Data

particle size passing - (μm)	percent in channel - by number		
704	0.10		0.08
592	0.53		0.47
497.8	2.54		2.58
418.6	10.06		11.13
352	27.45		30.50
296	37.89		38.02
248.9	18.49		15.26
209.3	2.94		1.96
176	0.00		0.00
148	0.00		0.00
124.5	0.00		0.00
104.7	0.00		0.00
88	0.00		0.00
74	0.00		0.00
62.23	0.00		0.00
52.33	0.00		0.00
44	0.00		0.00
37	0.00		0.00
31.11	0.00		0.00
26.16	0.00		0.00
22	0.00		0.00

Model

		Run			
		1	2	3	units
additional experimental data	torque	11	11	11	in-lb
	impeller speed	1200			rpm
	contact angle	42	44	48	deg
	contact angle	42	43	44	deg
	contact angle	43	39	44	deg
	contact angle	48	42	44	deg
	contact angle	43	43	43	deg
	contact angle	-	43	45	deg
	contact angle	-	-	44	deg
	contact angle	-	-	-	deg
	surface tension	57.22	57.35	58.88	N/m
	zeta potential	-8.9			mV
calculated data	power	24.86	24.86	24.86	Watt
	avg contact angle	43.60	42.33	44.57	deg
	overall contact angle	43.50			deg
	overall surface tension	57.82			N/m
	sauter particle diameter	294.1		298.9	μm
	avg sauter part diameter	296.5			μm
	avg bub. sauter diameter	467.4			μm
	model rate constant	**1.66E-02**	**7.84E-02**	**1.73E-02**	**min^{-1}**

Date performed	3/3/2004
Test number	17

Constants

solids density	2475	kg/m3
pressure differential distance	0.0994	m
cell diameter	13.97	cm

Experimental

		Run			
		1	2	3	units
experimental data	tailings wet weight - total	103.2	120.9	97.3	g
	tailings wet tare	26.733	25.830	26.570	g
	tailings dry weight - total	5.4	6.7	5.8	g
	tailings dry tare	3.3	3.3	3.3	g
	tailings time	14.69	13.64	13.62	sec
	product wet weight - total	143.7	131.7	137.6	g
	product wet tare	26.455	26.544	25.937	g
	product dry weight - total	19.0	18.1	17.4	g
	product dry tare	3.3	3.3	3.2	g
	product time	5.96	6.13	5.82	sec
	feed wet weight - total	169.0	143.7	138.0	g
	feed wet tare	18.574	18.713	18.778	g
	feed dry weight - total	20.6	16.9	16.6	g
	feed dry tare	3.2	3.2	3.2	g
	feed time	6.06	5.11	4.90	sec
	pressure differential - no air	0.116	0.110	0.122	psi
		0.117	0.115	0.124	psi
		0.116	0.110	0.125	psi
	pressure differential - with air	0.088	0.088	0.088	psi
		0.085	0.088	0.086	psi
		0.083	0.088	0.085	psi
	liquid height	10.0	10.2	10.5	cm
		9.9	10.4	10.4	cm
		10.0	10.4	10.8	cm
calculated	avg pressure dif. - no air	0.116	0.112	0.124	psi
	avg pressure dif. - with air	0.085	0.088	0.086	psi
	avg liquid height	10.0	10.3	10.6	cm
	air fraction	0.215	0.163	0.258	-
	active volume	1199	1325	1202	ml
	retention time	51.7	58.5	52.7	sec
mass balanced	feed percent solids	0.049	0.048	0.047	by vol
	feed flow rate	23.20	22.64	22.80	ml/sec
	tailings percent solids	0.012	0.015	0.014	by vol
	tailings flow rate	5.10	6.86	5.06	ml/sec
	product percent solids	0.060	0.062	0.057	by vol
	product flow rate	18.10	15.78	17.74	ml/sec
	exp. rate constant	**4.62E+00**	**2.99E+00**	**3.49E+00**	**min^{-1}**

Misc experimental data

	Run			
	1	2	3	units
temp	42	44	46	F
pH	7.37	7.4	7.43	

Particle Size Data

particle size passing - (μm)	percent in channel - by number		
704	0.00		0.00
592	0.00		0.00
497.8	0.00		0.00
418.6	0.00		0.00
352	0.00		0.05
296	0.05		0.27
248.9	0.58		1.39
209.3	5.25		6.66
176	25.28		22.44
148	44.44		38.52
124.5	21.34		24.83
104.7	3.06		5.84
88	0.00		0.00
74	0.00		0.00
62.23	0.00		0.00
52.33	0.00		0.00
44	0.00		0.00
37	0.00		0.00
31.11	0.00		0.00
26.16	0.00		0.00
22	0.00		0.00

Model

		Run			
		1	2	3	units
additional experimental data	torque	10	10	10	in-lb
	impeller speed	1200			rpm
	contact angle	41	40	38	deg
	contact angle	39	40	36	deg
	contact angle	40	43	36	deg
	contact angle	39	41	38	deg
	contact angle	39	41	39	deg
	contact angle	42	-	38	deg
	contact angle	-	-	-	deg
	contact angle	-	-	-	deg
	surface tension	59.11	59.29	59.59	N/m
	zeta potential	-16.0			mV
calculated data	power	22.60	22.60	22.60	Watt
	avg contact angle	40.00	41.00	37.50	deg
	overall contact angle	39.50			deg
	overall surface tension	59.33			N/m
	sauter particle diameter	140.5		139.8	μm
	avg sauter part diameter	140.2			μm
	avg bub. sauter diameter	467.4			μm
	model rate constant	**5.83E+00**	**4.46E+00**	**7.51E+00**	**min^{-1}**

Date performed	3/15/2004
Test number	18

Constants

solids density	2475	kg/m3
pressure differential distance	0.0994	m
cell diameter	13.97	cm

Experimental

		Run			
		1	2	3	units
experimental data	tailings wet weight - total	111.5	97.9	100.5	g
	tailings wet tare	26.077	25.982	26.387	g
	tailings dry weight - total	6.3	6.0	5.8	g
	tailings dry tare	4.2	4.1	4.2	g
	tailings time	16.23	13.71	14.40	sec
	product wet weight - total	123.6	123.6	143.6	g
	product wet tare	25.387	25.422	25.035	g
	product dry weight - total	16.8	15.4	16.1	g
	product dry tare	4.1	4.2	4.1	g
	product time	5.25	5.05	6.40	sec
	feed wet weight - total	136.9	139.4	161.6	g
	feed wet tare	18.871	18.429	18.360	g
	feed dry weight - total	17.8	15.1	17.0	g
	feed dry tare	4.2	4.1	4.2	g
	feed time	4.76	4.97	6.04	sec
	pressure differential - no air	0.127	0.125	0.119	psi
		0.120	0.120	0.123	psi
		0.123	0.122	0.124	psi
	pressure differential - with air	0.087	0.086	0.087	psi
		0.087	0.084	0.085	psi
		0.084	0.085	0.083	psi
	liquid height	9.0	9.5	10.0	cm
		9.5	10.0	10.2	cm
		0.0	0.0	0.0	cm
calculated	avg pressure dif. - no air	0.123	0.122	0.122	psi
	avg pressure dif. - with air	0.086	0.085	0.085	psi
	avg liquid height	9.3	9.8	10.1	cm
	air fraction	0.259	0.259	0.258	-
	active volume	1050	1107	1149	ml
	retention time	46.3	47.7	51.1	sec
mass balanced	feed percent solids	0.050	0.041	0.038	by vol
	feed flow rate	22.70	23.18	22.47	ml/sec
	tailings percent solids	0.010	0.010	0.009	by vol
	tailings flow rate	5.20	5.16	5.08	ml/sec
	product percent solids	0.062	0.050	0.047	by vol
	product flow rate	17.49	18.02	17.40	ml/sec
	exp. rate constant	**6.00E+00**	**4.70E+00**	**4.80E+00**	**min^{-1}**

Misc experimental data

	Run			
	1	2	3	units
temp	46	48	48	F
pH	7.65	7.68	7.71	

Particle Size Data

particle size passing - (μm)	percent in channel - by number		
704	0.00	0.00	0.00
592	0.00	0.00	0.00
497.8	0.00	0.00	0.00
418.6	0.00	0.00	0.00
352	0.00	0.00	0.00
296	0.00	0.00	0.00
248.9	0.00	0.01	0.00
209.3	0.03	0.03	0.00
176	0.10	0.10	0.00
148	0.38	0.37	0.20
124.5	1.53	1.51	1.39
104.7	5.75	5.72	6.89
88	16.80	16.85	21.08
74	30.89	30.91	34.21
62.23	28.63	28.54	25.48
52.33	12.65	12.66	8.87
44	3.24	3.30	1.88
37	0.00	0.00	0.00
31.11	0.00	0.00	0.00
26.16	0.00	0.00	0.00
22	0.00	0.00	0.00

Model

		Run			
		1	2	3	units
additional experimental data	torque	10	10	10	in-lb
	impeller speed	1200			rpm
	contact angle	30	35	27	deg
	contact angle	29	40	31	deg
	contact angle	36	30	29	deg
	contact angle	32	36	31	deg
	contact angle	31	37	33	deg
	contact angle	-	40	-	deg
	contact angle	-	35	-	deg
	contact angle	-	-	-	deg
	surface tension	60.8	60.43	60.26	N/m
	zeta potential	-13.2			mV
calculated data	power	22.60	22.60	22.60	Watt
	avg contact angle	31.60	36.14	30.20	deg
	overall contact angle	32.65			deg
	overall surface tension	60.50			N/m
	sauter particle diameter	66.5	66.5	68.5	μm
	avg sauter part diameter	67.2			μm
	avg bub. sauter diameter	467.4			μm
	model rate constant	**6.63E+00**	**6.68E+00**	**6.66E+00**	**min^{-1}**

Date performed	2/2/2004
Test number	19-a

Constants

solids density	2475	kg/m3
pressure differential distance	0.0994	m
cell diameter	13.97	cm

Experimental

		Run			
		1	2	3	units
experimental data	tailings wet weight - total	255.7	245.5	256.2	g
	tailings wet tare	26.077	25.982	26.387	g
	tailings dry weight - total	89.7	64.5	65.7	g
	tailings dry tare	8.4	8.6	8.5	g
	tailings time	14.43	11.76	11.72	sec
	product wet weight - total	148.6	158.4	134.2	g
	product wet tare	18.412	18.308	18.102	g
	product dry weight - total	25.3	27.9	19.8	g
	product dry tare	8.5	8.8	8.9	g
	product time	15.42	22.95	22.68	sec
	feed wet weight - total	215.3	231.5	243.6	g
	feed wet tare	25.846	25.543	25.293	g
	feed dry weight - total	52.4	55.3	56.0	g
	feed dry tare	8.6	8.6	8.6	g
	feed time	7.74	8.11	9.09	sec
	pressure differential - no air	0.179	0.171	0.178	psi
		-	0.176	0.181	psi
		-	0.168	0.177	psi
	pressure differential - with air	0.169	0.159	0.160	psi
		0.157	0.162	0.160	psi
		0.161	0.157	0.158	psi
	liquid height	14.3	14.6	14.0	cm
		14.2	14.7	14.2	cm
		-	-	-	cm
calculated	avg pressure dif. - no air	0.179	0.172	0.179	psi
	avg pressure dif. - with air	0.162	0.159	0.159	psi
	avg liquid height	14.3	14.7	14.1	cm
	air fraction	0.095	0.074	0.116	-
	active volume	1977	2080	1910	ml
	retention time	96.4	96.1	89.8	sec
mass balanced	feed percent solids	0.120	0.106	0.101	by vol
	feed flow rate	20.51	21.64	21.28	ml/sec
	tailings percent solids	0.162	0.122	0.118	by vol
	tailings flow rate	12.45	16.01	16.47	ml/sec
	product percent solids	0.055	0.060	0.040	by vol
	product flow rate	8.06	5.63	4.81	ml/sec
	exp. rate constant	**8.36E-02**	**8.01E-02**	**5.14E-02**	**min^{-1}**

Misc experimental data

	Run			
	1	2	3	units
temp	46	48	48	F
pH	6.91	7.21	7.53	

Particle Size Data

particle size passing - (μm)	percent in channel - by number		
704	0.11		0.16
592	0.60		0.82
497.8	2.83		3.28
418.6	10.75		10.68
352	27.89		26.14
296	37.02		36.39
248.9	17.87		19.23
209.3	2.93		3.30
176	0.00		0.00
148	0.00		0.00
124.5	0.00		0.00
104.7	0.00		0.00
88	0.00		0.00
74	0.00		0.00
62.23	0.00		0.00
52.33	0.00		0.00
44	0.00		0.00
37	0.00		0.00
31.11	0.00		0.00
26.16	0.00		0.00
22	0.00		0.00

Model

		Run			
		1	2	3	units
additional experimental data	torque	13	12	13	in-lb
	impeller speed	1200			rpm
	contact angle	45	50	50	deg
	contact angle	48	46	49	deg
	contact angle	47	42	50	deg
	contact angle	47	48	48	deg
	contact angle	-	-	52	deg
	contact angle	-	-	46	deg
	contact angle	-	-	-	deg
	contact angle	-	-	-	deg
	surface tension	60.4	60.6	60.39	N/m
	zeta potential	-15.0			mV
calculated data	power	29.38	27.12	29.38	Watt
	avg contact angle	46.75	46.50	49.17	deg
	overall contact angle	47.47			deg
	overall surface tension	60.46			N/m
	sauter particle diameter	296.2		295.9	μm
	avg sauter part diameter	296.1			μm
	avg bub. sauter diameter	467.4			μm
	model rate constant	**2.10E+00**	**2.33E+00**	**2.24E+00**	**min^{-1}**

Date performed	2/16/2004
Test number	19-b

Constants

solids density	2475	kg/m3
pressure differential distance	0.0994	m
cell diameter	13.97	cm

Experimental

		Run			
		1	2	3	units
experimental data	tailings wet weight - total	266.8	205.2	181.7	g
	tailings wet tare	26.733	25.830	26.569	g
	tailings dry weight - total	74.9	70.3	62.4	g
	tailings dry tare	8.7	8.4	8.4	g
	tailings time	12.26	16.54	14.86	sec
	product wet weight - total	126.3	94.9	84.7	g
	product wet tare	18.860	18.683	18.741	g
	product dry weight - total	12.8	12.2	9.7	g
	product dry tare	8.3	8.3	8.2	g
	product time	18.90	8.03	6.77	sec
	feed wet weight - total	232.1	230.2	215.6	g
	feed wet tare	26.169	26.574	25.974	g
	feed dry weight - total	56.8	57.6	53.6	g
	feed dry tare	8.3	8.5	8.4	g
	feed time	8.67	8.50	8.06	sec
	pressure differential - no air	0.134	0.132	0.175	psi
		0.132	0.127	0.171	psi
		0.133	0.130	0.172	psi
	pressure differential - with air	0.117	0.107	0.100	psi
		0.114	0.106	0.127	psi
		0.115	0.108	0.127	psi
	liquid height	13.8	14.2	13.7	cm
		14.0	14.5	14.0	cm
		14.0	14.7	14.0	cm
calculated	avg pressure dif. - no air	0.133	0.130	0.173	psi
	avg pressure dif. - with air	0.115	0.107	0.118	psi
	avg liquid height	13.9	14.5	13.9	cm
	air fraction	0.104	0.125	0.300	-
	active volume	1914	1940	1492	ml
	retention time	89.7	104.6	80.8	sec
mass balanced	feed percent solids	0.107	0.104	0.099	by vol
	feed flow rate	21.33	18.54	18.47	ml/sec
	tailings percent solids	0.137	0.187	0.194	by vol
	tailings flow rate	15.90	9.22	8.94	ml/sec
	product percent solids	0.017	0.021	0.009	by vol
	product flow rate	5.44	9.31	9.52	ml/sec
	exp. rate constant	**2.16E-02**	**3.24E-02**	**1.81E-02**	**min^{-1}**

Misc experimental data

	Run			
	1	2	3	units
temp	44	44	46	F
pH	6.99	7.19	7.24	

Particle Size Data

particle size passing - (μm)	percent in channel - by number		
704	0.08		0.10
592	0.46		0.57
497.8	2.25		2.70
418.6	9.11		10.37
352	26.39		27.50
296	39.20		37.53
248.9	19.63		18.34
209.3	2.88		2.89
176	0.00		0.00
148	0.00		0.00
124.5	0.00		0.00
104.7	0.00		0.00
88	0.00		0.00
74	0.00		0.00
62.23	0.00		0.00
52.33	0.00		0.00
44	0.00		0.00
37	0.00		0.00
31.11	0.00		0.00
26.16	0.00		0.00
22	0.00		0.00

Model

		Run			
		1	2	3	units
additional experimental data	torque	13	12	13	in-lb
	impeller speed	1200			rpm
	contact angle	49	42	47	deg
	contact angle	50	44	48	deg
	contact angle	47	44	47	deg
	contact angle	49	44	48	deg
	contact angle	-	46	46	deg
	contact angle	-	-	48	deg
	contact angle	-	-	-	deg
	contact angle	-	-	-	deg
	surface tension	59.93	55.48	60.81	N/m
	zeta potential	-4.4			mV
calculated data	power	29.38	27.12	29.38	Watt
	avg contact angle	48.75	44.00	47.33	deg
	overall contact angle	46.69			deg
	overall surface tension	58.74			N/m
	sauter particle diameter	291.3		295.0	μm
	avg sauter part diameter	293.1			μm
	avg bub. sauter diameter	467.4			μm
	model rate constant	**1.63E+00**	**3.21E+00**	**4.98E+00**	**min^{-1}**

Date performed	2/3/2004
Test number	20-a

Constants

solids density	2475	kg/m3
pressure differential distance	0.0994	m
cell diameter	13.97	cm

Experimental

		Run			
		1	2	3	units
experimental data	tailings wet weight - total	197.4	240.8	202.7	g
	tailings wet tare	25.455	25.843	25.663	g
	tailings dry weight - total	32.8	38.2	31.6	g
	tailings dry tare	8.5	8.5	8.4	g
	tailings time	21.71	19.43	27.22	sec
	product wet weight - total	89.6	81.8	86.0	g
	product wet tare	18.661	18.460	18.597	g
	product dry weight - total	32.4	27.0	26.7	g
	product dry tare	8.3	8.6	8.5	g
	product time	3.39	3.15	3.29	sec
	feed wet weight - total	185.1	198.2	143.3	g
	feed wet tare	26.411	26.003	26.042	g
	feed dry weight - total	50.6	51.4	36.3	g
	feed dry tare	8.3	8.3	8.0	g
	feed time	6.29	6.77	4.92	sec
	pressure differential - no air	0.171	0.157	0.130	psi
		0.165	0.162	0.133	psi
		0.171	0.157	0.134	psi
	pressure differential - with air	0.145	0.127	0.136	psi
		0.137	0.125	0.136	psi
		0.142	0.125	0.137	psi
	liquid height	13.4	13.2	12.8	cm
		13.3	13.4	13.0	cm
		13.5	13.6	13.0	cm
calculated	avg pressure dif. - no air	0.169	0.159	0.132	psi
	avg pressure dif. - with air	0.141	0.126	0.136	psi
	avg liquid height	13.4	13.4	12.9	cm
	air fraction	0.179	0.214	-0.026	-
	active volume	1687	1615	1593	ml
	retention time	74.1	65.9	72.5	sec
mass balanced	feed percent solids	0.133	0.114	0.112	by vol
	feed flow rate	22.75	24.50	21.98	ml/sec
	tailings percent solids	0.062	0.061	0.058	by vol
	tailings flow rate	7.13	9.44	5.85	ml/sec
	product percent solids	0.166	0.147	0.131	by vol
	product flow rate	15.62	15.06	16.13	ml/sec
	exp. rate constant	**1.49E+00**	**1.34E+00**	**1.38E+00**	**min^{-1}**

Misc experimental data

	Run			
	1	2	3	units
temp	48	46	48	F
pH	7.02	7.38	7.4	

Particle Size Data

particle size passing - (μm)	percent in channel - by number		
704	0.00		0.00
592	0.00		0.00
497.8	0.00		0.00
418.6	0.00		0.00
352	0.06		0.06
296	0.29		0.28
248.9	1.46		1.45
209.3	6.79		6.67
176	22.36		21.78
148	37.92		37.37
124.5	24.89		25.61
104.7	6.23		6.78
88	0.00		0.00
74	0.00		0.00
62.23	0.00		0.00
52.33	0.00		0.00
44	0.00		0.00
37	0.00		0.00
31.11	0.00		0.00
26.16	0.00		0.00
22	0.00		0.00

Model

		Run			
		1	2	3	units
additional experimental data	torque	11	11	11	in-lb
	impeller speed	1200			rpm
	contact angle	30	39	34	deg
	contact angle	32	37	35	deg
	contact angle	31	35	33	deg
	contact angle	31	36	34	deg
	contact angle	31	37	36	deg
	contact angle	-	34	-	deg
	contact angle	-	-	-	deg
	contact angle	-	-	-	deg
	surface tension	59.22	61.4	60.61	N/m
	zeta potential	-18.4			mV
calculated data	power	24.86	24.86	24.86	Watt
	avg contact angle	31.00	36.33	34.40	deg
	overall contact angle	33.91			deg
	overall surface tension	60.41			N/m
	sauter particle diameter	139.8		139.2	μm
	avg sauter part diameter	139.5			μm
	avg bub. sauter diameter	467.4			μm
	model rate constant	**3.34E+00**	**4.06E+00**	**3.57E+00**	**min^{-1}**

Date performed	2/17/2004
Test number	20-b

Constants

solids density	2475	kg/m3
pressure differential distance	0.0994	m
cell diameter	13.97	cm

Experimental

		Run			
		1	2	3	units
experimental data	tailings wet weight - total	146.5	131.1	147.2	g
	tailings wet tare	26.077	25.982	26.387	g
	tailings dry weight - total	18.2	13.3	13.1	g
	tailings dry tare	8.2	8.2	8.2	g
	tailings time	18.62	15.33	17.82	sec
	product wet weight - total	139.8	151.0	146.7	g
	product wet tare	25.387	25.422	25.035	g
	product dry weight - total	45.4	45.7	42.3	g
	product dry tare	8.2	8.2	8.1	g
	product time	6.77	7.39	7.35	sec
	feed wet weight - total	160.9	175.4	181.9	g
	feed wet tare	18.871	18.429	18.360	g
	feed dry weight - total	46.6	49.0	47.5	g
	feed dry tare	8.2	8.2	8.2	g
	feed time	6.07	6.84	7.34	sec
	pressure differential - no air	0.137	0.118	0.118	psi
		0.132	0.119	0.124	psi
		0.131	0.117	0.125	psi
	pressure differential - with air	0.089	0.093	0.094	psi
		0.082	0.088	0.093	psi
		0.081	0.087	0.095	psi
	liquid height	10.0	10.2	10.4	cm
		9.5	10.3	10.5	cm
		10.0	10.3	10.6	cm
calculated	avg pressure dif. - no air	0.133	0.118	0.122	psi
	avg pressure dif. - with air	0.084	0.089	0.094	psi
	avg liquid height	9.8	10.3	10.5	cm
	air fraction	0.331	0.196	0.195	-
	active volume	1009	1265	1295	ml
	retention time	51.1	62.5	64.9	sec
mass balanced	feed percent solids	0.126	0.114	0.104	by vol
	feed flow rate	19.74	20.24	19.97	ml/sec
	tailings percent solids	0.035	0.020	0.017	by vol
	tailings flow rate	6.10	6.42	6.37	ml/sec
	product percent solids	0.167	0.157	0.145	by vol
	product flow rate	13.65	13.82	13.59	ml/sec
	exp. rate constant	**3.83E+00**	**5.03E+00**	**5.42E+00**	**min^{-1}**

Misc experimental data

	Run			
	1	2	3	units
temp	41	42	42	F
pH	6.67	6.73	6.87	

Particle Size Data

particle size passing - (μm)	percent in channel - by number		
704	0.00		0.00
592	0.00		0.00
497.8	0.00		0.00
418.6	0.00		0.00
352	0.05		0.05
296	0.26		0.24
248.9	1.35		1.26
209.3	6.56		6.09
176	22.13		21.14
148	38.04		38.10
124.5	25.28		26.41
104.7	6.33		6.71
88	0.00		0.00
74	0.00		0.00
62.23	0.00		0.00
52.33	0.00		0.00
44	0.00		0.00
37	0.00		0.00
31.11	0.00		0.00
26.16	0.00		0.00
22	0.00		0.00

Model

		Run			
		1	2	3	units
additional experimental data	torque	11	11	11	in-lb
	impeller speed	1200			rpm
	contact angle	37	35	37	deg
	contact angle	35	35	36	deg
	contact angle	34	33	34	deg
	contact angle	36	34	36	deg
	contact angle	-	35	37	deg
	contact angle	-	-	-	deg
	contact angle	-	-	-	deg
	contact angle	-	-	-	deg
	surface tension	60.11	60.34	61.09	N/m
	zeta potential	-20.3			mV
calculated data	power	24.86	24.86	24.86	Watt
	avg contact angle	35.50	34.40	36.00	deg
	overall contact angle	35.30			deg
	overall surface tension	60.51			N/m
	sauter particle diameter	139.4		138.3	μm
	avg sauter part diameter	138.8			μm
	avg bub. sauter diameter	467.4			μm
	model rate constant	**5.86E+00**	**3.41E+00**	**3.47E+00**	**min^{-1}**

Date performed	2/18/2004
Test number	21

Constants

solids density	2475	kg/m3
pressure differential distance	0.0994	m
cell diameter	13.97	cm

Experimental

		Run			
		1	2	3	units
experimental data	tailings wet weight - total	75.0	154.5	119.1	g
	tailings wet tare	25.455	25.843	25.663	g
	tailings dry weight - total	10.8	16.1	14.1	g
	tailings dry tare	8.3	8.3	8.2	g
	tailings time	27.22	20.72	12.58	sec
	product wet weight - total	139.7	152.0	136.3	g
	product wet tare	26.396	25.840	25.814	g
	product dry weight - total	43.0	47.2	44.3	g
	product dry tare	8.2	8.2	8.3	g
	product time	5.82	7.70	7.36	sec
	feed wet weight - total	137.8	139.6	124.5	g
	feed wet tare	18.676	18.623	18.825	g
	feed dry weight - total	39.9	39.5	34.5	g
	feed dry tare	8.2	8.2	8.1	g
	feed time	5.37	5.81	4.71	sec
	pressure differential - no air	0.124	0.124	0.113	psi
		0.125	0.124	0.114	psi
		0.127	0.126	0.112	psi
	pressure differential - with air	0.093	0.110	0.094	psi
		0.095	0.109	0.095	psi
		0.096	0.110	0.091	psi
	liquid height	9.0	9.0	8.5	cm
		0.0	0.0	9.0	cm
		0.0	0.0	0.0	cm
calculated	avg pressure dif. - no air	0.125	0.125	0.113	psi
	avg pressure dif. - with air	0.095	0.110	0.093	psi
	avg liquid height	9.0	9.0	8.8	cm
	air fraction	0.210	0.102	0.134	-
	active volume	1090	1239	1162	ml
	retention time	60.4	66.3	60.5	sec
mass balanced	feed percent solids	0.133	0.118	0.115	by vol
	feed flow rate	18.06	18.68	19.22	ml/sec
	tailings percent solids	0.022	0.026	0.027	by vol
	tailings flow rate	1.78	5.79	7.08	ml/sec
	product percent solids	0.145	0.159	0.167	by vol
	product flow rate	16.28	12.89	12.14	ml/sec
	exp. rate constant	**6.02E+00**	**3.88E+00**	**3.95E+00**	**min^{-1}**

Misc experimental data

	Run			
	1	2	3	units
temp	41	42	42	F
pH	7.27	7.31	7.35	

Particle Size Data

particle size passing - (μm)	percent in channel - by number		
704	0.00	0.00	0.00
592	0.00	0.00	0.00
497.8	0.00	0.00	0.00
418.6	0.00	0.00	0.00
352	0.00	0.00	0.00
296	0.00	0.00	0.00
248.9	0.00	0.00	0.00
209.3	0.01	0.00	0.02
176	0.05	0.04	0.07
148	0.18	0.17	0.30
124.5	0.74	0.77	1.28
104.7	3.04	3.36	5.03
88	10.41	11.83	15.23
74	24.26	27.09	29.27
62.23	31.10	32.30	29.37
52.33	20.23	18.51	14.84
44	7.57	5.93	4.59
37	2.41	0.00	0.00
31.11	0.00	0.00	0.00
26.16	0.00	0.00	0.00
22	0.00	0.00	0.00

Model

		Run			
		1	2	3	units
additional experimental data	torque	11	11	11	in-lb
	impeller speed	1200			rpm
	contact angle	34	37	36	deg
	contact angle	37	38	37	deg
	contact angle	39	39	37	deg
	contact angle	37	42	38	deg
	contact angle	40	37	38	deg
	contact angle	-	-	40	deg
	contact angle	-	-	-	deg
	contact angle	-	-	-	deg
	surface tension	60.26	60.3	61.04	N/m
	zeta potential	-12.5			mV
calculated data	power	24.86	24.86	24.86	Watt
	avg contact angle	37.40	38.60	37.67	deg
	overall contact angle	37.89			deg
	overall surface tension	60.53			N/m
	sauter particle diameter	60.5	62.3	65.0	μm
	avg sauter part diameter	62.6			μm
	avg bub. sauter diameter	467.4			μm
	model rate constant	**1.06E+01**	**4.97E+00**	**6.58E+00**	**min^{-1}**

Vita

Ian Michael Sherrell was born on September 18, 1976 in San Francisco, CA. He graduated from Tabb High School, Virginia in 1994. He then enrolled in Virginia Polytechnic Institute and State University and graduated with a Bachelor of Science degree in Mining and Minerals Engineering in May of 1999. He continued his enrollment at VPI and obtained a Master of Science degree in Mining and Minerals Engineering in May of 2001. He remained at VPI to pursue his Doctorate Degree in Mining and Minerals Engineering.